Journal of Materials Chemistry A

REVIEW

View Article Online
View Journal

Cite this: DOI: 10.1039/c9ta07552f

Colloidal nanoparticle inks for printing functional devices: emerging trends and future prospects

Minxiang Zeng and Yanliang Zhang *

Colloidal nanoparticles have been widely studied and proven to have unique and superior properties compared to their bulk form and are attractive building blocks for diverse technologies, including energy conversion and storage, sensing, electronics, *etc.* However, transforming colloidal nanoparticles into functional devices while translating their unique properties from the nanoscale to the macroscale remains a major challenge. The development of advanced manufacturing methodologies that can convert functional nanomaterials into high-performance devices in a scalable, controllable and affordable manner presents great research opportunities and challenges for the next several decades. One promising approach to fabricate functional devices from nanoscale building blocks is additive manufacturing, such as 2D and 3D printing, owing to their capability of fast prototyping and versatile fabrication. Here, we review recent progress and methodologies for printing functional devices using colloidal nanoparticle inks with an emphasis on 2D nanomaterial-based inks. This review provides a comprehensive overview on four important and interconnected topics, including nanoparticle synthesis, ink formulation, printing methods, and device applications. New research opportunities as well as future directions are also discussed.

Received 12th July 2019
Accepted 16th September 2019

DOI: 10.1039/c9ta07552f

rsc.li/materials-a

1. Introduction

Colloidal nanoparticles are attractive building blocks for a wide range of emerging technologies, including electronics, optoelectronics, sensors, energy devices, *etc.* In the past several decades, various device fabrication technologies, such as photolithography, electroless plating, and physical/chemical vapor deposition, have been extensively investigated.[1,2] However, these technologies rely on expensive equipment and/or multi-stage processes, which are not only difficult for fast prototyping and low-cost manufacturing, but also not compatible/sophisticated enough for building functional devices with colloidal nanoparticles. An alternative method to fabricate flexible/functional devices is additive manufacturing, such as three-dimensional (3D) printing.[3,4] In the past several

Department of Aerospace and Mechanical Engineering, University of Notre Dame, Notre Dame, IN, USA. E-mail: yzhang45@nd.edu

Minxiang Zeng received his BS degree from the University of Science and Technology of China in 2014. He completed his PhD under the supervision of Dr Zhengdong Cheng from Texas A&M University in 2018. He is currently a postdoctoral researcher in the group of Dr Yanliang Zhang at the University of Notre Dame. His research interests include self-assembly of two-dimensional materials, additive manufacturing of functional devices, and development of colloidal nanomachines.

Yanliang Zhang is an Assistant Professor in the Department of Aerospace and Mechanical Engineering at the University of Notre Dame, where he directs the Advanced Manufacturing and Energy Lab (AMEL). He received his Ph.D. degree in Mechanical Engineering from Rensselaer Polytechnic Institute in 2011. Dr Zhang was the recipient of the U.S National Science Foundation CAREER Award (2017). His research focuses on additive and nanomanufacturing of multifunctional and multiscale devices, thermal science and energy conversion, and advanced sensors and flexible electronics.

decades, significant development of printing technologies has been witnessed for converting printable nanoparticle inks into complex device architectures.[5–7] A wide range of functional nanomaterials from zero-dimensional (0D) quantum dots to one-dimensional (1D) nanowires/nanofibers and two-dimensional (2D) nanosheets have been adopted as printable colloidal inks (Fig. 1). All this progress has created almost infinite possibilities for rapid prototyping and scalable and low-cost manufacturing of functional devices.[8]

Among various types of nanomaterials, 2D nanomaterials (2DMs) are ultrathin nanostructures with unique optical, electrical, chemical, thermal and mechanical properties.[12,13] Since the rise of the graphene family, a great variety of 2D nanomaterials have been synthesized and developed by a bottom-up strategy from molecular precursors or a top-down approach from their layered crystals.[14] As shown in Fig. 2, common 2D nanomaterials include graphene/graphene oxide/reduced graphene oxide (Gr/GO/rGO), transition metal dichalcogenides (TMDs), transition metal carbides/carbonitrides/nitrides (MXenes), black phosphorus (BP), hexagonal boron nitride (h-BN), graphitic carbon nitride (g-C_3N_4), layered double hydroxides (LDHs), transition metals/metal oxides (TMOs/MOs), and other novel 2D nanostructures.[12] Graphene is monolayer graphite with every carbon atom bonded to adjacent ones by σ bonds, forming a hexagonal 2D network with a thickness of around 3.4 Å. TMDs also have a hexagonal surface structure similar to that of graphene, with the in-plane anion atoms in each layer split into two identical layers. MXenes have the general formula $M_{n+1}X_nT_x$ ($n = 1$–3), where M is a transition metal (*e.g.*, Ti or V), X is C and/or N, and T is a surface anion (O, OH, and F). For naturally occurring 2DMs, clay minerals have 2D sandwich structures with octahedral metal hydroxide layers and tetrahedral silicate layers.[15] LDHs, also known as anionic clays or hydrotalcite-like compounds, are often described by the general formula $[M_{1-x}^{2+}M_x^{3+}(OH)_2]^{x+}A_{x/n}^{n-}\cdot yH_2O$, where M is a metal ion and A represents an interlayer anion.[16,17]

The extreme chemical diversity of 2D nanomaterials provides many opportunities, but also poses challenges for comprehensive assessment of specialized roles of 2DMs in device fabrication processes, such as printing-based manufacturing. In addition, high-performance 2D nanomaterials are not necessarily convertible into high-quality inks for printing processes. The collective behaviour of 2D nanoparticles in colloidal inks can be influenced by many factors, such as particle size and surface chemistry, tendency of aggregation, and ionic strength of the dispersion. Although several articles have made great effort towards reviewing printing technologies of nanomaterials,[3,4,7,19–22] a comprehensive review that covers nanoscale building blocks (*e.g.*, synthesis and surface engineering), mesoscopic colloidal interaction (*e.g.*, aggregation and sedimentation), and macroscopic printing processes (*e.g.*, 2D, 3D, and 4D printing) and device applications is missing. This review therefore proposes a framework for seeking a systematic understanding on fundamental correlations of materials chemistry and physics of 2DMs, ink properties, printing processes, and corresponding device applications. With this in mind, the framework thus considers four key interactive aspects: 2D nanomaterial synthesis, ink formulation, printing processes, and device applications. Our vision is to perform a meticulous examination of current research trends over the last decade with a focus on 2DMs compatible with printing processes. The review ends with a conclusion and outlook, suggesting future directions to inform researchers about potentially disruptive printing technologies and applications of 2DMs.

2. Synthesis of 2D nanomaterials

Since the discovery of graphene, significant efforts have been invested towards the synthesis of 2D materials, including liquid phase exfoliation, hydrothermal synthesis, *etc.* In this section, we mainly focus on solution-processable 2D nanomaterials so some synthetic methods such as chemical vapor deposition will not be discussed. The synthetic strategies of 2D nanomaterials typically can be categorized into two kinds: bottom-up synthesis and top-down synthesis. Despite some exceptions, Table 1 aims to summarize the common preparation methods of 2D nanomaterials. Despite the fact that not all of these synthetic

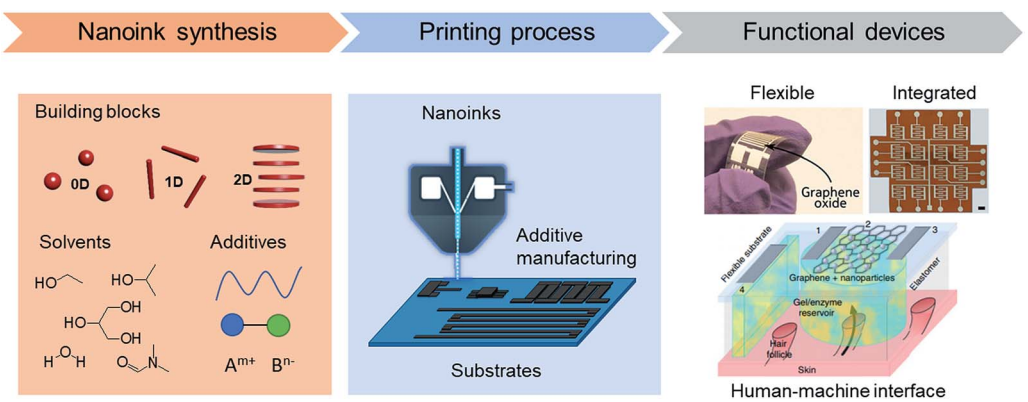

Fig. 1 Additive manufacturing enables the rapid transformation from nanoscale building blocks into macroscale functional devices. Adapted and reprinted with permission from Springer Nature.[9,10] Copyright 2017 & 2018 Nature Publishing Group. Reproduced with permission from ref. 11. Copyright 2013 American Chemical Society.

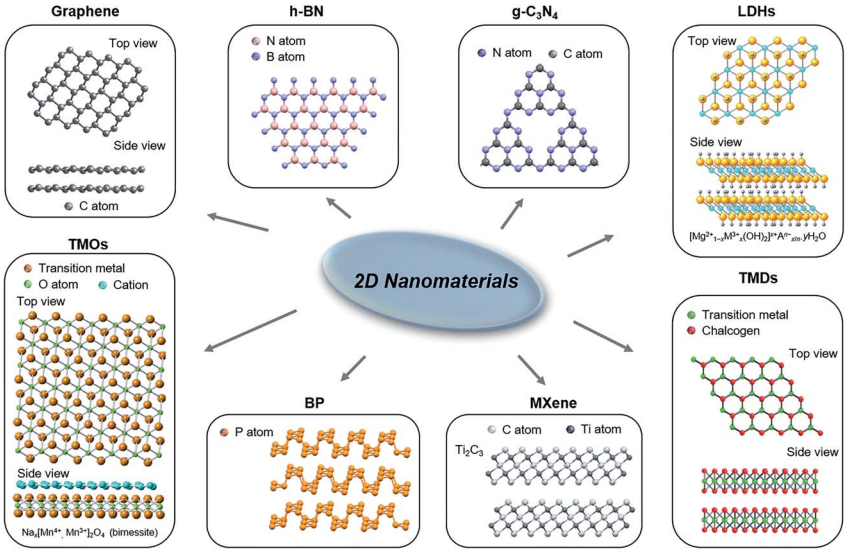

Fig. 2 2D nanomaterials and their structures. Adapted with permission from ref. 18. Copyright 2015 Wiley-VCH.

methods have been explored for ink preparation, significant research opportunities still exist for synthesizing novel printable 2D nanostructures and establishing a next-generation material library in the field of printing technology.

2.1. Bottom-up synthesis

2.1.1. Hydrothermal/solvothermal synthesis. As a representative wet-chemical synthesis approach, hydrothermal/solvothermal synthesis involves water or other solvents in a sealed vessel, where the reaction temperature can be higher than the boiling point of the solvent in order to generate high pressure to assist the reaction kinetics and increase the quality of the crystal phase of the as-prepared 2D nanomaterials.[12] Remarkably, the solvent and additives, such as ligands or surfactants, are crucial factors in determining the synthesis, morphology, and properties of 2D nanosheets. For example, ultrathin cobalt nanosheets with a tunable oxide state can be prepared by using hydrothermal conditions of butylamine and dimethylformamide (Fig. 3a).[50] Single-layer noble metal nanosheets with lateral sizes of a few hundred nanometers can be prepared using polyvinylpyrrolidone (PVP) as a surfactant. Besides metal nanosheets, metal oxide and TMD nanosheets have also been produced by hydrothermal/solvothermal techniques.

Although hydrothermal/solvothermal synthesis is a facile and possibly scalable technique for producing 2DMs, it is difficult to fully understand the mechanisms in every single reaction as all the reaction kinetics occur in a sealed system, which makes it challenging to apply the same experimental condition to other 2DM systems. Noteworthily, hydrothermal synthesis is relatively sensitive to the experimental settings, which increases the challenge of precisely controlling the resulting 2D nanomaterials in different batches or different laboratories.

Table 1 Overview of various 2D nanomaterials with their common preparation methods

	Bottom-up			Top-down		
	Hydrothermal/solvothermal	Ligand/template attachment	Self-assembly	Micro-mechanical cleavage	Liquid exfoliation	Selective etching
Gr/GO/rGO	+[23,24]			+[25,26]	+[27,28]	
TMDs	+[29]	+[30]	+[31]	+[32]	+[33,34]	
h-BN	+[35,36]			+[37]	+[38]	
Black phosphorus				+[39]	+[40]	
Metal oxides	+[41]	+[42,43]	+[44]		+[45]	
MXene		+[46]				+[47]
Clays	+[48]				+[49]	
Comments	Facile and applicable to large-scale production	Provide good control on particle size and morphology	Versatile but low structural robustness due to non-covalent bonding	Good quality but often low yield	High scalability and relatively low cost	Strongly corrosive agents are often required

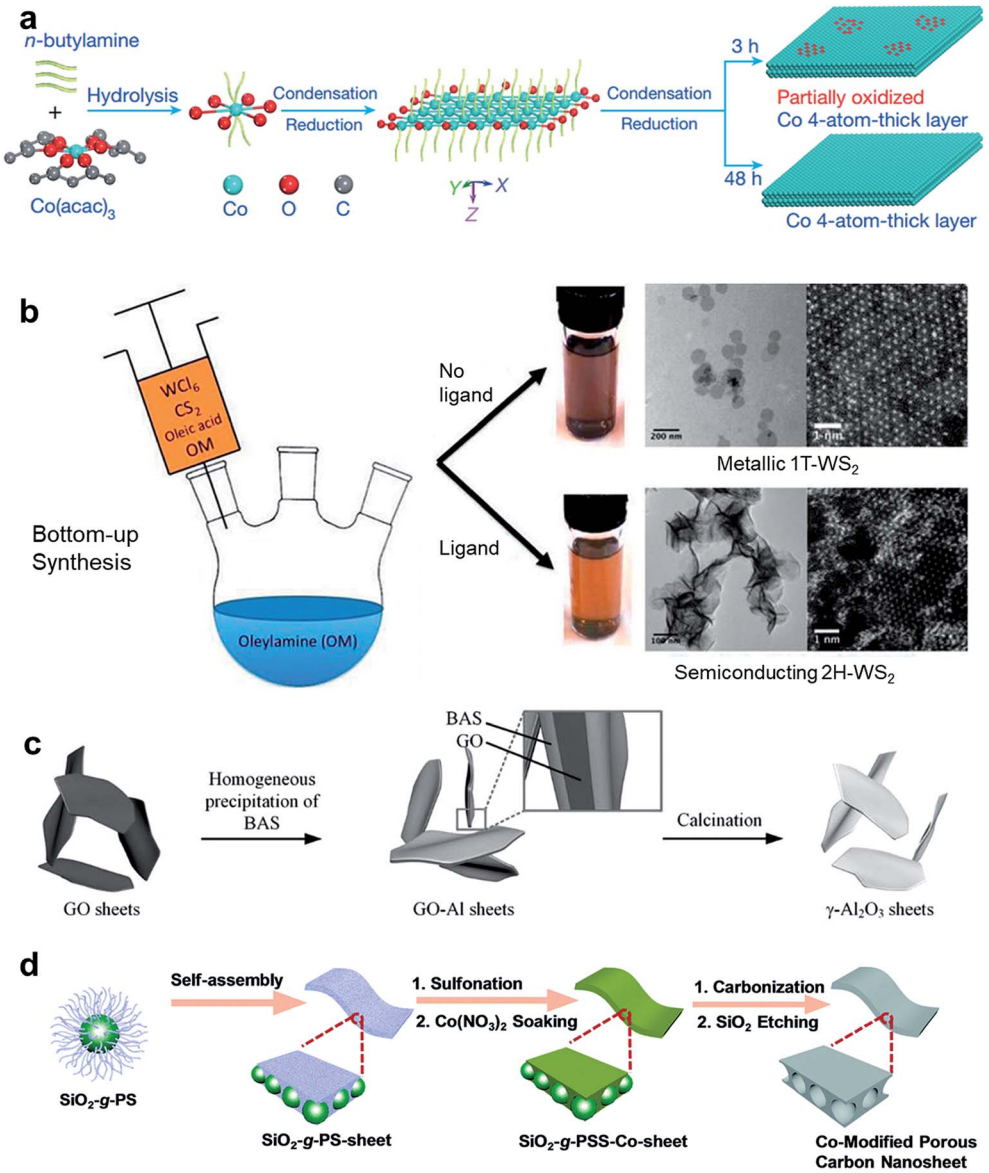

Fig. 3 Examples of bottom-up synthesis of 2D nanomaterials. (a) Hydrothermal synthesis of cobalt nanosheets. Reprinted with permission from Springer Nature.[50] Copyright 2016 Nature Publishing Group. (b) Colloidal synthesis of WS_2 from small molecules. The formation of 1T-WS_2 and 2H-WS_2 can be actively controlled by adjusting the reaction conditions. Reprinted with permission from ref. 51. Copyright 2014 American Chemical Society. (c) The bottom-up synthesis of Al_2O_3 nanosheets based on the 2D templates of GO reacting with basic aluminum sulfate (BAS). Reproduced with permission from ref. 30. Copyright 2016 Wiley-VCH. (d) Evaporation-induced bottom-up self-assembly approach for fabricating 2D porous carbon nanosheets. Reprinted with permission from ref. 52. Copyright 2019 the Royal Society of Chemistry.

2.1.2. Ligand/template attachment method. Compared with traditional hydrothermal mechanisms, the ligand attachment method demonstrates a tunable growth progression and realizes nanostructures with well-defined shapes.[53] During this process, neighboring nanocrystals or precursors are accumulated, attached, and fused with each other, forming single-crystalline 2D sheets to reduce high interfacial energy facets.[12] For example, taking advantage of the strong bonding of oleic acid on the [100] facet, small PbS nanocrystals can grow into single-crystalline 2D PbS sheets. Studies also showed that other reagents, such as chlorine-containing reactants, can assist in activating the oriented attachment progression. In general, the growth mechanism is typically based on the oriented attachment of small crystals, after which epitaxial recrystallization into large 2D nanostructures occurs. Similar to hydrothermal mechanisms, surfactants are critical for determining the size, shape, and nanostructures of 2DMs in the ligand attachment method. As shown in Fig. 3b, Mahler *et al.* demonstrated that the formation of either 2H-WS_2 or 1T-WS_2 highly depends on the ligand choice.[51] Introducing a small amount of hexamethyldisilazane (HMDS) into the reaction system can lead to the formation of semiconducting 2H-WS_2 rather than metallic 1T-WS_2.

Similar to the ligand attachment method, other templated strategies have been investigated for synthesizing anisotropic

nanostructures. As shown in Fig. 3c, 2D GO nanosheets were used as a 2D template to direct the growth of inorganic Al_2O_3 sheets.[30] During the synthesis, a thin layer of aluminum hydroxide was first deposited on GO sheets which was then removed using calcination treatment at 800 °C, leading to the transformation of aluminum hydroxide into Al_2O_3 nanosheets. As another 2D-templated example, hexagonal close-packed (hcp) gold nanosheets can be prepared by using GO as a starting template.[54] In addition, CuO nanoplates were also reported for the templated synthesis of α-Fe_2O_3 nanosheets, in which the CuO template was etched away during the nanosheet growth.[55] Numerous 2D semiconductor nanosheets, including $CuInS_2$, $CuIn_xGa_{1-x}S_2$, and Cu_2ZnSnS_4, have also been fabricated by 2D-templated synthesis processes.[56]

2.1.3. Self-assembly of building blocks. Driven by the improvement of nanocrystal production, self-assembly of small building blocks has been developed to form architectures with nanocrystal building blocks in an orientationally/positionally ordered manner, where pre-synthesized building blocks instinctively assemble with each other by physical/chemical interactions including electrostatic interactions, van der Waals interactions, hydrogen bonds, *etc.*[57] Both nanoparticles and nanowires were shown to self-assemble into 2D materials, such as polycrystalline 2D CdTe nanosheets or assembled Au nanosheets.[31,58] For example, the self-assembly of PbS nanowires has been demonstrated to produce anisotropic PbS nanosheets.[59] To better control the assembly process, interface-based self-assembly has been proposed to fabricated functional 2D nanomaterials.[52] As shown in Fig. 3d, spherical polystyrene-functionalized SiO_2 nanoparticles can self-assemble at the interface of the saturated NaCl solution and air. The 2D intermediate was then dispersed in sulfuric acid to preserve its nanosheet morphology followed by Co treatment to dope Co element in 2D sheets. After a simple carbonization and etching process, functional Co-modified carbon nanosheets were obtained.[52]

In addition to nanocrystals, organic molecules can also be used as building blocks for self-assembly into 2D nanosheets by electrostatic interactions, van der Waals interactions, and hydrogen bonds. Well-organized photonic nanosheets were demonstrated by self-assembly of nonionic surfactant hexadecylglyceryl maleate.[60] It is reasonable to expect that more novel 2D materials would be developed *via* the strategy of self-assembly of building blocks.

2.2. Top-down synthesis

2.2.1. Micromechanical cleavage. The ability to synthesize 2D materials with a desired chemical composition, dimensions, crystalline phase, and surface properties is of particular significance. The micromechanical cleavage technique was used to prepare 2D nanosheets by exfoliating layered crystals. For example, using mechanical forces with Scotch tape, single/few layers of nanosheets can be achieved as the interlayered van der Waals forces have been overcome in bulk crystals. In 2004, Geim and co-workers first reported the micromechanical cleavage of graphite, where the bulk graphite can be attached to Scotch tapes followed by peeling into thin platelets with another adhesive surface.[61–64] By repeating such a process several times, the desired thin flakes can be obtained. After attaching freshly cleaved thin films to a flat substrate and removing scope tapes, single- or few-layers of graphene can be acquired.

This micromechanical cleavage technique can be extended to exfoliate other layered materials, including MoS_2, $NbSe_2$, and h-BN.[63] Recently, the micromechanical cleavage technique has been employed to synthesize several ultrathin 2D nanomaterials ranging from TMDs,[65] to topological insulators,[66] and antimonene.[67] As a general method capable of fabricating all categories of nanosheets of which bulk crystals are layered structures, additional novel ultrathin 2D crystals are expected to be synthesized by this method. This methodology can be considered as a nondestructive process as no chemical reactions were required during the manufacturing process. Consequently, the exfoliated nanosheets retained the pristine crystal quality of their layered counterparts. The dimensions of the formed 2D structures can reach micrometer levels, which enables the mechanically cleaved nanosheets to become an ideal candidate to investigate the intrinsic mechanical, optical, and electronic properties of 2D nanomaterials.

Despite several advantages of the micromechanical cleavage method, disadvantages still remain: (1) the fabrication yield of this method is relatively low, and impurities such as thick flakes always coexist with single- or few-layer flakes; (2) the manufacturing speed is not competitive with other methods such as solution-based approaches. The low yield together with the slow manufacturing rate makes it problematic to meet the requirements for many printing applications, especially for large-scale additive manufacturing; (3) the dimensions of the prepared 2D materials are hard to regulate as the exfoliation route lacks the exactness, controllability, or repeatability; (4) additional substrates are prerequisites to hold the formed 2D crystals during exfoliation, making it challenging for fabricating freestanding 2DM-based devices. Recently efforts have been made to improve the micromechanical cleavage method, showing that using oxygen plasma treatment with additional heating during the exfoliation substantially improved the uniformity of the interface contact and thus increased the production yield of 2D nanosheets.[68]

2.2.2. Mechanical liquid exfoliation. Sonication has been commonly used as a source of mechanical forces for exfoliating layered bulk materials, which are generally dispersed in a particular solvent. As the liquid cavitation is induced by sonication, the waves of mechanical vibrations through the layered crystals produce an intensive tensile stress, resulting in the exfoliation of starting materials into thin sheets.[69] The 2D nanosheets can be separated from the suspension using centrifugation. To maximize the efficiency of liquid phase exfoliation, matching the interfacial energy between the solvent and 2D materials can be an important factor. As it is relatively simple and effective without any complicated equipment, this sonication technique offers a low-cost approach for high-yield fabrication of 2D nanosheets. For example, a fairly high concentration of graphene nanosheet suspension was achieved by sonicating bulk graphite in isopropanol and chloroform.[70,71] In addition to graphene, other 2D nanomaterials, including

$NbSe_2$, Bi_2Te_3, and h-BN, have also been prepared by this technique.[72] The solvent systems play significant roles in the production of exfoliated nanosheets. It is noteworthy that although pure H_2O was constantly thought to be unsatisfactory for efficiently exfoliating layered bulk materials, a recent study showed that direct exfoliation and dispersion of 2D nanomaterials in pure H_2O can be achieved at elevated temperatures.[73] The exfoliated nanosheets can be stabilized due to the presence of colloidal surface charges brought about by edge functionalization or high polarity, leading to enhanced colloidal stability of 2D nanosheets. Such an approach of exfoliating bulk materials in pure water makes this process promising for practical applications due to its environmentally friendly and low-cost features.

It is challenging to find an appropriate solvent for each layered bulk material, as the surface energy differs in different bulk crystals. Instead, the addition of polymers or surfactants provided another promising pathway for exfoliating 2D layered materials. The surface energy of the aqueous dispersion can be simply adjusted by introducing suitable surfactants, thus reducing the interfacial energy between layered bulk crystals and solvent and realizing effective exfoliation of layered constituents. For instance, pyrene derivatives are commonly used as dispersants for manufacturing graphene dispersions owing to their ability to form π–π stacking interaction with graphene sheets.[74,75] Through introducing repulsive electrostatic forces on the graphene surface, pyrene derivatives can prevent sheet aggregation and consequently stabilize graphene in water.[76–78] In addition to pyrene derivatives, other species have been employed for dispersing 2D nanosheets in inks: polystyrene (PS), polyvinyl chloride (PVC), ethyl cellulose (EC), polyvinylpyrrolidone, poly(isoprene-*b*-acrylic acid) (PI-*b*-PAA), poly[styrene-*b*-(2-vinylpyridine)] (PS-*b*-P2VP), P-123-polyoxyethylene orbitanmonooleate, polyoxyethylene sorbitan-trioleate, polyoxyethylene dodecyl ether, polyoxyethylene octadecylether, polyoxyethyleneoctyl phenyl ether, bovine serum albumin (BSA), Pluronic P-123, *n*-dodecyl β-D-maltoside (DBDM), and Arabic gum from acacia tree.[79–82]

Although the sonication-assisted exfoliation method can be applicable for a wide range of 2D materials with a higher fabrication rate than that of micromechanical cleavage processes, the fabrication rate remains relatively low to meet the requirement for industrial scale applications. In order to scale up the process, a shear force-assisted method was proposed. Using a high-shear rotor-stator mixer, high shear rates in suspension can trigger the exfoliation process and produce exfoliated nanosheets in a much more efficient manner.[83] The shear-force device contains a mixing head consisting of a rotor with a stator. Such a technique was also used for exfoliating BP crystals into few-layer platelets. Additionally, the synthesis of exfoliated WS_2, MoS_2, and h-BN nanosheets was reported by using a kitchen blender.[84] Such results suggest that it is possible to use industrial stirring tank reactors for large-scale 2D material production.

2.2.3. Intercalation-assisted liquid exfoliation. As a typical top-down approach, the ion intercalation strategy has been widely adopted to fabricate ultrathin 2D nanosheets. Small molecules and ionic species, including Li^+, Na^+, and K^+, can intercalate into the spaces between neighboring layers in layered bulk crystals, leading to the formation of intercalated compounds (Fig. 4).[33,34] Consequently, the ion intercalation can considerably enlarge the interlayer distance of unexfoliated bulk crystals, facilitating the exfoliation process with a shorter time. A high yield of mono- to few-layer nanosheets can be achieved using a separation step to eliminate unexfoliated flakes by methods such as high-speed centrifugation. For example, the layered materials were treated with *n*-butyl lithium to yield a Li-intercalated structure in refluxed hexane solution for several days, and subsequently the nanosheet dispersion can be readily formed under sonication in water.

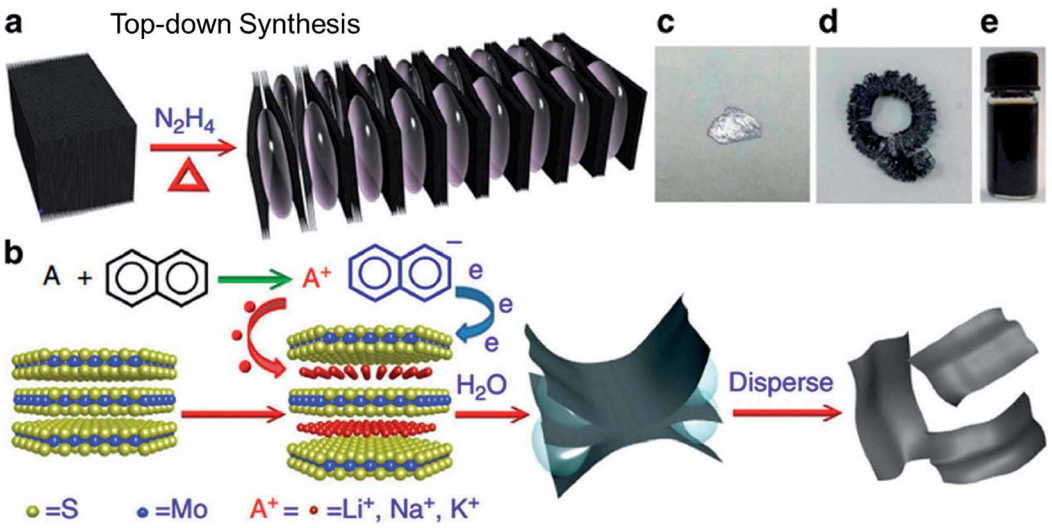

Fig. 4 Examples of top-down synthesis of 2D nanomaterials. (a) The intercalation and (b) the exfoliation of MoS_2 using hydrazine and naphthalenide. (c) Unexfoliated MoS_2 crystal. (d) Intercalated MoS_2. (e) Exfoliated MoS_2 in dispersion. Reprinted with permission from Springer Nature.[34] Copyright 2014 Nature Publishing Group.

In spite of the accelerated exfoliation facilitated by ion intercalation, the intercalation process itself requires an extended reaction time (for example, several days) and elevated temperature (for instance, 100 °C) for some compounds. The lateral dimensions, quantity of deficiencies, sheet concentration, and number of layers can be approximately adjusted by changing the tentative settings, including the starting size of layered crystals, exfoliation time, exfoliation agents, and reaction temperature. During ion-intercalation, phase alteration sometimes occurs from semiconducting hexagonal (2H) and metallic octahedral (1T) phases for MoS_2 and WS_2, presenting a potent method for the phase engineering of TMDs.[85] Despite the fact that some ions are able to intercalate into layered metal tellurides or selenides, the use of the ion intercalation strategy for exfoliating metal tellurides or selenides remains challenging, as intercalated metal tellurides or selenides are commonly unstable, leading to the decomposition of metal tellurides/selenides during sonication.[12]

The ion intercalation route, such as the use of butyl lithium, is difficult to regulate precisely, making it challenging to circumvent inadequate or over ion-intercalation. Recently, safer salt choices including NaCl and $CuCl_2$ were proposed as intercalates for the exfoliation of graphite powder into graphene. Upon heating at 100 °C to vaporize the water, Cu^{2+} or Na^+ can be intercalated into the interlayer spacing of graphite.[86] After sonicating in DMF or NMP for a short time, up to 65% (1–5 layers) yield of graphene sheets can be produced with large lateral sizes up to tens of micrometers.

2.2.4. Oxidation-assisted liquid exfoliation. In oxidation-assisted exfoliation of graphite, commonly known as Hummers' method, strong oxidizing agents, such as potassium permanganate or sodium persulfate, were applied to oxidize graphite, and the oxidation of graphite produces hydrophilic functional groups on each graphene layer, resulting in enlarged *d*-spacing of bulk graphite.[87,88] With increased treatment time and temperature, the expanded graphite oxide bulk materials were exfoliated into 2D graphene oxide monolayers, or possibly transformed into small-sized 2D graphene quantum dots. This technique enables large-scale synthesis of single-layer GO nanosheets in aqueous solution. It is noteworthy that the oxygen-containing functional groups of GO can be partially eliminated using the reduction strategy to form reduced GO nanosheets. Up to now, electrochemical reduction, thermal annealing, photochemical reduction, and chemical reduction have been reported to remove GO's oxygen-containing groups.[89] Since the residual groups may still exist, the conductivity of reduced GO commonly cannot compete with graphene nanosheets produced from the CVD method or mechanical exfoliation.

2.2.5. Selective etching. The selective etching method can prepare 2D nanosheets of MXenes, a class of metal carbides or carbonitrides.[90,91] MAX phases have a common formula of $M_{n+1}AX_n$ (n = 1, 2, or 3), where M, A, and X represent an early transition metal, element of group IIIA or IVA, and C and/or N, respectively.[92–94] A clear difference between MAX phase materials and conventional van der Waals layered crystals lies in the metallic bonds between $M_{n+1}X_n$ layers which shows much more robust interaction than weak forces of TMDs, graphite, and BP. Consequently, a selective etching technique based on acidic HF solution is often required to remove the "A" layers without destroying the bonds in $M_{n+1}X_n$ layers. The resulting etched materials with loosely packed layers can be readily exfoliated into 2D nanosheets under sonication. Up to now, this technique has been magnificently useful for synthesizing many different types of MXenes including Al_3C_3, Ta_4C_3, Mo_2TiC_2, Nb_2C, Ti_4N_3, $Mo_2Ti_2C_3$, Ti_3CN, Mo_2CT_x, Cr_2TiC_2, Ti_2C, V_2C, $(Ti_{0.5},Nb_{0.5})_2C$, and $(V_{0.5},Cr_{0.5})_3C_2$. However, several limitations still exist in this technique as it is difficult to apply this process to prepare other ultrathin 2D nanosheets, such as TMDs.

3. Ink formulation

While 2D materials show intriguing properties at the nanoscale, these particles cannot be directly used until being processed and formulated into printable inks for device fabrication. One important goal of ink formulation is to convert or integrate nanoscale building blocks into a stable colloidal dispersion. The use of 2DM-based inks for printing has received increasing research interest in recent years, likely due to: (i) significant advances in solution-processable 2DMs and 2DM derivatives for which the surface chemistry and nanostructure can be on-demand controlled and (ii) fast development of printing technologies which provides a variety of processing options. Herein, the major principles of colloidal ink systems and recent developments in 2DM-based inks are discussed.

3.1. The colloidal stability of 2D nanomaterials

For most nanoparticle-based inks, the colloidal stability of the ink particles is one of the most essential elements in the preparation of high-quality inks. In a liquid medium, the colloidal behavior of 2D nanomaterials can be estimated through Derjaguin–Landau–Verwey–Overbeek (DLVO) theory, which predicts the aggregation trend of nanoparticles quantitatively. As shown in Fig. 5a, DLVO theory combines the potential energy of the van der Waals attraction (P_A, red) and the electrostatic repulsion (P_R, blue) because of the electric double layers. Fig. 5a also presents a typical total energy profile (P_{total}, green) along with the separation distance of particles: the primary minimum and secondary minimum represent the aggregation state and colloidally stable state, respectively. For 2D particles, DLVO theory can be represented as in eqn (1)–(4):[95]

$$P_A = -\frac{A}{12\pi}\left\{\frac{1}{d^2} + \frac{1}{(d+2\delta)^2} - \frac{2}{(d+\delta)^2}\right\} \quad (1)$$

$$P_R = \frac{64 k_B T I N_A}{\kappa}\left\{\tanh\left(\frac{e\psi_0}{4k_B T}\right)\right\}^2 e^{-\kappa d} \quad (2)$$

$$\kappa^{-1} = \sqrt{\frac{k_B T \varepsilon_0 \varepsilon_r}{2 N_A e^2 I}} \quad (3)$$

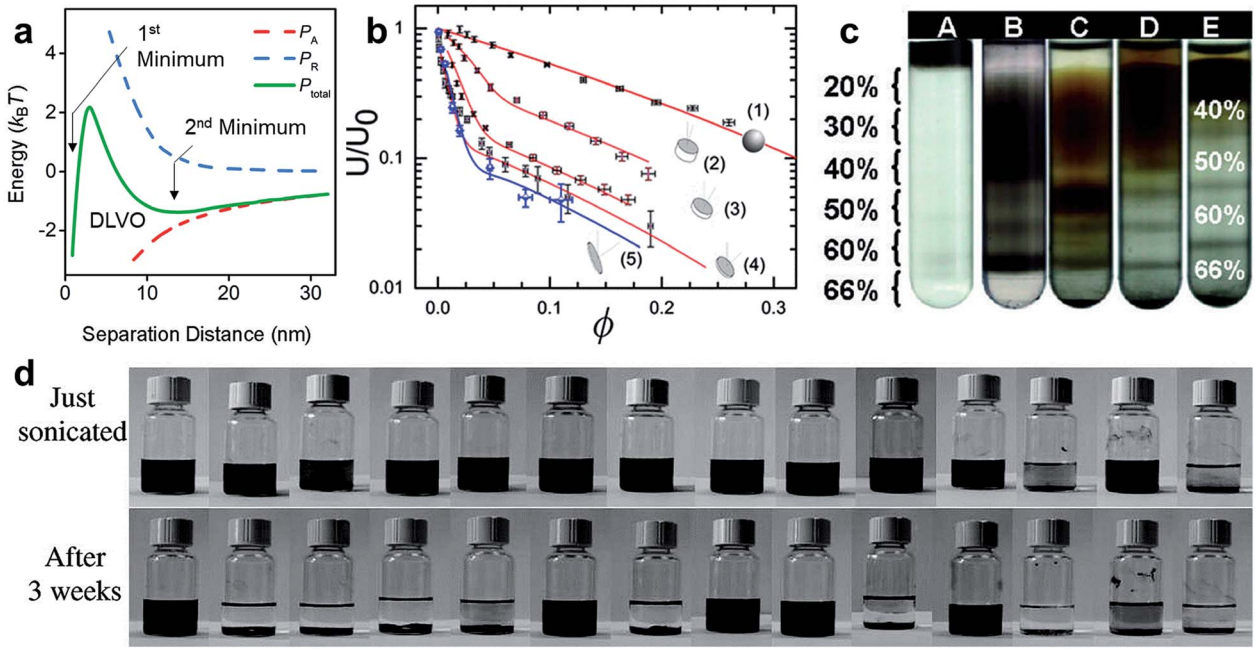

Fig. 5 (a) DLVO theory of colloidal particles in dispersion. (b) Dimensionless sedimentation speed of 2D particles. Reproduced with permission from ref. 99. Copyright 2010 American Physical Society. (c) Ultracentrifuge separation of monodisperse graphene using density gradient. Reproduced with permission from ref. 100. Copyright 2010 American Chemical Society. (d) The colloidal stability of graphene oxide in different solvents. From left to right, the solvents are water, acetone, methanol, ethanol, 1-propanol, ethylene glycol, dimethyl sulfoxide, dimethylformamide, *N*-methyl-2-pyrrolidone, pyridine, tetrahydrofuran, dichloromethane, xylene, and hexane. Reproduced with permission from ref. 101. Copyright 2008 American Chemical Society.

$$P_{total} = P_A + P_R = -\frac{A}{12\pi}\left\{\frac{1}{d^2} + \frac{1}{(d+2\delta)^2} - \frac{2}{(d+\delta)^2}\right\} + \frac{64k_BTIN_A}{\kappa}\left\{\tanh\left(\frac{e\psi_0}{4k_BT}\right)\right\}^2 e^{-\kappa d} \quad (4)$$

where δ is the thickness of 2D materials, A is the Hamaker constant of materials, d is the average distance of 2D materials, κ^{-1} is the Debye screening length, N_A is 6.02×10^{23} mol^{-1} (Avogadro constant), ε_0 is the vacuum permittivity, ε_r is the relative permittivity of water, k_B is the Boltzmann constant, ψ_0 is the surface potential of 2D materials, and I is the ionic strength.

Despite being a simplified model of colloidal particle interaction, DLVO theory provides some important insights to understand the aggregation of 2D nanoparticles. A small Debye length κ^{-1} (the thickness of the diffuse electric double layer) often leads to a reduced repulsive potential energy which is likely to cause aggregation. For example, Chowdhury *et al.* observed that GO nanosheets tend to aggregate at a high salt concentration due to electrical double layer compression.[96] It is also intuitive that the aggregation occurs when 2D particles are processed at a high volume concentration (a small average distance d), as shown in Fig. 5a. However, there are studies showing that DLVO theory is not effective in describing colloidal nanosystems in dilute dispersions with low salt concentrations.[97,98]

In addition to the tendency to aggregate, gravitational sedimentation can also have an important effect on the colloidal stability of the ink system. According to Stokes' law, the terminal sedimentation velocity of an individual spherical particle in a fluid is a function of the particle size, the force of gravity, the viscosity of the fluid and the density difference between the particle and the fluid, as shown in eqn (5):[102]

$$U_0 = \frac{D^2\Delta\rho g}{18\mu} \quad (5)$$

where D is the diameter of the sphere, $\Delta\rho$ is the density difference between the particle and the solvent, g is the gravity constant, and μ is the solvent viscosity.

According to Stokes' law, reducing particle size and increasing solution viscosity can promote particle dispersibility, preventing rapid sedimentation due to gravity. Indeed, these sedimentation parameters have been used to develop methods for the preparation and separation of monodispersed 2D materials (Fig. 5c). For example, Sun *et al.* reported a density-gradient ultracentrifuge separation method to separate chemically modified graphene by sheet size and surface chemistry.[100] By optimizing the parameters, including the density gradient and centrifugation speed/time, graphene nanosheets with reduced polydispersity were obtained.

In addition to the particle size, the particle shape and volume fraction (ϕ) can also strongly affect the sedimentation speed. Compared with spherical nanoparticles, He *et al.*[99] found that anisotropic 2D nanosheets showed a higher resistance to

sedimentation owing to a stronger backflow of particles, as shown in Fig. 5b. There is a clear decreasing trend of the dimensionless sedimentation rate upon increasing the particle volume fraction ϕ. For batch sedimentation, backflow moves in a direction opposite to the sedimentation direction to compensate for the volume flux of settling colloidal particles. Such a hydrodynamic force from the backflow can retard the sedimentation of colloidal particles. Thus, increasing ϕ can decrease the dimensionless sedimentation speed U/U_0. These results indicated the unique advantages of 2D nanomaterials in preparing high-quality nanoinks.

Appropriate solvents are often critical to promote the colloidal stability of 2DMs. The desirable features of solvents include suitable viscosity, matched surface tension, and optimal Hansen/Hildebrand solubility parameters.[103,104] Having been used in industries such as paints and coatings, the Hansen distance (R_a, often refers to as the Hansen solubility parameter) can be expressed as follows:

$$R_a = \sqrt{(\delta_{D,A} - \delta_{D,B})^2 + (\delta_{P,A} - \delta_{P,B})^2 + (\delta_{H,A} - \delta_{H,B})^2} \quad (6)$$

where δ_D is the energy from dispersion forces of molecules A and B, δ_P is the energy from dipolar intermolecular force between molecules A and B, and δ_H is the energy from hydrogen bonds between molecules A and B.

The two molecules are likely to dissolve if R_a is a small value. Hernandez *et al.*[105] evaluated the dispersibility of graphene in 40 solvents and obtained the Hansen solubility parameters of graphene sheets. It was found that some high boiling point organic solvents showed optimal Hansen solubility parameters for graphene, such as dimethylformamide and *N*-methyl-2-pyrrolidone. The dispersion stability of GO in various solvent systems is shown in Fig. 5d.[101] Due to the hydrophilic nature of GO, several hydrophobic solvents, including dichloromethane and hexane, showed poor solubility for dispersing GO. The boiling point of solvents is another important factor. For example, screen printing prefers solvents of relatively slow evaporation rates to circumvent possible clogging of the screen mesh related to rapid drying. On the other hand, more volatile solvents, such as isopropanol (IPA), are required for high-speed processes such as gravure and flexographic printing. In the aspect of the environment, the development of good green solvents can be highly beneficial for large-scale application of printing processes.[106] It is worth mentioning that using mixtures of solvent can allow additional control on the boiling point, surface tension and solubility parameters.[107,108]

Alternatively, surfactants can be employed for electrostatic and/or steric stabilisation.[77,109,110] As shown in Fig. 6a, surfactants are amphiphilic species that have hydrophobic groups as well as hydrophilic groups. These molecules can be strongly adsorbed on the surface of 2D materials to further reduce the interfacial tension between particles and solvents, facilitating the colloidal stability of inks. The addition of surfactants commonly allows higher concentrations of 2DMs for printing applications. It has been demonstrated that ionic surfactants, such as cetyltrimethylammonium bromide (CTAB) and sodium dodecyl sulfate (SDS), can be used to prepare monolayer MoS_2 nanosheets in water.[111] The dispersions are stabilized by electrostatic repulsive force between MoS_2 nanosheets, and interestingly the sign of surface charge on nanosheets, either positive or negative, can be controlled by the choice of surfactants (Fig. 6b). A recent study also suggested that the surfactant sodium dodecyl benzene sulfonic acid sodium salt (SDBS) can not only enhance the colloidal stability of nanoparticles (*e.g.*, carbon nanotubes (CNTs)), but also improved the film adhesion through an ink aging process.[112]

Among various types of surfactants, facial amphiphiles with a quasi-flat molecular structure (*e.g.* sodium cholate (SC) and sodium deoxycholate (SDC)) are particularly effective for dispersing 2D materials.[115] When SC surfactants and 2D materials interact in water, the surfactant molecules are adsorbed onto the surface of the 2D flakes, leading to the formation of temporary charge. This can balance the aggregation forces (*e.g.*, van der Waals force) and hence facilitate dispersion or exfoliation processes.[115] The induced charge of exfoliated 2D sheets can enhance electrostatic repulsion which further prevents reaggregation.[116] Smith *et al.* systematically investigated SC in stabilizing aqueous dispersions of WS_2, $MoTe_2$, $MoSe_2$, $NbSe_2$, $TaSe_2$, and h-BN nanosheets.[113] As shown in Fig. 6c, it was found that the dispersed concentration increased monotonically with the surfactant concentration (C_{sc}), initial concentration of unexfoliated bulk materials (C_I), and sonication time (t_{sonic}). It is worth mentioning that if the surfactant concentration is above the critical micelle concentration (CMC), the excess addition of the surfactant would not continuously improve the concentration of 2DMs as the surfactant molecules will spontaneously assemble into micelles. The CMC values of surfactants can be easily determined by measuring interfacial tension with increasing surfactant concentration (Fig. 6d).[114] Below the CMC, further addition of the surfactant causes a considerable decrease in the surface tension as the surfactant molecules assemble at the solution–particle or solution–air interface. It is also worth noting that the addition of a co-surfactant, such as tetrahydrofuran and pentanol, may increase the CMC so the surfactant needs to reach a higher concentration to form micelles.[117] This co-solvent strategy could be valuable for preparing a highly concentrated 2DM dispersion, though a systematic study on the co-solvent effect and corresponding mechanism for printing processes has not been conducted so far.

In addition to surfactants, other additives (normally <5 wt%) may be used to modify or tailor specific properties of ink systems. Examples of 2D nanomaterials with the corresponding ink formulations are shown in Table 2. A recent study also demonstrated that the use of an ionic liquid electrolyte can reduce the overall fabrication cost of solar cells by avoiding one extra cell sealing step in the conventional solar cell sealing process.[118] In addition, various types of polymers have been added during ink formulation, such as sodium carboxymethylcellulose (Na-CMC), polyvinylpyrrolidone, and ethyl cellulose.[119,120] The polymers can attach onto or encapsulate 2D material flakes, and hence provide a physical separation between the flakes to allow enhanced exfoliation and stabilization.[121] Liang *et al.* demonstrated the addition of ethyl cellulose in ethanol for exfoliation and stabilization of graphene

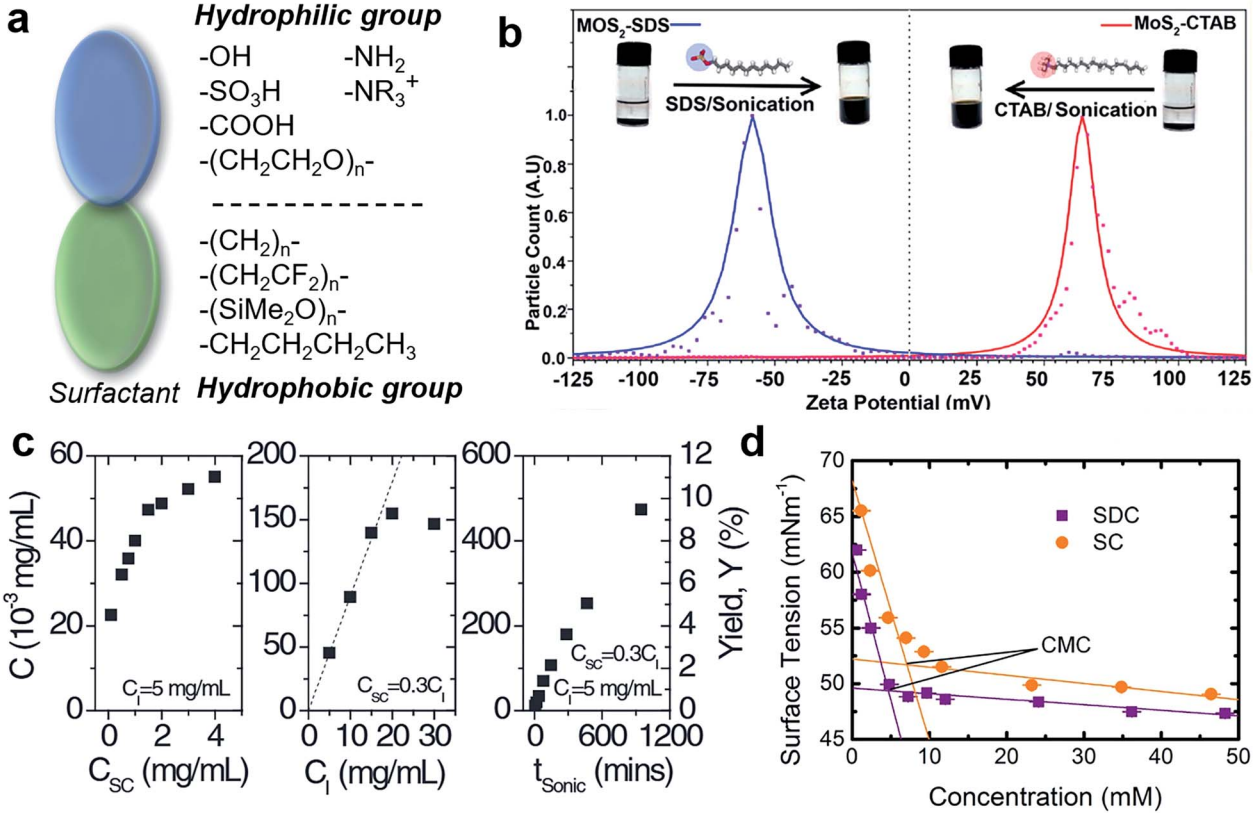

Fig. 6 (a) Schematic illustration of examples of hydrophilic and hydrophobic groups of surfactants. (b) Electrostatic stabilization of MoS_2 in water by cationic (cetyltrimethylammonium bromide, CTAB) or anionic surfactants (sodium dodecyl sulfate, SDS). Reproduced with permission from ref. 111. Copyright 2015 American Chemical Society. (c) The dispersed particle concentration C increases monotonically with the concentration of surfactant sodium cholate (C_{sc}), initial concentration of unexfoliated bulk materials (C_i), and sonication time (t_{sonic}). Reproduced with permission from ref. 113. Copyright 2011 Wiley-VCH. (d) The surface tension of sodium cholate (SC) and sodium deoxycholate (SDC) solutions decreases with surfactant concentration until reaching the critical micelle concentration (CMC). Reproduced with permission from ref. 114. Copyright 2016 Wiley-VCH.

flakes using this strategy.[122] The authors suggested that the ethyl cellulose worked as a colloidal stabilizer and prevented the graphene flakes from aggregation.[122] Additives may also be selected to modify certain functionalities. For instance, defoaming agents (*e.g.* short-chain alcohols) may be used to suppress undesired bubble formation during the printing of aqueous inks. Alkalis can be added into inks to carefully adjust the pH value to improve the solubility of polymer binders (*e.g.*, ethyl cellulose). In fact, the binders can be either polymers (*e.g.*, cellulose and its derivatives) or inorganic precursors (*e.g.*, chalcogenidometallate).[21,123] Binders can form an integral part of formulated inks, connecting the nanomaterials to each other

Table 2 Examples of 2D nanomaterials with the corresponding ink formulations and printed device applications. *The ink formulation includes the main solvents and applicable additives in parentheses

	Synthesis	Ink formulation*	Printed device applications
MoS_2	Liquid exfoliation	Terpineol/ethanol (ethyl cellulose)	Inkjet inks for FETs[124]
WS_2	Liquid exfoliation	Propylene glycol/water (Triton X-100)	Inkjet inks for photodetectors[125]
SnS_2	Liquid exfoliation	Ethanol	Inkjet inks for gas sensors[126]
Black phosphorus	Liquid exfoliation	Acetonitrile	Inkjet inks for humidity sensors[127]
MXene	Selective etching	Water	Direct ink writing for supercapacitors[128]
$Bi_2Te_{2.8}Se_{0.2}$	Solvothermal	Terpineol (Disperbyk-110)	Screen-printing inks for thermoelectrics[129]
$Bi_2Te_{2.7}Se_{0.3}$	Solvothermal	Ethanol/glycol/glycerol	Aerosol jet inks for thermoelectrics[130]
h-Boron nitride	Liquid exfoliation	Water (Na-CMC)	Inkjet inks for dielectrics[131]
Gr	Liquid exfoliation	IPA (PVP)	Inkjet inks for humidity sensors[132]
Gr	Commercial Gr	Water/IPA (Na-CMC)	Flexographic inks for solar cells[133]
Gr	Liquid exfoliation	Terpineol/ethanol (ethyl cellulose)	Gravure inks for conductive devices[134]
Gr	Commercial Gr	Ethanol (PANI)	Screen printing inks for supercapacitors[135]
GO	Hummers' method	Water	Direct ink writing for batteries[136]
rGO	Hummers' method, $NaBH_4$	Water/ethanol	Gravure printing inks for functional substrates[137]

and/or to the substrate. Such a binding process can occur by simply drying and solidifying during solvent evaporation, while sometimes curing processes (*e.g.* thermal annealing or exposure to UV light) are required in order to form cross-linked structures. The appropriate choice of binders can improve certain properties and performance of printed devices, such as mechanical strength or stability/durability against hazardous conditions. For example, hydrophobic polymers can promote the resistance of printed composites to moisture.[21]

3.2. Ink rheology of 2D nanomaterials

The rheological properties of nanomaterial-based inks (*e.g.* viscosity and elasticity) can significantly affect their printing consistency and performance. The viscosity of inks describes the resistance to flow at a certain shear due to internal friction and is defined as the ratio of shear stress to shear rate.[138] Ink viscosity is a crucial factor for most printing techniques. For example, inkjet printing generally requires low viscosity of 2D material dispersion, whereas viscous yet fluent inks are preferred for screen printing. Fig. 7a shows the common range of viscosities for 2D and 3D printing of 2DMs. A higher viscosity means that the fluid is more difficult to flow and is more resistant to stress. A typical fluid can be categorized into Newtonian fluids or non-Newtonian fluids. A Newtonian fluid is a fluid with a linear shear stress/shear rate relationship, *i.e.* a constant viscosity. However, the dispersion of 2D materials commonly shows reduced shear stress at an increased shear rate, which is known as shear thinning. Yang *et al.*[139] investigated the shear-induced properties of aqueous dispersions of GO nanosheets. As shown in Fig. 7b, the authors found strong shear-thinning behaviour of GO which showed a yield stress for all concentrations. Holmqvist *et al.* reported that 2D gibbsite suspensions showed the same shear-thinning behavior.[140] Such an effect of 2D materials is caused by the alignment of ordered structures along the shear direction. These shear-thinning fluids were also termed pseudoplastic fluids, enabling the ink to flow with a less resistance force at higher shear rates. The pseudoplastic behaviour is important for ink formulation, as in this case the ink particles are more

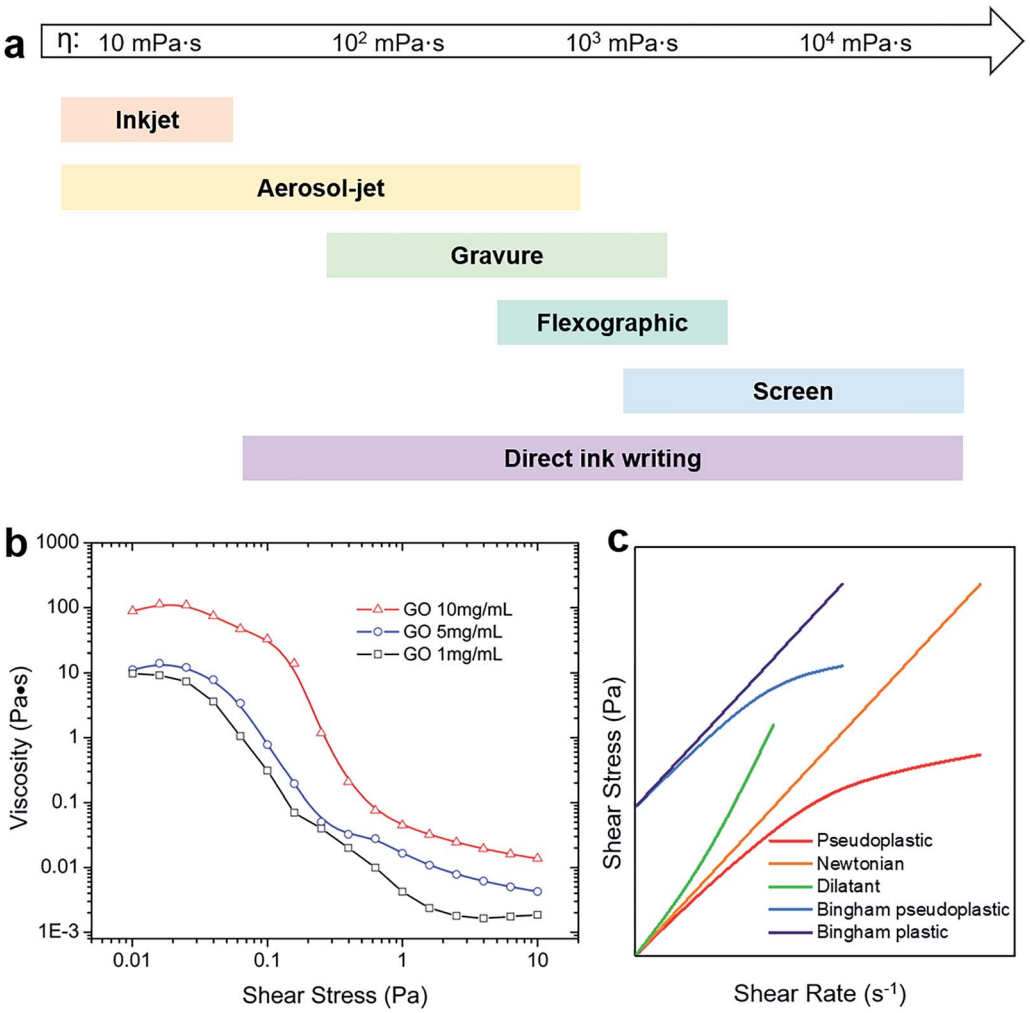

Fig. 7 (a) Typical viscosity range of functional inks for different printing technologies. (b) Shear thinning behaviour of GO nanosheets. Reproduced with permission from ref. 139. Copyright 2013 American Chemical Society. (c) Newtonian and non-Newtonian fluids with shear stress as a function of shear rate.

readily dispersed under stress due to better shear-driven mixing. For example, the pseudoplastic nature allows the ink to smoothly flow during the printing process by transferring from component to component and from roll to roll (high shear rate), but is prevented from overspreading once printed onto substrates (low shear rate).[141] For 3D printing of polymers, shear thinning limits the entanglement of polymer chains, allowing smooth extrusion of viscous inks, such as biological hydrogels, through a nozzle. Owing to these benefits, many researchers have tried to enhance the shear thinning properties of bioinks.[142]

As opposed to pseudoplastic fluids, a dilatant fluid shows increased viscosity under shear. A dilatant fluid is usually a highly concentrated suspension in a colloidal form. On the other hand, Bingham fluids exhibit yield stress, so the fluids need to overcome this finite stress to flow. A Bingham fluid may behave as a Bingham plastic for which the viscosity is constant upon stress, or a Bingham pseudoplastic for which the viscosity decreases under stress. The rheology behaviors of these non-Newtonian fluids are summarized in Fig. 7c.

3.3. Ink drying and particle assembly

The interaction of ink droplets on the substrate after deposition is another essential step during printing. Depending on the droplet velocity and material properties, the droplet may splash or keep its shape after deposition. The spreading of ink over a solid surface is determined by the wettability of substrates toward inks.[143] In general, a good wetting of ink on the substrate results in a small contact angle ($\ll 90^\circ$), while a large contact angle ($\gg 90^\circ$) indicates a poor wetting (Fig. 8a). For instance, a contact angle of 0° indicates superwetting and spreading, while 180° indicates a perfect non-wetting case. A good wetting means that the ink is capable of spreading over and maintaining contact with the solid surface for a continuous feature, in which the interfacial tension between the substrate and inks is much smaller than that of the substrate and air or that of the ink and air. Therefore, for aqueous inks, hydrophilic substrates (*e.g.* glass) with low interfacial energies for water are easy to wet, while hydrophobic polymers (*e.g.* polytetrafluoroethylene) are relatively difficult to wet.[22,144] In the case of poor wetting, the printed ink tends to retract and bead up due to the high interfacial tension, leading to a discontinuous material deposition. To change the wetting of substrates, several strategies including surface modification, polymer coating, and plasma etching have been developed.[22,28,145–147] For example, to address the poor wetting of PDMS, Trantidou *et al.* proposed a two-step method of the deposition of polyvinyl alcohol after a plasma treatment.[148] PDMS with a hydrophilic surface was achieved and remained stable in air for 9 days (Fig. 8b).

Although good wetting and spreading can improve the continuity of printed films, the over spreading of inks on substrates tends to increase drop size, which limits the printing resolution for most nozzle-based printing processes.[150,151] To overcome this challenge, several strategies based on surface modification of substrates have been developed. For example, Sirringhaus *et al.* demonstrated that the surface patterning of substrates can greatly improve the printing resolution of inkjet-printed polymer transistors.[152] Alteration of the surface charge can enhance the printing resolution.[153] The surface alteration can be used for printing dots or lines on 2D substrates. Also, an appropriate amount of drop overlap is beneficial and interaction between the droplets can be an important factor for precisely printing micro-lines of different sizes. For inkjet

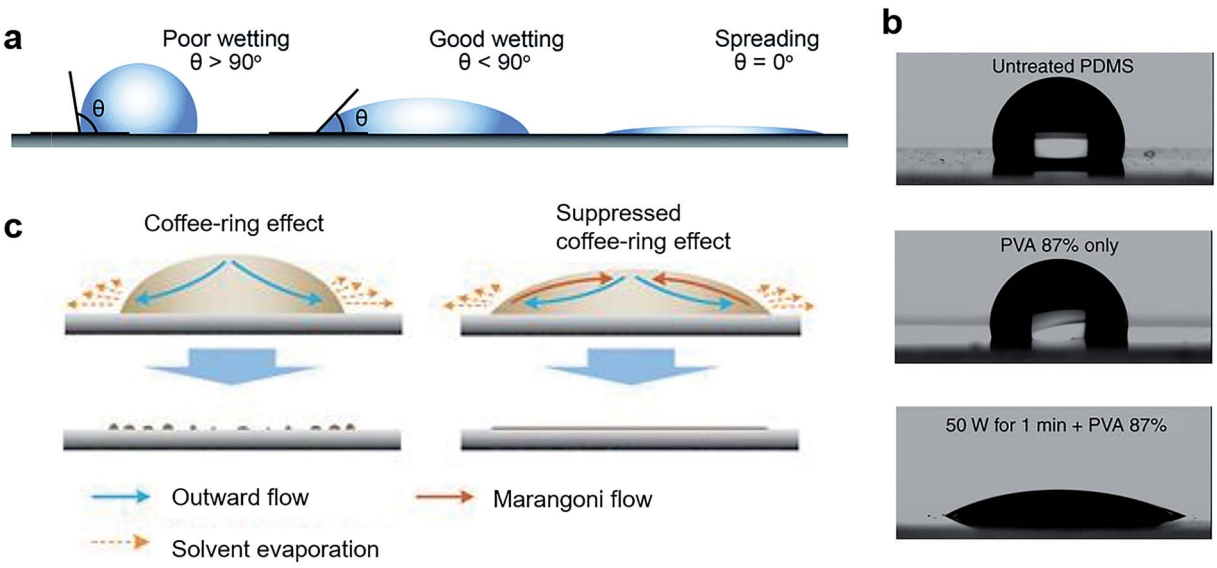

Fig. 8 (a) The ink–substrate interaction showing poor wetting (left), good wetting (middle), and spreading behaviour (right). Reproduced with permission from ref. 21. Copyright 2018 Royal Society of Chemistry. (b) An example of surface modification of PDMS. The plasma etching followed by PVA treatment allows for hydrophilic coating of PDMS for a long period of time. Reprinted with permission from Springer Nature.[148] Copyright 2017 Nature Publishing Group. (c) Coffee ring effect (left) and suppressed coffee-ring effect (right) by Marangoni flow. Reprinted with permission from Springer Nature.[149] Copyright 2017 Nature Publishing Group.

printing of biomaterials (such as tissue), the interfacial energy is vital for drop interactions, and printed bio-inks should be stable enough to keep their shape prior to solidification.[154] For nozzle-based 3D printing, surface modification methods may not be feasible as ink droplets are collected on top of each other, making interactions between drops even more significant than generating 2D structures with droplet overlap.[151,155]

During ink drying, the coffee ring effect is a common and unwanted phenomenon.[156] Such an effect can be attributed to non-uniform solvent evaporation across the droplet during the ink drying process. Fig. 8c shows a droplet deposited onto a substrate, where the evaporation of the solvent occurs.[149] During drying processes, the solvent evaporation speed is typically highest at the edge of printed drops due to the highest surface area to volume ratio. Such uneven evaporation of the solvent results in an outward convection flow that moves from the droplet centre to the edges to replenish the evaporated solvents.[156] During the outward flow, the dispersed nanomaterials are carried and deposited at the droplet edges, leaving little to no material at the droplet centre. To mitigate the coffee-ring effect, significant efforts have been made. For example, Song's group reported a kinetics-controlled deposition mechanism to overcome the coffee-ring effect.[157] It was found that higher temperature enabled a surface capture effect and thus uniform particle deposition. In addition to elevated temperature, introducing a co-solvent with a different boiling point can also help reduce the coffee-ring effect. In preparation of BP-based inks, Hu *et al.* included 10 vol% 2-butanol (boiling point 100 °C) to induce a recirculating Marangoni flow that compensates for the strong capillary outflow.[149] Therefore, a reduced coffee-ring effect was observed and an improved printing resolution was achieved.

Overall, considering the rapid development of printing processes and vast chemical diversity of 2D materials, much more research will be needed to realize molecular-level understanding and control of the colloidal behavior of 2DMs in inks that would benefit the design of printing processes.

4. Printing strategies

The use of printing originates from ancient China where replaceable/moveable wooden or ceramic letterpress was used for letter reproduction. Nowadays, the ability of printing for efficient conversion of materials into devices has been considered as one of the most promising solutions for rapid prototyping and advanced manufacturing. In the past few decades, a large number of new printing strategies based on nanomaterials, including metals, semiconductors, and insulators have emerged for a wide variety of applications.[20,158] Based on the dimensionality of printing processes, additive printing of nanomaterials can be mainly categorised into three types: 2D printing, 3D printing, and 4D printing. Several factors, such as printing mechanisms, dispensing pressure, printing speed, nozzle diameter, and stage temperature, are crucial for successful printing of 2D materials. In this section, we will discuss the printing strategies of colloidal nanomaterials (particularly 2DMs) and critically evaluate their performances in these three kinds of printing processes. Some common examples of 2D printing, 3D printing, and 4D printing methods and their features and applications are shown in Table 3.

4.1. 2D printing

Template-based and nozzle-based printing are probably two most studied methodologies for 2D printing of 2DMs. As examples of nozzle-based printing, inkjet printing and aerosol jet printing are non-contact, high-resolution, mask-less patterning technologies, while common template-based printing including gravure printing, flexographic printing, and screen printing is particularly advantageous in low-cost and large-scale manufacturing.

Inkjet printing techniques are regarded as a versatile manufacturing tool *via* pushing the ink to form discrete droplets from a nozzle. As shown in Fig. 9a, a thermal inkjet printer uses a thin-film heater to heat a thin layer of fluid, producing a vapor bubble in a few microseconds, which ejects a liquid drop.[172] During printing, the initial actuation pressure of thermal inkjet printer is close to the saturated vapor pressure of the solvent at the superheat limit.[173] The piezoelectric inkjet printing process is another popular type of inkjet printing, which is based on the mechanical force of piezoelectric units to create pulses for droplet formation.[174] Nozzles of inkjet printing have a typical size of 10–30 μm in diameter, while droplet volume is normally in the range of 1–20 pL.

To ensure smooth inkjet printing of colloidal nanoparticles, the size of 2DMs should not be more than 2% of the nozzle diameter to avoid nozzle clogging.[176] For example, small-sized WS_2 and h-BN particles can be directly used for inkjet printing in a low-cost and scalable manner.[165] In addition to particle size, inkjet printing requires relatively low ink viscosity (normally <50 mPa s), which limits the types of polymer additives for ink formulation.[177,178] One common option is ethyl cellulose which can behave as a colloidal stabilizer for 2D sheets.[177] The polymeric binders may be removed by thermal sintering or photonic sintering.[177,179] These post-printing treatments, although very effective, may lead to additional cost, and more importantly, can limit the choices of substrates due to the temperature intolerance.

The aerosol jet printing uses the aerodynamic focusing of aerosolized droplets to reliably transfer inks to surfaces.[180] This approach starts with aerosolizing inks using sonication force or shear pressure, forming aerosolized droplets with a size of 2–5 microns (Fig. 9a). Then, nitrogen was used as the carrier gas to transport the aerosol cloud to a printhead, where a co-flowing sheath gas focuses the droplets to a 10–100 μm-diameter jet with a velocity of ~80 m s^{-1}. One striking advantage of aerosol jet printing lies in its flexibility, as it can tolerate a wide viscosity range from 1 mPa s to around 1000 mPa s, far beyond the range of conventional inkjet printing systems (5–50 mPa s). Aerosol jet printing techniques have emerged as a powerful tool in electronics manufacturing.[181] To date, a variety of materials, including nanoparticles, polymers, and biomaterials, have been printed by aerosol jet printing onto various substrates such as glass, polyimide, silicon, and PDMS.[181–185] It is worth noting that

Table 3 Common examples of colloidal ink printing methods, their printing dimensionality, capabilities and features, and application examples. *The viscosity data are collected from ref. 20–22 and 158–171. **The viscosity of the ink filament for fused deposition modelling (FDM) is highly dependent on the fusing temperature and the nature of filament polymers.[159] ***The direct ink writing (DIW) method also includes micro-extrusion-based bioprinting, with higher-viscosity inks for constructing structural materials and lower-viscosity inks to provide a suitable environment for maintaining cell viability and function[158]

Printing methods	Dimensionality	Capabilities & features	Ink viscosity* (mPa s)	Application examples
Screen	2D	Tolerate high viscosity, high particle load	1000–10 000	Flexible electronics,[160] electrocatalysis[161]
Flexographic	2D	Good uniformity and low production cost	1000–2000	Solar cells[133]
Gravure	2D	High throughput, thickness control	100–1000	Acetone sensor,[162] conductive pattern[134]
Aerosol jet	2D/3D	High resolution, expanded material types	1–1000	Thermoelectrics,[130,163] stretchable interconnects[164]
Inkjet	2D/3D/4D	High accuracy and uniformity, good spatial resolution	1–50	FETs,[165] photodetector,[125] strain probe,[166] all-solid-state supercapacitor,[167] shape-changing soft actuators[168]
FDM	3D/4D	Good for polymer–particle composites	10^5–10^7**	Flexible circuits,[169] shape memory composite[170]
DIW	3D/4D	Easy to print, low cost	30–10^7***	Lithium ion batteries,[136] soft robotics[171]

the aerosol jet print head can work relatively far from the substrates so aerosol jet printing is capable of printing on a curved surface. With appropriate design of the printing model and precise modulation of printing parameters, the conformal printing of nanomaterials on 3D curved substrates can be readily achieved with reliable quality.

Screen printing is a template-based process whereby ink is transferred onto the substrate through a stencil screen made of a fine, porous mesh of fabric, silk, synthetic fibres or metal threads. As shown in Fig. 9b, the pores of the mesh are selectively blocked (typically using photo-polymerised resins) in the non-printing areas, whereas the remaining pores are kept

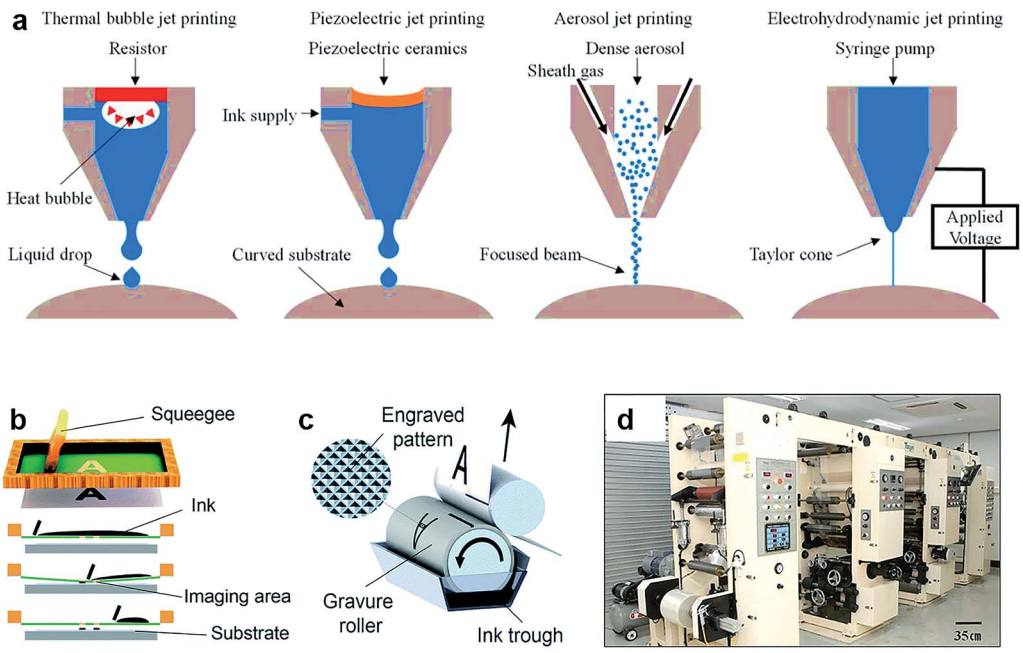

Fig. 9 (a) Schematic illustration of various nozzle-based printing technologies. Reproduced with permission from ref. 172. Copyright 2019 the Royal Society of Chemistry. (b) Schematic illustration of screen printing of inks on substrates. (c) Schematic figure showing the working principles of gravure printing. Reproduced with permission from ref. 21. Copyright 2018 the Royal Society of Chemistry. (d) Photo of a commercial gravure printer for printing electrodes on plastic foil. Reproduced with permission from IEEE.[175] Copyright 2010 IEEE.

exposed to allow ink to flow through.[186] Screen-printing ink formulations typically include polymeric binders due to the requirement of high ink viscosities. Several polymer binders show satisfactory performances for screen printing applications, including ethyl cellulose, polyaniline (PANI),[187] and PVP/polyvinyl alcohol (PVA).[160] Screen printing of 2D nanomaterials has recently attracted attention due to the ability to process a high concentration of 2DMs. For example, Zhang *et al.* developed a rGO-based ink using ethyl cellulose as the polymer binder.[188] Owing to the good conductivity of 2D rGO, such a 2DM-based ink was used to fabricate counter electrodes for dye-sensitized solar cells.[188] However, high-temperature annealing was required to effectively remove organic binders from the rGO composite, which undermined the attachment of rGO on substrates. Although graphene has typically been the most studied 2D nanomaterial, other 2DMs, such as MoS_2 (ref. 161) and h-BN,[189] have also been reported recently.

As a large-scale commercial technology, high-speed roll-to-roll (R2R) printing (*e.g.*, gravure and flexographic) has been extensively used to fabricate labels, smart packaging, and organic light-emitting diode.[190,191] For R2R gravure printing (Fig. 9c), a predesigned pattern is first scratched on plastic/metal cylinders that are then used to print the pattern on substrates. Such a procedure may be repeated several times to print multiple layers of functional inks which is important for high-throughput continuous operation (Fig. 9d).[175] In 2014, Secor *et al.* reported a gravure printing process of graphene for the fabrication of conductive patterns.[134] The graphene was prepared by liquid phase exfoliation (LPE) and then transferred into a terpineol/ethanol system during ink formulation, in which ethyl cellulose was used to adjust ink properties for smooth gravure printing.[134] To ensure high-resolution gravure printing, it was found that the small platelet size of the LPE graphene (~50 nm in diameter with an average thickness of ~2 nm) was beneficial. It was demonstrated that a high-resolution (~30 μm) patterning of graphene on Kapton was obtained, leading to the formation of electrically conductive stripes.[134] Compared with gravure printing, flexographic printing requires a slightly more complex ink transfer process. To form graphic patterns, soft and flexible relief printing plates are mounted onto a plate cylinder. Ink is first applied to the surface of a screened anilox roller, which is rolled through an ink trough to fill the cells with ink. Unlike gravure printing, the cells of the anilox roller are not the graphic-forming part and are used primarily for determining the amount of ink to ensure continuous patterns. Baker *et al.* demonstrated the flexographic printing of graphene in 2014.[133] A graphene/sodium carboxymethylcellulose ink was first formulated in water/IPA solutions, and then printed on indium tin oxide (ITO) glass to prepare counter electrodes for photovoltaics. The graphene/polymer binder ratio was controlled to suit flexographic printing.[133]

The various types of 2D printing techniques offer a straightforward, flexible, and cost-effective solution for the fast fabrication of functional devices with satisfactory resolution. Owing to the continuous operation and high printing efficiency, 2D flexographic printing and gravure printing have shown tremendous potential for large-scale manufacturing of electronic circuits and sensors. However, the printing of bulk 3D devices using conventional 2D printing techniques remains a challenge.

4.2. 3D printing

Since its conception in the 1980s, three-dimensional printing has attracted unprecedented levels of interest from the academic community as well as industry, leading to inestimable possibilities for fast prototyping. The 3D printing begins with the formation of a virtual model, followed by the deposition/polymerization of ink materials, and post-treatment of the printed objects. 3D-printing technologies are commonly grouped into the following major categories:[4] (1) material jetting (*e.g.* inkjet printing), (2) extrusion/micro-extrusion (*e.g.* direct ink writing), (3) photopolymerization, (4) powder-bed fusion, and (5) lamination. Herein, we will only discuss the most commonly used methods for additive 3D printing of colloidal 2D materials, which are (1) and (2). A comprehensive review of 3D printing can be found in other recent literature.[7,151]

Direct ink writing (DIW) and inkjet printing are arguably two most prevalent strategies for 3D printing of colloidal nanoparticles because of their straightforward procedure, cost effectiveness, flexible choice of materials, and ability to construct highly sophisticated 3D structures without additional masking requirements.[5] After being extruded under an external pressure (Fig. 10a) or ejected in the form of droplets by nozzles (Fig. 10b), the inks solidify to form 3D objects either through gelation, phase transition, or simply solvent evaporation.[20] The printing resolution of direct ink writing is normally determined by the size of printing nozzles, and various predesigned substrates may be used during DIW, such as hemispherical antennas (Fig. 10c), suggesting its broad utility in electronics and optoelectronics.[192,193] One striking feature of DIW is the flexibility of printable ink options that include not only shear-thinning nanoparticle dispersions, but also exceedingly viscous hydrogels. Such an advantage of DIW allows for an unrivalled freedom of material choices and preparation of suitable inks.[158,194,195] The viscoelastic properties of certain inks have enabled self-supporting structures, such as 3D butterfly design (Fig. 10d).[194] As early as 2015, García-Tuñon *et al.*[196] formulated GO inks that possessed a good elastic shear modulus to construct self-supporting 3D structures *via* DIW (Fig. 10e). After drying and thermal reduction, an ultra-light graphene device was obtained with elastomeric behavior and decent conductivity.

Fused deposition modelling (FDM) is another popular 3D-printing technique that has been commercialized for years.[198] FDM is capable of layer-by-layer constructing complex three-dimensional structures by extruding liquefied plastic or metal filaments, while a nozzle moves along the x, *y*, and *z* axes. After extrusion from the nozzle and landing onto the substrate, solidification of inks occurs, which relies on the temperature-induced phase transition of polymers. Despite relatively low resolution and precision, the FDM method still has several advantages including easy operation and low operating costs.[199] Among various types of polymer filaments, poly(lactic acid)

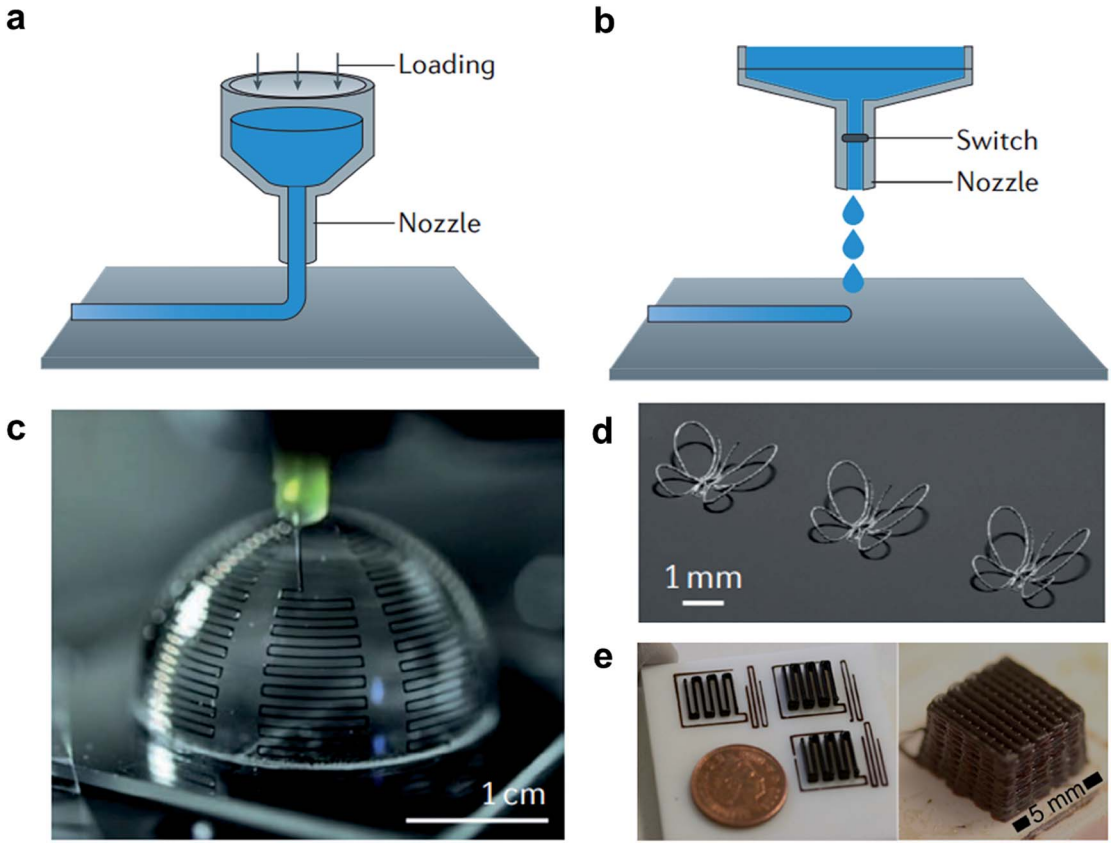

Fig. 10 (a) Schematic illustration showing the working principle of extrusion-based 3D printing. (b) Schematic of jetting-based 3D printing. Reprinted with permission from Springer Nature.[197] Copyright 2017 Nature Publishing Group. (c) Photo of a printed antenna on a hemispherical surface. Reproduced with permission from ref. 193. Copyright 2011 Wiley-VCH. (d) Self-supported structures by 3D printing. Reprinted with permission from ref. 194. Copyright 2016 National Academy of Sciences. (e) Optical images of 3D printed graphene devices. Reproduced with permission from ref. 196. Copyright 2015 Wiley-VCH.

(PLA) and acrylonitrile–butadiene–styrene (ABS) are the two popular choices for FDM. To date, FDM printing of nanocomposites including ABS/graphene,[200] PLA/graphene,[201] and PLA/LFP/carbon[202] has been reported. In the preparation of filaments of PLA/graphene, rGO and polylactic acid were blended at elevated temperature to form composite powders.[169] After the FDM printing, the obtained 2D and 3D flexible circuits showed good mechanical performance. However, it is worth noting that a high content of PLA (94 wt%) may lower the electrical conductivity (476 S m^{-1}), whereas increasing the concentration of rGO or post-treatment (such as thermal sintering) may mitigate this issue.

As discussed previously, inkjet and aerosol-jet printing are non-contact fabrication techniques that were originally developed for 2D printing. However, these two printing techniques can be redesigned for 3D printing purposes. Owing to their drop-on-demand characteristics, inkjet printing and aerosol jet printing are promising solutions toward rapid and economical deposition of inks on various substrates according to predesigned patterns.[203] In 2017, Panat's group demonstrated highly intricate microscale 3D networks based on aerosol jet printing techniques.[164] Without using any supporting materials, sophisticated nanoarchitectures with nearly fully dense truss elements, including microscaffolds as well as microlattices, were realized. In the past decade, inkjet printing of 3D graphene aerogels or hydrogels has attracted enormous interest and achieved some progress.[204] For instance, Chi *et al.* reported an inkjet printable graphene/polyaniline (Gr–PANI) composite ink that was prepared by ball milling and ultrasonication.[167] Such a 2DM-based ink was printed on freestanding graphene paper to form a three-dimensional hybrid electrode. With good mechanical flexibility, the printed Gr–PANI and gel electrolyte created an all-solid-state symmetric supercapacitor that showed a decent energy density as well as high cycling durability.

Although various types of 2D nanomaterials have been successfully printed in the past decade, the 3D printing of 2DMs has mainly focused on extrusion-based processes (*e.g.* direct ink writing and fused deposition modelling). Innovative printing approaches are highly desirable to expand the scope of printable 3D devices and to make full use of 2DM functionalities, which may lead to the development of intelligent structures that are multifunctional, adaptive, and programmable.

4.3. 4D printing

The ability of some 3D fabricated materials to evolve into a predefined shape, pattern, and structures over time has given

rise to a new term called "4D printing".[205] However, not all 3D printing technologies that generate active components such as printed flexible hinges are regarded as 4D printing as they do not exhibit 'smart' behaviour such as self-folding, self-actuating and shape changing.[206] It has been suggested that some of the distinguishing features of 4D printing involve fabricating a physical object using suitable additive manufacturing techniques, and laying down successive layers of stimuli-responsive materials with varying properties.[207] After the printing process, the object responses to stimuli from the natural environment or through human intervention, leading to a physical/chemical change of state over time. The 4D printing with shape-morphing features has been considered as a powerful paradigm for designing and fabricating multi-functional hierarchical structures.[208]

In the past few years, several research fields have emerged, including shape memory alloys (SMAs),[212] self-evolving structures,[213] soft actuators/robotics,[168,214] active origami, and controlled sequential folding.[215] For example, 4D printing of a hydrogel was demonstrated based on the swelling ability of a composite ink coupled with anisotropic design of printing patterns (Fig. 11a).[197,209] The anisotropic swelling properties of different filament layers induced a controlled deformation and curvature of printed hydrogels. Reversible changes in 3D shapes are feasible with deswelling using external stimuli, such as heat. As shown in Fig. 11b, several key factors including printed patterns, swelling ratios, and elastic moduli can be used to tailor the final structural and properties of 4D-printed products. Theoretical mechanics models that expand the classical Timoshenko theory can be useful guidelines for predicting and developing new 4D-printed devices.[216] In addition, hydrogels are able to be laminated against passive materials for producing a self-evolving joint capable of twisting, curling, and folding upon swelling.[205,213]

Owing to the atomically thin structure and ultralow bending stiffness of 2D materials, many of these 2DMs have huge

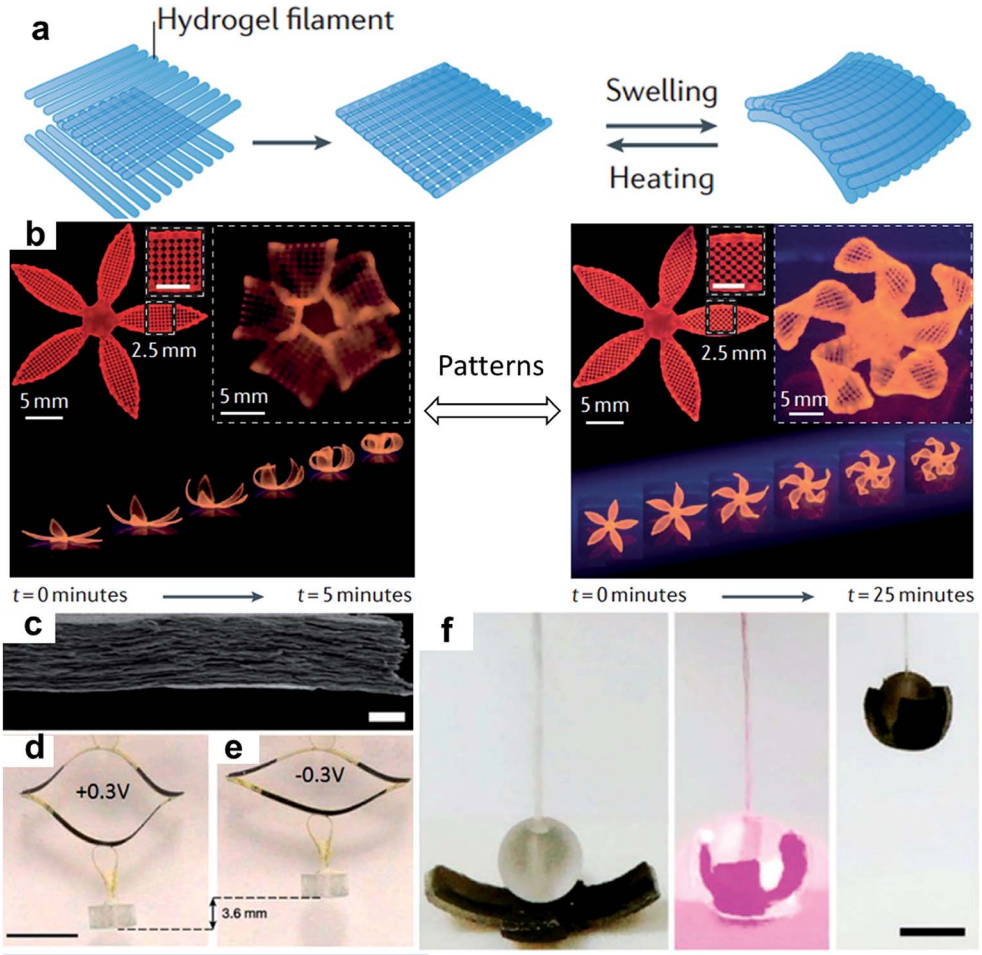

Fig. 11 (a) Schematic showing the working principle of 4D printing of a hydrogel. Upon swelling, the shape of the printed hydrogel tends to deform to enable additional control of the final structure. (b) Two hydrogel patterns with flower geometries and different petal patterns. Reprinted with permission from Springer Nature.[197,209] Copyright 2016 & 2017 Nature Publishing Group. (c–e) Dynamic expansion and contraction of a MoS_2 electrode. Scale bars of (c) and (d) are 2 μm and 1 cm, respectively. Reprinted with permission from Springer Nature.[210] Copyright 2017 Nature Publishing Group. (f) Photos of MoS_2 composite hydrogels showing shape deformation and self-wrapping motions under remote control of light or heat. Scale bar is 1 cm. Reprinted with permission from ref. 211. Copyright 2016 the Royal Society of Chemistry.

potential for fabricating stimuli-responsive materials, which are the key components for successful 4D printing.[217] Acerce *et al.* showed that the dynamic expansion and contraction of electrode films prepared by restacking exfoliated metallic MoS_2 nanosheets can produce considerable mechanical forces (Fig. 11c–e).[210] MoS_2 electrode films can lift masses that are more than 150 times that of the electrode on the scale of ~cm. Such actuation of MoS_2 films can be attributed to the suitable elastic modulus and good conductivity of the metallic 1T phase. In addition to voltage response, Lei *et al.* reported a MoS_2 composite hydrogel that showed anisotropic actuation with thermo- and photo-responses. In this composite hydrogel, MoS_2 worked as a photothermal transduction component, allowing for remote control of hydrogel actuators (Fig. 11f).[211] The structural deformation and self-wrapping actions of the hydrogels were demonstrated using light or heat as an external stimulus.

Duncan *et al.*[218] established self-folding of pre-strained polymer films by microwaves (Fig. 12a). Printed graphene composite films absorbed and converted microwave energy into heat which causes the polymer to shrink and fold. The dihedral angle is directly proportional to the hinge width printed on the polymer sheet and it is possible to self-fold all the way to 180°. As shown in Fig. 12b, Yang *et al.*[219] showed the transformation of robotic materials from a GO/cellulose template into various soft metal oxide (MO) composites. Metalized GO glue enabled the fabrication of complex MO origami and origami assemblies. After thermal treatment to remove the template (Fig. 12c), the reproduced MO origami were further stabilized with thin elastomers, forming composite origami that can be used as functional backbones of soft robotics. The functionalities of MO backbones can be thoroughly controlled by introducing different metal precursors into the GO/cellulose template. Despite these advances, 4D printing of 2D nanomaterials remains an underexplored avenue for the fabrication of multifunctional, programmable, and smart structures/devices.

5. Device applications of printed 2D nanomaterials

Although significant development of 2DM-based devices has been seen in the past decade, device applications based on additive manufacturing of 2D nanomaterials are only beginning to emerge. This section provides a snapshot of some representative device applications based on 2DM printing, with an emphasis on energy and sensing devices.

5.1. Energy conversion and storage

The generation/storage of electric energy from sustainable sources, such as waste heat, wind and sun light, is one of the pressing challenges for modern society in the 21st century.[220,221] A great number of energy technologies are emerging as possible solutions for bridging the gaps between global energy supply and demand. Here, thermoelectrics, supercapacitors, batteries, and solar cells are used as a few representative examples to illustrate potential energy applications of additive printing using 2DMs.

5.1.1. Thermoelectrics. When it comes to global energy consumption and supply, sustainable energy is one of the most crucial sources for securing long-term electricity supply. Thermoelectric (TE) materials have attracted huge attention due to their ability to convert waste heat to electric energy.[222–226] Printing techniques that rapidly transform thermoelectric inks into TE devices with predesigned shapes have great potential to accelerate the practical applications of TE technology.[227,228] Up

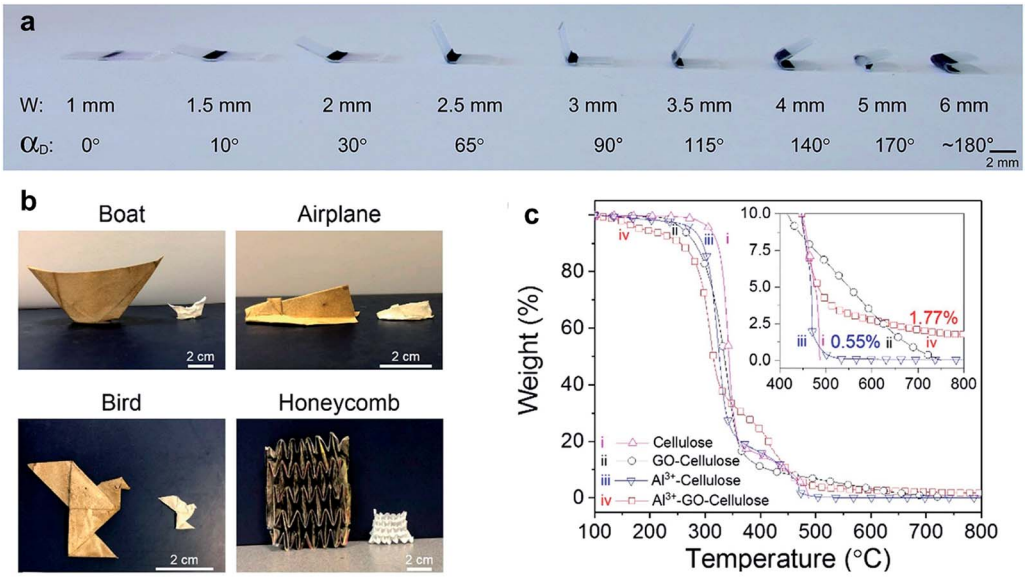

Fig. 12 (a) 4D-printed self-folding graphene composite induced by microwaves. Reproduced with permission from ref. 218. Copyright 2015 the Royal Society of Chemistry. (b) Photographic images of various reconfigurable origami enabled by GO-template inks. (c) The removal of the GO template using heat. Reproduced with permission from ref. 219. Copyright 2019 American Chemical Society.

to now, a great variety of TE materials ranging from inorganic nanoparticles (such as Bi_2Te_3, Sb_2Te_3, $Bi_{0.5}Sb_{1.5}Te_3$, $Bi_2Te_{2.7}Se_{0.3}$, PbTe, $Ca_3Co_4O_9$, *etc.*) to organic polymers (such as poly(3,4-ethylenedioxythiophene) polystyrene sulfonate) have been successfully integrated in printing techniques.[130,229–232] As printable 2D nanomaterials, few-layer graphene has been reported in inkjet printing processes for fabricating flexible thermoelectric thin films (Fig. 13a–c).[233] The printed graphene films exhibit electrical transport akin to that of few-layer graphene, and glassy thermal transport originated from disordered nanostructures. The thermoelectric power factor of the printed films is determined to be 18.7 ± 3.3 μW m^{-1} K^{-2}. Such inkjet-printed thermoelectric devices confirmed the feasibility of low-cost thermoelectric applications, allowing for the harvest of electric energy from body heat in wearable applications.

In addition to graphene, additive printing of other 2D nanomaterials has been reported. For example, Zhang's group demonstrated high-performance flexible films and devices by screen printing bismuth telluride based nanoplate inks synthesized using a microwave-stimulated wet-chemical method (Fig. 13d).[129] The films showed an unprecedented peak *ZT* of 0.43 at 175 °C and superior flexibility with negligible changes of electrical conductivity after 150 bending cycles. A flexible thermoelectric device fabricated using the printed films produces a high-power density of 4.1 mW cm^{-2} under a temperature difference of 60 °C. A high-performance PbTe based flexible film was also demonstrated by Zhang's group by scalable and low-cost printing, with a conservative estimate of *ZT* above 1 at 350 °C.[234] These high-performance and flexible thermoelectric devices present an important step to make thermoelectrics a viable technology for a broad range of applications.

Although significant efforts have been made in printable TE materials, the large-scale applications of printed TE devices remain a challenge due to two main reasons: (1) the electrical conductivity of printed TE materials is often lower than that of their single-crystalline bulk counterparts, leading to unsatisfactory output power and low figure-of-merit *ZT* values; (2) conformal printing of TE devices on different shapes that can fit the geometries of heat sources, such as hot pipelines, remains difficult. To address these issues, Kim *et al.* proposed a extrusion-based 3D-printing approach to fabricate thermoelectric materials with geometries suitable for heat sources.[123] Bi_2Te_3-based TE materials were integrated with inorganic binders using Sb_2Te_3 chalcogenidometallate during ink formulation. After printing and sintering, various shapes of TE devices were obtained and readily integrated into pipeline systems (Fig. 13e–f). Homogeneous thermoelectric performance was observed in 3D-printed materials, for which the *ZT* values of 0.9 for p-type and 0.6 for n-type were comparable to those of their bulk counterparts. The TE devices showed a maximum output voltage of 27.0 mV and a maximum power of 1.62 mW at a temperature difference of 39 °C (Fig. 13g). In addition to extrusion-based 3D-printing methods, 3D conformal aerosol jet printing was demonstrated to deposit solution-processed $Bi_2Te_{2.7}Se_{0.3}$ nanoplate inks onto both 2D planar and 3D curved substrates.[235] Within seconds of the photonic sintering process, the electrical conductivity of the printed film was dramatically improved from non-conductive to 2.7 × 10^4 S m^{-1}. A power factor of 730 μW m^{-1} K^{-2} was achieved for the printed flexible films with good stability after 500 bending cycles.

5.1.2. Supercapacitors. Based on the double-layer effect, supercapacitors enable rapid charging and discharging through the storage and release of electrical energy in a short period of time.[236,237] Owing to their large specific surface area, 2D materials have emerged as encouraging candidates for developing high-performance supercapacitors/ultracapacitors.[14,238,239] For example, Pumera's group and Banks' group have applied graphene/PLA to functional electrodes for supercapacitors through fused deposition modelling printing.[240,241] In another example, the micro-extrusion 3D printing method was effectively used for the fabrication of rGO-based micro-supercapacitors.[242] The printed GO films were first treated with hydrogen iodide (HI), followed by the deposition of PVA–H_2SO_4 gel as the electrolyte. A capacitance of 41.8 F cm^{-3} at 0.06 A cm^{-3} was obtained for the printed micro-supercapacitor. To further improve the capacity of supercapacitors, Jiang *et al.* fabricated graphene aerogel microlattices with rich hierarchical pores and high electrical conductivity.[243] During the printing process, a facile ion-induced gelation method was demonstrated to directly print aerogel microlattices from GO-based ink (Fig. 14a–c). Using Ca^{2+} as an ionic gelator, aqueous GO solution was transformed into a printable gel ink, leading to the formation of free-standing 3D structures with programmable microlattices under ambient conditions. The gravimetric capacitance (C_s) of supercapacitors is 213 F g^{-1} at 0.5 A g^{-1} and 183 F g^{-1} at 100 A g^{-1}, and retains over 90% after 50 000 cycles.

In addition to graphene, other conductive 2D materials have also been investigated for fabricating supercapacitors. Recently, Zhang *et al.* developed a stamping strategy to transform 2D titanium carbide or carbonitride inks into supercapacitors.[244] As shown in Fig. 14d, this process started with stamp fabrication by the FDM method using PLA filaments. Next, the 3D-printed stamp was covered with MXene inks ($Ti_3C_2T_x$ or Ti_3CNT_x), and hard-pressed onto flexible substrates to generate all-MXene supercapacitors. Several MXene-based micro-supercapacitors were rapidly manufactured with a wide variety of designs (Fig. 14e), which showed good cycle life (>10 000 cycles) and excellent capability (capacitance retention of 82% at 800 μA cm^{-2}).

5.1.3. Batteries. Supercapacitors are ideal when rapid charging is desirable to fill a short-term power demand, while batteries are required to supply long-term electric energy. Thanks to the rapid development of printing technologies, direct printing of 2D nanomaterials has been increasingly investigated for applications including Li–O_2 batteries,[245] Li–S batteries,[246] and Na-ion batteries.[247] For example, graphene/PLA composites have been used in the rapid manufacturing of 3D printed freestanding anodes for lithium-ion batteries.[240,248] In 2016, Hu's group developed a fully 3D-printed lithium-ion battery by additive printing of GO-based inks as well as gel polymer electrolytes (Fig. 15).[136] Lithium titanium oxide ($Li_4Ti_5O_{12}$, LTO) and lithium iron phosphate ($LiFePO_4$, LFP) were added into anode and cathode materials, respectively. The

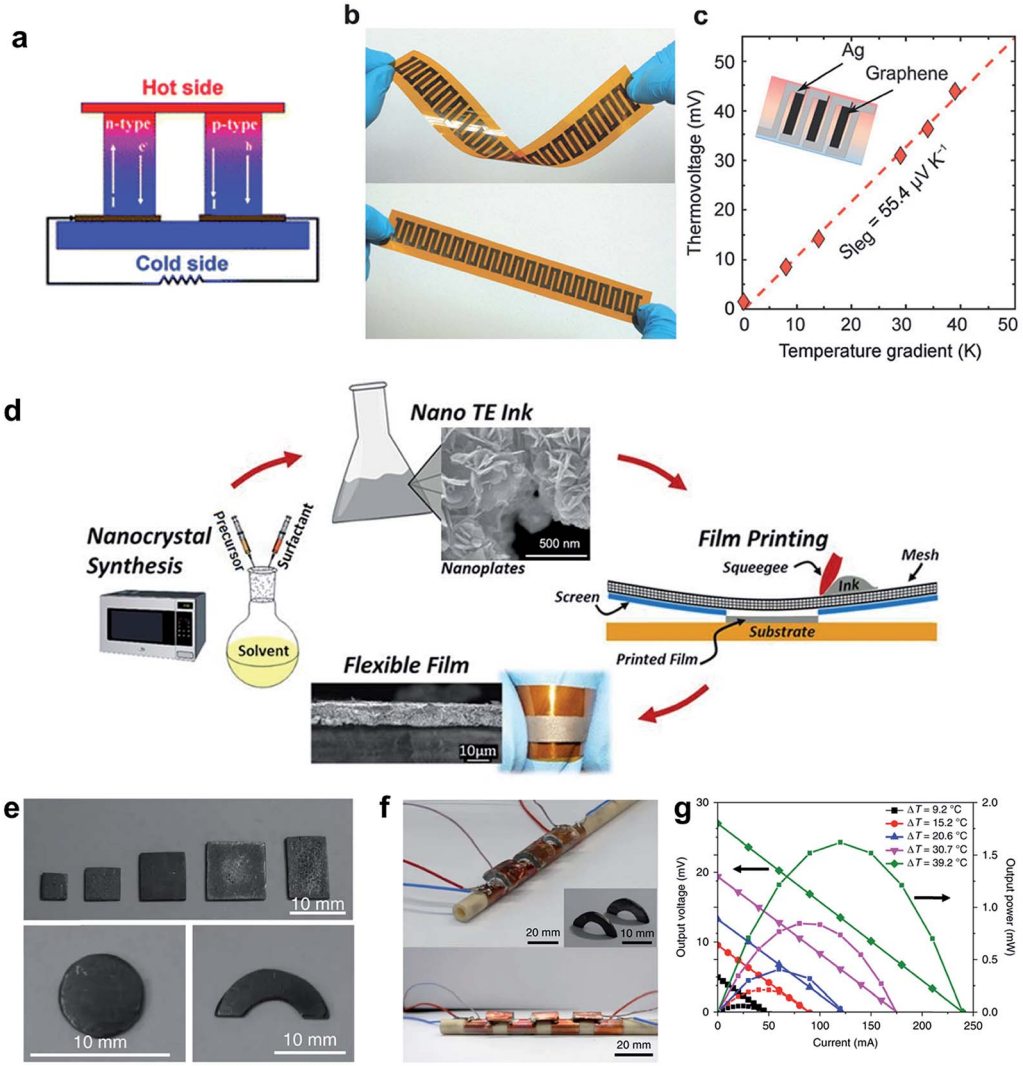

Fig. 13 Printable 2D materials for thermoelectric (TE) applications. (a) Schematic demonstration of a thermoelectric device for power generation. Reproduced with permission from ref. 226. Copyright 2009 the Royal Society of Chemistry. (b) Printed flexible TE devices. (c) Voltage output of Ag/graphene devices as a function of temperature gradient. Reproduced with permission from ref. 233. Copyright 2018 Wiley-VCH. (d) Screening printing process of flexible TE films using $Bi_2Te_{2.8}Se_{0.2}$ nanoplate ink. Reprinted with permission from Springer Nature.[129] Copyright 2016 Nature Publishing Group. (e) Photos of the printed TE materials with different shapes. (f) Images of the printed conformal TE devices. (g) Output voltage and power of the printed TE devices. Reprinted with permission from Springer Nature.[123] Copyright 2018 Nature Publishing Group.

3D-printed LTO anode and LFP cathode showed stable cycling performance with specific capacities of ≈170 mA g^{-1} and ≈160 mA h g^{-1}, respectively. A fully 3D-printed cell presented a high electrode mass loading of 18 mg cm^{-2} when normalized to the overall area of the battery. The full cell delivered initial charge and discharge capacities of 117 and 91 mA h g^{-1}. In 2018, the same group described the use of holey graphene oxide (hGO) for 3D printing of a lithium–oxygen battery without the use of additives or binders.[245] The 3D printed hGO meshes exhibited hierarchical porosity: nanoscale (4–25 nm holes on hGO), microscale (~10 μm pores introduced by lyophilization), and macroscale (<500 μm square pores of the mesh). The 3D printed mesh's multi-level porosities improved active-site utilization as well as mass/ionic transport, leading to enhanced $Li–O_2$ battery performance in comparison with the vacuum filtration method. In order to explore the role of hierarchical porosity, specifically nanoporosity, on electrochemical performance, GO nanosheets without nanoholes were prepared and compared with regards to their performance in batteries. The mesh cathodes of hGO outperformed conventional GO under full discharge conditions, and showed better cycling depth and stability.

5.1.4. Solar cells. Owing to their extraordinary optical and electrical properties, several colloidal nanoparticles (*e.g.* graphene) have been widely used in various solar cell systems including heterojunction solar cells (HSCs),[249] organic solar cells (OSC),[250] dye/QD sensitized solar cells (DSSCs),[251,252] and perovskite solar cells (PSCs).[253–256] For example, Hashmi *et al.*

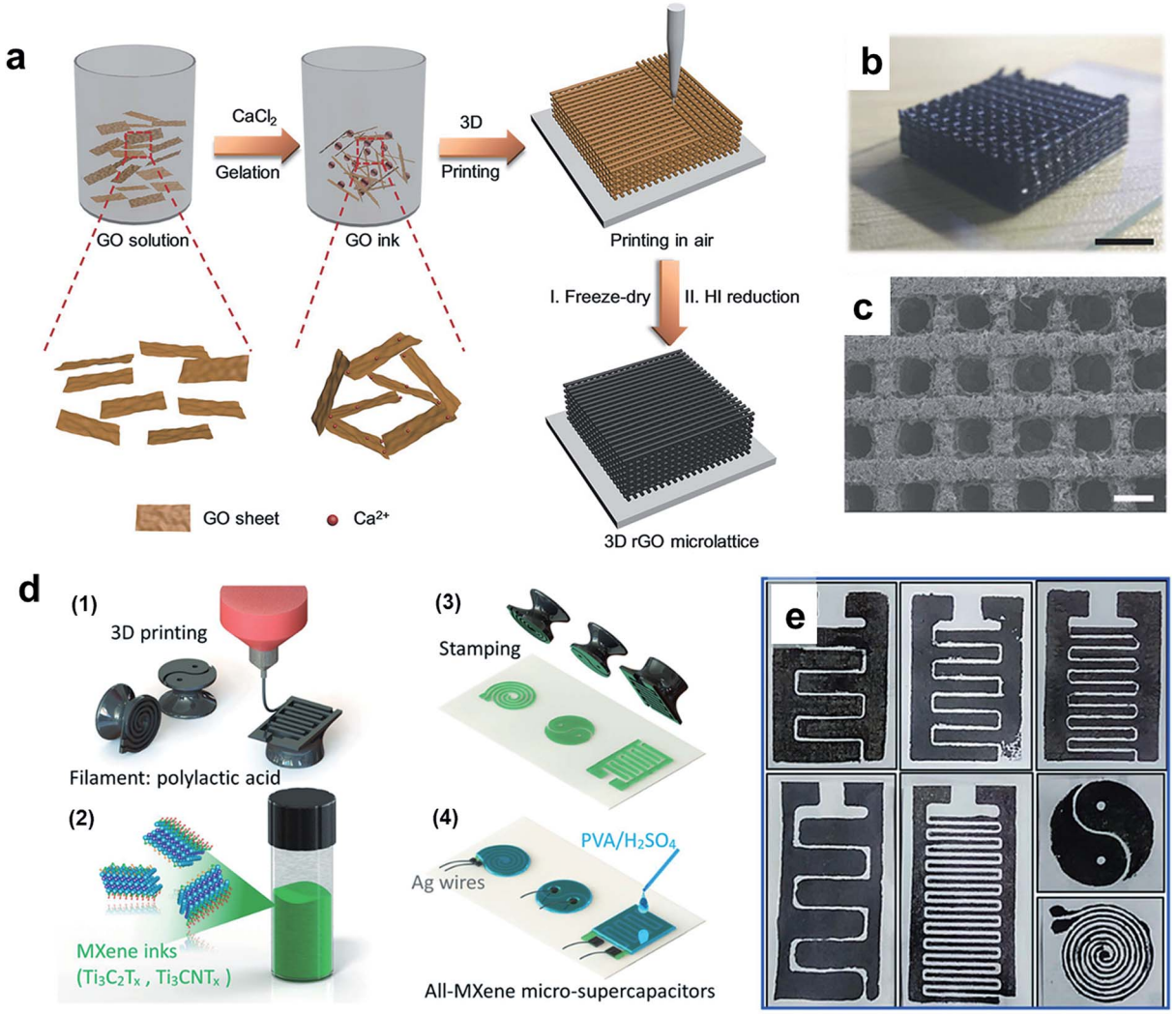

Fig. 14 Printable 2D materials for supercapacitors. (a) 3D printing of graphene oxide into supercapacitors. (b) Photographic image of a printed supercapacitor with a microscopic porous morphology. (c) SEM image of a printed graphene supercapacitor. Scale bars of (b) and (c) are 5 mm and 500 μm, respectively. Reproduced with permission from ref. 243. Copyright 2018 Wiley-VCH. (d) The fabrication of MXene-based supercapacitors by 3D printing and ink transferring using stamps. (e) Photos of several MXene-based supercapacitors. Reproduced with permission from ref. 244. Copyright 2018 Wiley-VCH.

developed inkjet infiltrated carbon-based printed perovskite solar cells with high stability and reproducibility.[257] As shown in Fig. 16a–e, the authors demonstrated that the perovskite precursor ink is highly stable, printable, and controllable, and can directly be used to fabricate porous triple layered printed PSCs with a high overall conversion efficiency of 9.53% without the need for hole transporting materials. Owing to their high conductivity, 2D MXene nanosheets were used in silicon solar cells to form an ohmic junction with n^{+}-Si (Fig. 16f).[258] The metallic feature enabled MXenes to effectively extract the photogenerated electrons from the active layer, leading to a decrease in device contact resistance and the suppression of charge carrier recombination. An improved open-circuit voltage and a high short-circuit current density were observed with a maximum power conversion efficiency of 11.5%. Despite the fact that spin/drop coating was used for the majority of the photovoltaic studies published in the literature to date, printing techniques have emerged as a promising approach for fast prototyping and scalable manufacturing of solar cells.[259,260] A wide range of materials including graphite,[257] carbon nanotubes,[261] and dye molecules[262] have been incorporated in the printing of solar cells. In particular, the printing of 2D nanomaterials has been increasingly investigated in the past few years. For example, the Hasan group demonstrated the use of graphene ink for fabricating dye-sensitized solar cells.[263] In the fabrication of counter electrodes (CEs), graphene ink showed good uniformity and consistency, as shown in Fig. 16g. The authors also investigated the use of different dyes including natural dye extracts from *Pennisetum glaucum*, *Hibiscus sabdariffa* and *Caesalpinia pulcherrima* as well as the synthetic ruthenium-based dye N719, showing a maximum performance of ~3.0% conversion efficiency (Fig. 16h). The inkjet-printed

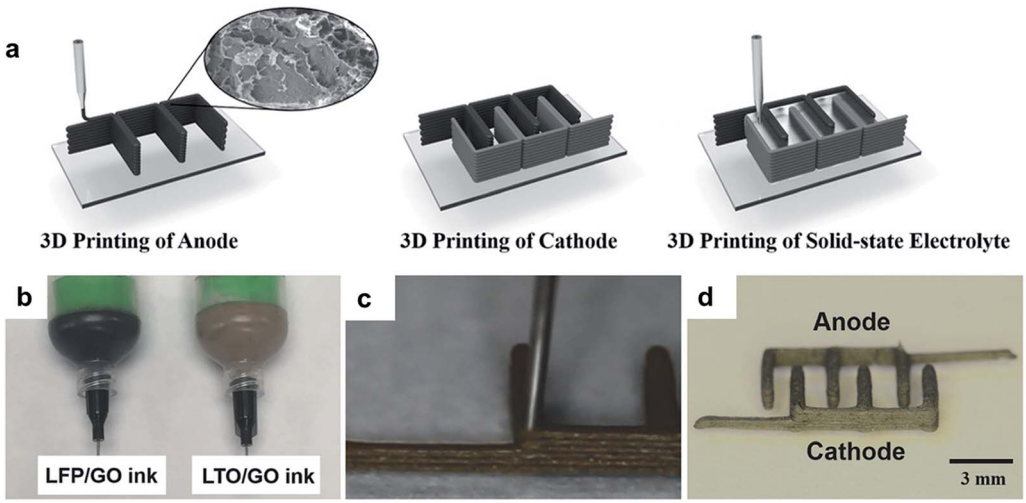

Fig. 15 Printable 2D materials for batteries. (a) Schematic illustration of the 3D-printed battery electrodes as well as the electrolyte. (b) Photos of LFP/GO and LTO/GO inks. (c) Digital image displaying the printing process. (d) Optical images of 3D-printed interdigitated electrodes. Reproduced with permission from ref. 136. Copyright 2016 Wiley-VCH.

graphene electrode provided a cost-effective alternative, which has a material cost of only ~2.7% of that of equivalent solution processed Pt-based electrodes. As another example of printed solar cells, MXene/CuSe nanosheets were screen-printed onto graphite sheets to form a counter electrode in quantum dot-sensitized solar cells.[264] The authors combined the high electrical conductivity of MXenes (Ti_3C_2) and rich active sites of CuSe for polysulfide electrolyte reduction.[264] Therefore, such a 2D composite CE enabled a photovoltaic device with an

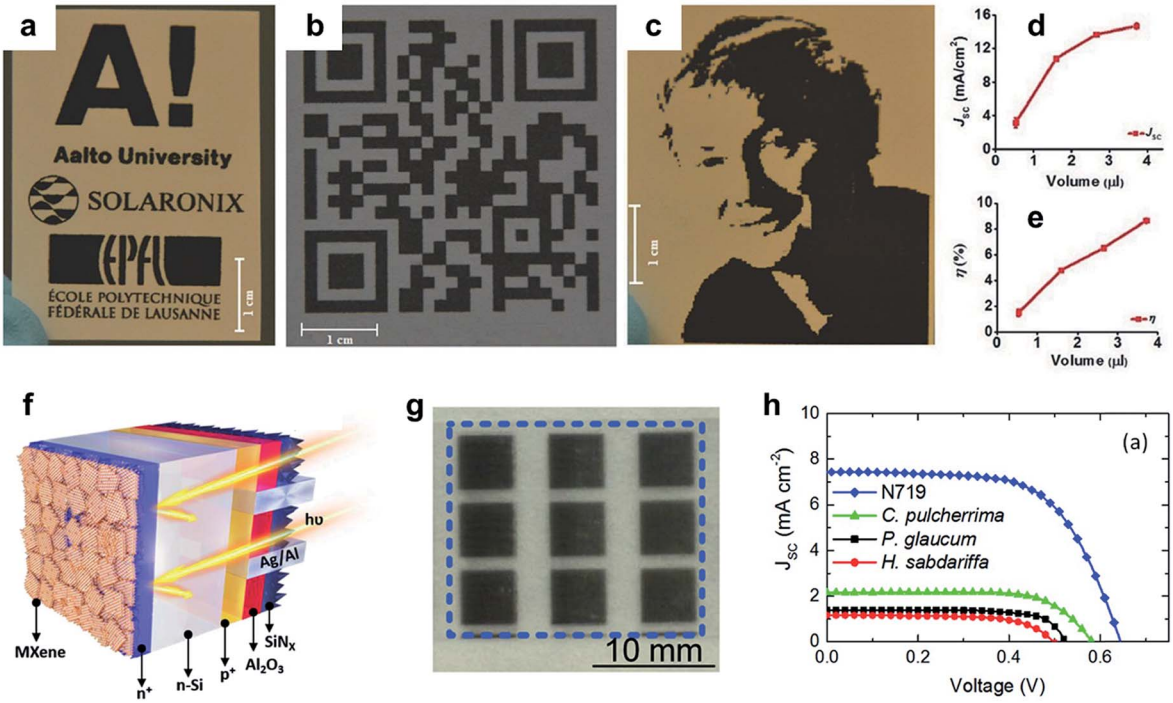

Fig. 16 Printable colloidal nanomaterials for solar cells. (a–c) Demonstrations of inkjet-printed patterns using a stable perovskite precursor ink, including (a) logos, (b) quick response (QR) code, and (c) digital image. (d and e) The short circuit current density (J_{sc}) and efficiency (η) of PSCs by adjusting the volume of printing perovskite precursor ink, leading to the precise tuning of photovoltaic performance. Reproduced with permission from ref. 257. Copyright 2017 Wiley-VCH. (f) Schematic illustration of MXene-based silicon solar cells. Reproduced with permission from ref. 258. Copyright 2019 Wiley-VCH. (g) Image of printed graphene electrodes showing good printing consistency. (h) Current–voltage characteristic curves of graphene-based solar cells sensitized with different dyes (natural tropical dye: extracts from *Pennisetum glaucum*, *Hibiscus sabdariffa* and *Caesalpinia pulcherrima*. Synthetic dye: N719). Reproduced with permission from ref. 263. Copyright 2016 Elsevier B.V.

improved efficiency of 5.12%, which is higher than that of pristine CuSe CE (3.47%) or pristine Ti_3C_2 CE (2.04%).

The printing of 2DM-based inks provides a versatile platform for the design and development of a broad range of devices for energy conversion and storage. With suitable printing methods, these energy devices can be printed on a wide variety of substrates, such as flexible and transparent films, adjusting the conventional stereotypes of energy conversion and storage using rigid structures. More importantly, the printing technologies enable energy devices with low dimensions, high resolution and short fabrication time, which would serve as power supplies for the development of next-generation wearable electronics and sensors.

5.2. Sensing

The ability of 2DMs to respond to the environment with ultrahigh surface sensitivity has been demonstrated as the key characteristic for sensing applications. Moreover, 2DMs' exceptional optical/electrical properties, combined with the structural robustness and flexibility, enable these materials to be desired candidates for manufacturing next-generation sensors. Combined with printing technologies, we will highlight recent advances in functional devices for sensing physical, chemical, and biological stimuli/inputs.

5.2.1. Optoelectronic sensors. The fast-expanding market of optoelectronic devices, including photodetectors and UV sensors, calls for innovative production of nanostructures from optoelectronic materials in a low-cost, high-throughput, and large-scale fashion.[19,265] Printing is a versatile technology for deposition of ink materials and an emerging tool toward fast prototyping and manufacturing of optoelectronic sensors. As many optoelectronic sensors involve charge transfer or energy transfer processes, the electronic structure of 2DMs plays an essential role in developing functional optoelectronics based on desired donor–acceptor pairs. In particular, the versatility of the band gaps of 2D materials provides enormous opportunities in the field of optoelectronics (Fig. 17a).

Semiconducting TMDs and BP have attracted a lot of attention because of their tunable band gaps as well as atomically thin structures. For example, Kim *et al.* reported highly transparent MoS_2 phototransistor arrays on flexible polymer substrates by a drop-on-demand inkjet-printing technique.[267] To fabricate the phototransistor arrays, MoS_2 monolayers were selectively patterned using a reactive ion etching system with O_2 plasma (Fig. 17b and c), followed by inkjet printing of electrodes and dielectric layers. As shown in Fig. 17d, the printed phototransistors showed good responsivity and detectivity in the wavelength range of 400 to 800 nm. In addition to MoS_2,

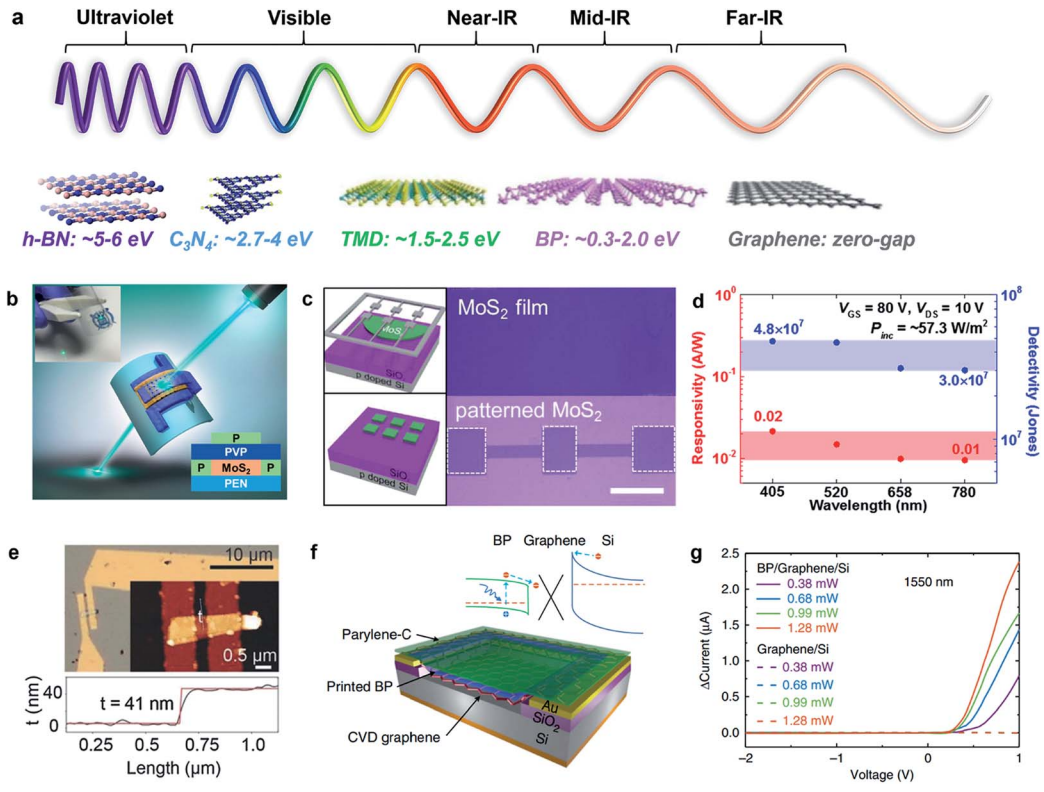

Fig. 17 Optoelectronic sensors based on printable 2D nanomaterials. (a) The electromagnetic wave spectrum and the band gap ranges of different 2D nanomaterials. Reproduced with permission from ref. 266. Copyright 2015 National Academy of Sciences. (b–d) MoS_2 based phototransistors. Reproduced with permission from ref. 267. Copyright 2017 American Chemical Society. Scale bar in (c) is 400 μm. (e) In_2Se_3 thin-film photodetectors with a thickness of 41 nm. Reproduced with permission from ref. 40. Copyright 2018 Wiley-VCH. (f) Schematic illustration of a printed black phosphorus (BP) photodetector. (g) The BP/graphene/Si heterostructure showing high photoresponsivity to 1550 nm light. Reprinted with permission from Springer Nature.[149] Copyright 2017 Nature Publishing Group.

solution-processable indium selenide (InSe) flakes were used to fabricate a photodetector with high photoresponsivities ($\approx 5 \times 10^7$ A W^{-1}) that surpass those of previously reported solution-processed monolithic semiconductor photodetectors by three orders of magnitude (Fig. 17e).[40] The pristine InSe flakes were prepared by liquid-phase exfoliation in surfactant-free, deoxygenated co-solvent mixtures and the field-effect transistors were fabricated by vacuum filtration and electron-beam lithography. Such a solution-based process possesses huge potential for the scalable synthesis of InSe and its thin films, which showed excellent responsivity for film-based photodetectors.

Recently, two-dimensional black phosphorus has drawn significant research attention owing to its unique structural and electrical properties.[266] An inkjet-printable BP ink was developed for fabricating a hybrid photodetector.[149] As shown in Fig. 17f, printed BP was combined with a graphene/Si Schottky junction to fabricate optoelectronic devices. To avoid possible oxidation or degradation in air, a layer of parylene-C was used to encapsulate the hybrid structure. Under a 450 nm light source, a photoresponsivity of up to 164 mA W^{-1} was observed. Interestingly, owing to the layer-dependent bandgap of BP (0.3–2.0 eV), the device can also respond to 1550 nm light (1.8 mA W^{-1} photoresponsivity), as shown in Fig. 17g.

For graphene, MXenes and other low band-gap 2DMs, they have also been extensively studied as an electrical contact or a photoactive layer in optoelectronics. In addition, the good solution processability of GO allows the full inkjet printing for graphene-based photodetectors. Manga *et al.* formulated an ionic solution ink by combining GO nanosheets with titanium bis(ammonium lactate)dihydroxide (TBA), and printed the ink on coplanar graphene-based electrodes, producing a fully inkjet-printed photodetector.[268] A heterostructure graphene/WS_2/graphene junction was also utilized for photodetection.[125]

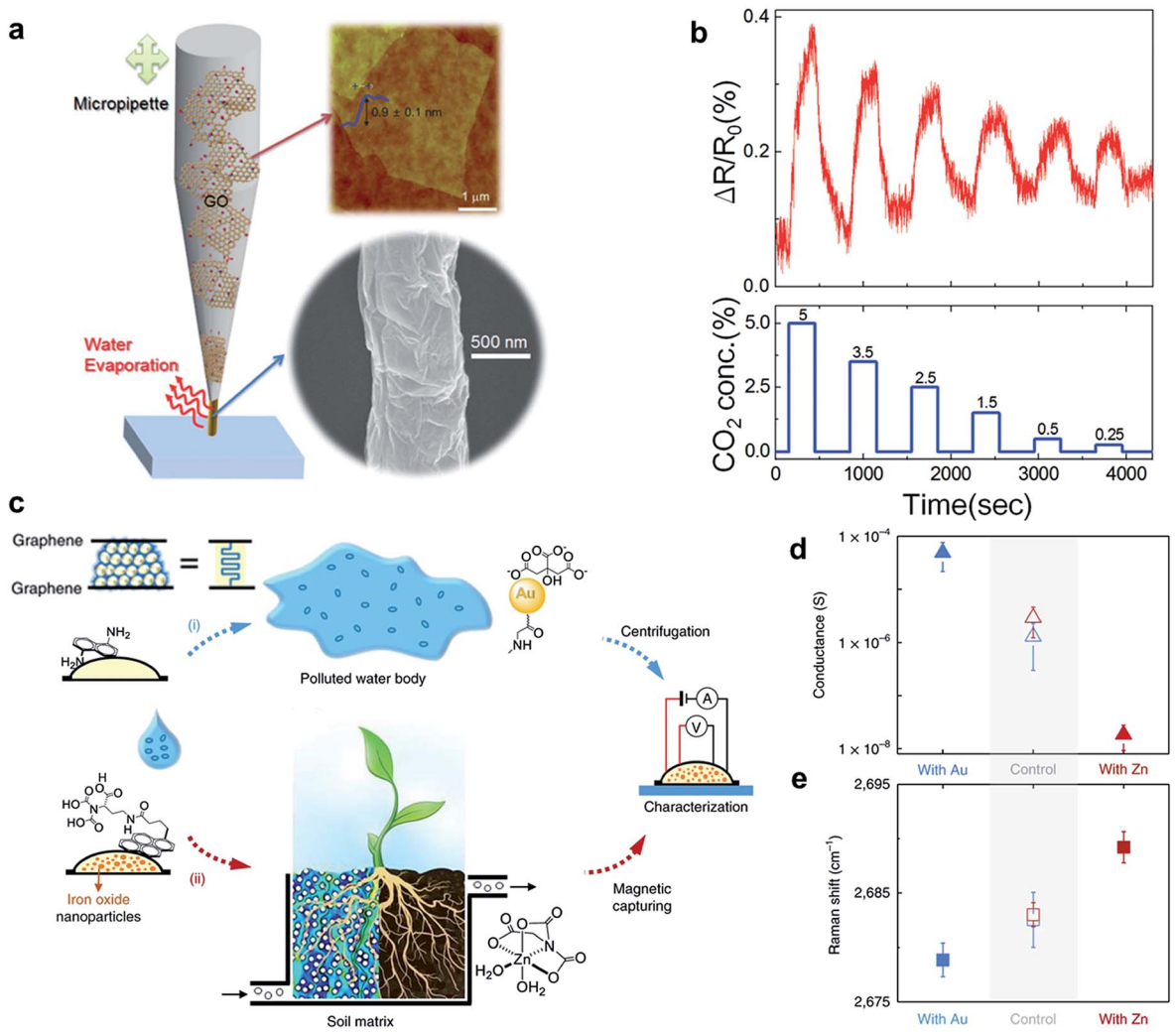

Fig. 18 Printable 2D materials for chemical sensors. (a) 3D printing of reduced GO-based wires. (b) rGO nanowires for CO_2 sensing. Reproduced with permission from ref. 274. Copyright 2015 Wiley-VCH. (c) Chemical sensors based on microprinted graphene–PS–graphene microparticles. (d) Surface conductance of graphene–PS–graphene microparticles on detecting gold nanoparticles and Zn^{2+}. (e) Raman shift of graphene–PS–graphene microparticles on detecting gold nanoparticles and Zn^{2+}. Reprinted with permission from Springer Nature.[275] Copyright 2018 Nature Publishing Group.

This heterostructure device exhibited a photoresponsivity >1 mA W^{-1} (at 514 nm).

5.2.2. Chemical sensor. Recently, graphene, rGO, TMDs, and other 2D nanomaterials have emerged as active constituents for electrochemical sensing due to their superior electrical conductivity, excellent electrochemical properties, and large surface to volume ratios compared to traditional metal oxides and conducting polymers.[269–272] A printed 2DM chemical sensor was first reported in 2010, where inkjet printing of rGO platelets was achieved using aqueous surfactant-supported dispersions of rGO powder.[273] Despite its relatively low electrical conductivity ($\sigma \approx 15$ S cm^{-1}), the rGO-based chemical sensor was able to detect chemically aggressive vapours at the parts per billion level using an air sample at room temperature. An increase in electrical conductivity was observed when the rGO sensor was exposed to highly oxidizing vapours, while there was an increase in resistance when it was exposed to organic vapours and reducing species, including hexanes, CH_3OH, and NH_3. In addition to 2D printed sensors, 3D printing of reduced graphene oxide nanowires was realized to detect CO_2 concentrations between 0.25 and 5% (Fig. 18a and b).[274] By accurately tuning the printing parameters, the authors fabricated 3D printed rGO wires with complex features, demonstrating controlled deposition direction as well as deposition positions. The 3D printing of 2DM-based nanowires shows enormous potential to fabricate components of electrochemical sensing devices such as flexible sensing transducers.[274]

Recently, the Strano group integrated a micro-printing technique with CVD-grown 2D materials to develop an "auto-perforation" technique that provides a means of spontaneous assembly for surfaces composed of two-dimensional molecular scaffolds.[275] This innovative approach was based on controlled crack propagation in CVD-grown 2DM thin films, creating microparticles with a pair of enveloping 2D layers. In their work, the authors showcased a graphene–polystyrene–graphene (G–PS–G) microparticle which was used as a platform to detect and monitor environmental stimuli. Such G–PS–G microparticles with amine groups can interact with gold nanoparticles (Fig. 18c), and those with nitrilotriacetic acid (NTA) ligands can probe Zn^{2+} ions. Therefore, amine-modified devices revealed a significant increase in the surface conductivity for sensing gold nanoparticles, whereas a huge reduction was witnessed for the NTA-modified particles upon Zn^{2+} exposure (Fig. 18d). Raman shift of the printed microsensor was also observed upon these chemical stimuli (Fig. 18e).

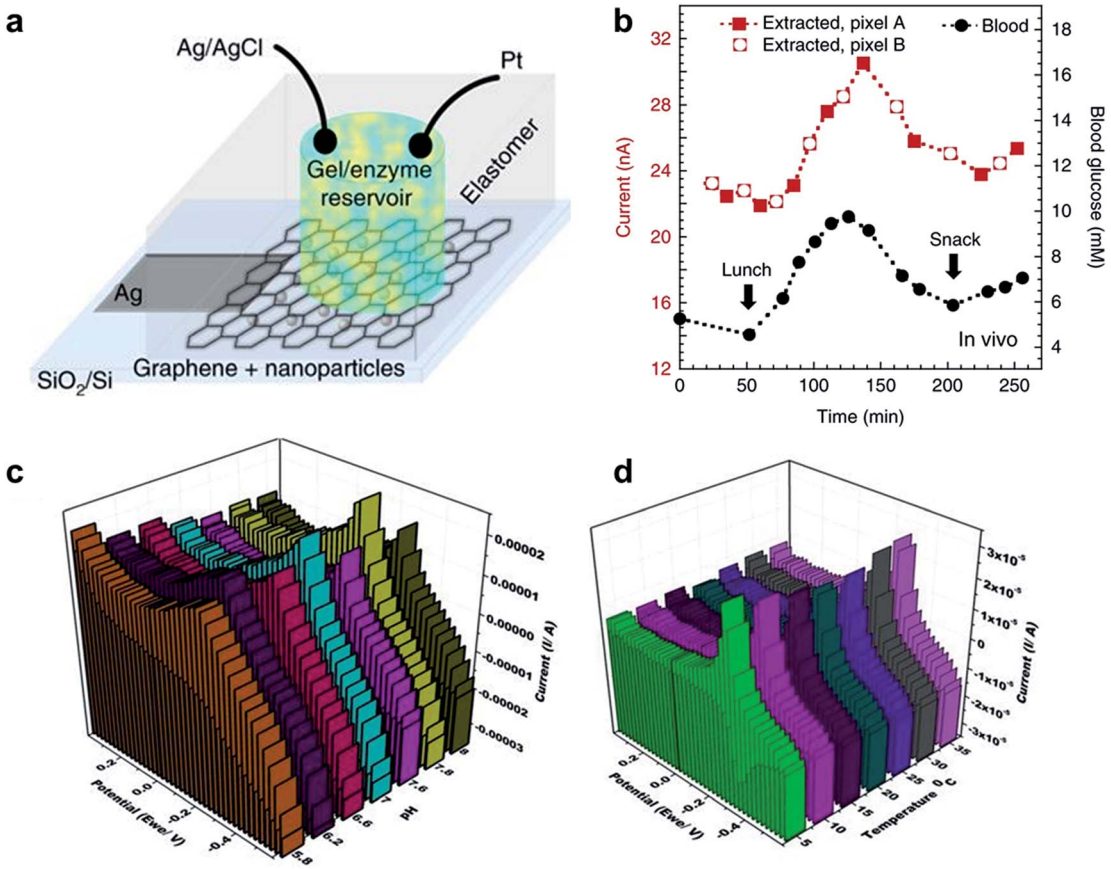

Fig. 19 Printable 2D materials for biosensors. (a) Schematic demonstration of glucose sensing devices. A 3D electrochemical cell is formed by contacting the gel with Ag/AgCl (reference) and Pt (counter) electrodes. (b) The *in vivo* testing in which the glucose levels of healthy volunteers were monitored. Reprinted with permission from Springer Nature.[9] Copyright 2018 Nature Publishing Group. (c and d) MoS_2-based biosensor for detecting chikungunya virus DNA under the pH effect (c) and temperature effect (d). Reprinted with permission from Springer Nature.[280] Copyright 2018 Nature Publishing Group.

In addition, there is an increased emphasis on two areas in chemical sensing: (1) real-time monitoring; (2) ultrahigh-sensitivity detection.[276] The real-time monitoring commonly relies on non-covalent interactions of 2D nanomaterials that enable a quick response and a fast recovery rate. Such non-covalent interactions, dependent on the type of analyte, include electrostatic force, hydrogen bonding, π–π interaction, *etc.* To detect the trace amount of pollutants, strategies based on covalent linkages between analytes and 2D nanomaterials sometimes can be more suitable. As it allows analytes to immobilize on the surface and to be stable during the assay, covalent linkages overcome the weakness of the supramolecular forces, particularly for biomolecule systems. The careful engineering of surface chemistry of 2D materials and novel designs enabled by printing techniques would be desirable to realize next-generation high-performance chemical sensors.

5.2.3. Biosensors. 2D materials appear to be a promising carrier platform for biological recognition elements owing to their high surface sensitivity and exceptional electronic properties.[277–279] To monitor glucose levels in the interstitial fluid, Lipani *et al.*[9] developed a path-selective, non-invasive, transdermal glucose monitoring system by screen printing of a graphene film, as shown in Fig. 19a. It was suggested that glucose reacted with glucose oxidase to produce hydrogen peroxide, which was detected by the electrochemical sensor. With an increased density of graphene-decorating Pt nanoparticles, the limit of detection was improved to about 0.76 μM. The authors also performed *in vivo* testing in which the glucose levels of healthy volunteers were monitored by two of the array's pixel devices, during which lunch and a snack were ingested (Fig. 19b). The results showed well-matched readout values that provided further confidence in the performance of the array.

In addition to graphene, other 2D materials have been extensively investigated for printable biosensors, particularly MoS_2.[281–283] Recently, Singhal *et al.* developed a biosensor based on MoS_2 nanosheets for the selective detection of chikungunya virus.[280] Owing to MoS_2's exceptional biocompatibility, good electrochemical activity, and high specific surface, the biosensor exhibited a wide linear range of 0.1 nM to 100 μM towards chikungunya virus DNA. The biosensor also showed a low limit of detection of 3.4 nM in a 3σ rule. As shown in Fig. 19c and d, the pH response and temperature effect of the biosensor were studied, showing the highest current response at 7.8 pH and 35 °C.

5.2.4. Other sensors. The rapid development of printing technology has enabled many other sensing and monitoring systems, such as temperature sensors, pressure gauges, and humidity detectors. Based on solution-processable colloidal nanoparticles, several printed temperature sensors have been demonstrated, showing strong potential in various research and industrial processes.[284–286] Due to their excellent electrical, mechanical, and thermal properties, graphene and its derivatives have been widely used in developing sensors for temperature probing and monitoring.[287–289] For example, a flexible resistive temperature sensor was inkjet-printed using graphene/PEDOT:PSS ink.[290] The sensing device showed a negative

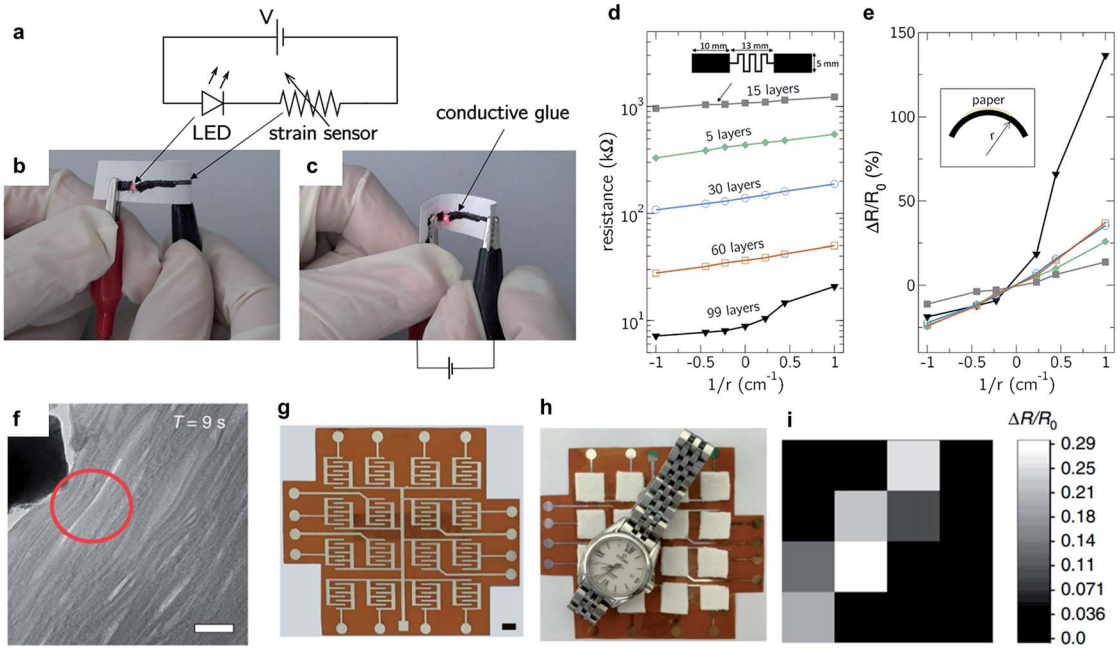

Fig. 20 (a) Schematic of the simple circuit for the graphene strain sensor. (b and c) Graphene sensing system under (b) tensile and (c) compressive strain. (d) Resistance as a function of the inverse of the bending radius and under different layer thicknesses. (e) Sensitivity as a function of 1/*r* under different layers. Reproduced with permission from ref. 166. Copyright 2018 Elsevier. (f) The *in situ* dynamic monitoring of MXenes under an external pressure, showing the change of the interlayer distance (scale bar is 40 nm). (g) 4 × 4 MXene-based sensor pixel arrays for sensing pressure distribution (scale bar is 5 mm). (h) A watch was positioned on the arrays. (i) The corresponding resistance change was evaluated at each pixel. Reprinted with permission from Springer Nature.[10] Copyright 2017 Nature Publishing Group.

Table 4 Examples of emerging trends of printing-related technologies and their applications in functional devices

	Emerging fields	Capabilities & features	Example applications	Reference
Ink formulation	Orientation engineering	Ink particles can self-assemble or be directly assembled into functional structures with high orientational ordering	Ordered/aligned devices	320 and 321
	Nanosurfactant	QD nanosurfactants stabilize graphene in water with high colloidal stability	Photonic materials	28
	Semiconductor binder/solder	Connecting semiconductor particles under mild conditions	Thermoelectrics, FETs	123 and 308
	Green solvent	Providing a low hazardous and highly scalable method	Transistors	106
Printing methodology	High throughput printing	A bar-coating technique (speed of 6 m min^{-1}) enables large-area polymer circuits	Large-area electronics	314
	Volumetric printing	Printing entire complex objects on a time scale of seconds	Custom objects	315 and 316
	Embedded printing	Fabricating devices within extensible elastomeric matrices	Strain sensors	319
	Multi-material printing	Direct printing and mixing of multiple, high-quality materials by one printing process	Shape memory circuit	317 and 318
Substrate	Surface coating	Improve the printability of substrates	Microfluidics	148
	Prepatterned	Providing a customizable platform for generating 1D/2D patterns	Microcontact printing	22 and 144
	Smart substrate	Thermo-responsive polymers were used as reversible shape changing substrates	Soft actuators	169
Sintering/annealing	Microwave annealing	Reduce GO to pristine graphene using 1- to 2-second pulses of microwaves	Hydrogen evolution	325
	Photonic sintering	Sintering of printed films on polymer substrates within seconds	Thermoelectrics	130

temperature dependence of resistance with 0.06% per degree Celsius sensitivity. Very recently, Zhao *et al.* developed a printed tandem line-type temperature sensor based on reduced graphene oxide.[289] The authors also used the DIW printing method to fabricate an MXenes/CNT positive electrode and rGO/CNT negative electrode, which were used as a supercapacitor to power the temperature sensors. The authors found that the temperature sensitivity of the printed integrated electronic device can reach 1.2% per degree Celsius in resistance.

Owing to 2D nanomaterials' exceptional mechanical properties and ultrathin thicknesses, they are emerging as an attractive platform for strain sensors.[291–294] In a typical printed strain sensor, a conductive pattern can respond to geometric deformation that changes one or several key parameters of the sensor, such as resistance or capacitance.[295–297] Casiraghi *et al.* reported inkjet printed strain gauges based on liquid-exfoliated graphene (Fig. 20a–c).[166] By adjusting several key printing parameters such as the number of printing passes (Fig. 20d and e), a gauge factor up to 125 was obtained, which led to high sensitivity (>20%) under small strains (0.3%). In another recent study, a 2D MXene has been used to develop a flexible pressure sensor with interdigital electrodes based on their change in *d*-spacing upon external pressure.[10] An *in situ* transmission electron microscopy study directly illustrated a decrease in interlayer distances under pressure (Fig. 20f), providing a qualitative understanding of the working mechanism of the MXene-based sensor. A wide range of pressure can be detected using the MXene-based piezoresistive sensor with a decent gauge factor (GF $\sim$ 180), good mechanical reversibility (over 4000 times), and short response time (<30 ms). The authors also demonstrated an MXene-based sensor pixel array (4 $\times$ 4) for mapping the pressure distribution, as shown in Fig. 20g–i. When an object (*e.g.* a watch) was positioned on the sensor arrays, the

corresponding output at each pixel was recorded and measured, allowing for mapping local pressure distribution quantitatively.

Due to the ability to attract or interact with water molecules, numerous hydrophilic nanomaterials have recently attracted research interest in humidity sensing[279,298] and water-level monitoring.[299,300] Owing to the strong hydrophilic feature enabled by surface functional groups, 2DMs such as graphene oxides and MXenes have been used in developing flexible/wearable humidity sensors.[301–304] For example, Yuan's group developed a flexible humidity sensor based on poly(3,4-ethylenedioxythiophene)/reduced graphene oxide/Au nanoparticles.[298] Using inkjet printing techniques, the thin-film humidity sensor showed high conductivity and sensitivity with superior stability after 200 bending cycles. The sensor can respond to a wide range of humidity (11–98% relative humidity), while producing a wide resistance change of 7–52%. For some 2DMs (*e.g.*, black phosphorus) for which the intrinsic conductivity is sensitive to ambient water, humidity sensors can also be developed through rational device design.[305–307] For example, a thick-film black-phosphorus humidity sensor was fabricated with a high response to humidity change.[305] Such humidity-response properties showed decent stability after 3 month exposure to ambient conditions with 25% relative humidity. Compared with conventional thin-film sensors, the authors suggested that a thick film of BP nanosheets can be more robust for long-term humidity sensing under moderate humidity conditions.

6. Conclusions and future prospects

In the past decade, colloidal nanoparticles have been extensively employed in a variety of printing processes because of their unique properties. In this review, we summarized and evaluated state-of-the-art progress on colloidal nanoparticle synthesis, ink formulation, printing and device applications, and suggested high-priority areas for future research. As a perspective on possible future directions, we listed some emerging technologies and research topics that could be potentially leveraged in the development of next-generation printed functional devices (Table 4).

The properties of 2D materials vary significantly, as expected from their diversity in chemical/electronic structures, from zero/small band gaps for some materials (*e.g.* graphene and MXenes) to large band gaps for others (*e.g.* MoS_2 and h-BN). The rich diversity of 2D materials in chemistry/physics offers numerous opportunities for formulating high-performance inks and printing functional devices, but also presents challenges for comprehensive understanding of specialized roles of 2DMs in the printing process. The review considered four key aspects: 2D material synthesis, ink formulation, printing processes, and device applications.

In the section of 2D material synthesis, the rapid development of nanoparticle synthesis has accelerated progress in preparing advanced 2D nanomaterials with controlled nanostructures. By using bottom-up or top-down approaches, ultrathin 2D nanomaterials have been synthesized with a high yield and fast production speed. However, the commercial production (*e.g.* 1–100 kg level) of high-performance 2D nanomaterials remains a major challenge. For example, many LPE-based monolayer syntheses rely on ultrasonication for hours and even days, which makes it challenging for large-scale manufacturing of 2DMs. Methods that can consistently produce high-quality 2DMs with low cost and on an industrial scale are yet to be developed.

For processing inks, the ingredients (*e.g.* solvents, surfactants, and binders) play significant roles in determining the quality of inks, and thus innovations in ink additives can further improve the performance of printed devices. For example, the development of composition-matched molecular "solders" has demonstrated considerable improvement in device carrier mobility.[308] In addition, surfactants can greatly reduce the interfacial tension and form steric and/or provide electrostatic stabilization for 2D nanomaterials in inks. However, the residual surfactant in printed devices often limits the overall functionalities of the 2D materials, which requires post-treatments to remove the surfactant. Therefore, one practical need for the large-scale applications of 2DM-based inks is the development of compatible ink additives so they wouldn't compromise the performance of printed devices. A possible solution is to develop semiconducting/conducting nano-surfactants that do not undermine or even improve the device functionalities of 2D materials. For instances, recent advances in colloidal nano-surfactants or so-called Pickering surfactants have shown that quantum dots,[28] graphene,[309] MoS_2,[310] and 2D clays[311–313] can reduce surface tension and show "surfactancy" upon appropriate surface functionalization of nanoparticles. This could be a promising approach for preparing organic-free functional inks, and more work needs to be done on this aspect.

In the past decade, the emergence of 2D/3D/4D printing has enabled rapid prototyping of macroscale functional devices from nanoscale building blocks.[314–320] Despite considerable progress, there is still much to be done for comprehensive understanding and further optimization of ink rheological properties, the drying process, and substrate–ink interactions. In addition, the fundamental understanding of the effect of the 2D structure and chemical characteristics of 2DMs on the above processes is critically important. As mentioned in Section 3.1, the colloidal stability of 2D particles in fluids is fundamentally different from spherical nanoparticles, such as the electrostatic repulsion energy and sedimentation rate. However, the impact of the unique dimensionality of 2DMs on printing technology remains poorly understood. Another possible direction to improve the overall performance of printed 2DMs is to design and develop novel printing processes. For example, multi-material printing that integrates two or more 2D functional materials *in situ* during printing may enable fast prototyping and high-throughput discovery of novel heterostructures or nanocomposites. Successful examples of heterogeneous nanocompositing have been witnessed in the field of sensing. For instance, SnS_2, WS_2, MoS_2, and Ni_3S_2 have been adopted to enhance the performance of graphene/CNT based electrochemical sensors.[269–272]

On the other hand, although significant efforts have been made in printing functional devices, the electrical performance

of printed 2D materials is often if not always lower than that of their single-crystalline counterparts. In order to further improve the charge/energy carrier transport of printed 2DM devices, methods that can align 2D materials with minimal defects are highly desirable. To achieve high alignment, the liquid-crystalline assembly of 2D nanoparticles into ordered structures seems to be a promising approach. As 2D materials are intrinsically anisotropic, the dispersions of 2D particles have shown a fascinating diversity of liquid crystal phases, *i.e.* forming orientationally or positionally ordered structures.[321,322] This approach, combined with directed assembly tools, has been reported to significantly improve the device performance in terms of thermal conductivity and electrical capacity,[323,324] and could be applicable to additive printing processes. Innovative approaches of post-treatment (*e.g.* photonic sintering[130] or microwave treatment[325]) have also demonstrated great potential in improving the performance of solution-processed nanoparticle films.

For device design and development, a wider selection of 2D materials should be included. Newly discovered 2D materials, including tellurene and hematene,[326,327] have not been fully characterized and may enable translational applications. These and other undiscovered materials may have unprecedented properties that could hold the key to new research breakthroughs. To push forward the development of a new generation of printable structures of 2D materials, it is of utmost importance to establish a fundamental structure–processing–property relationship by innovative theoretical efforts, such as machine learning methods. For example, Rajan *et al.* developed machine-learning models to predict the band gap of MXenes using kernel ridge (KRR), support vector (SVR), Gaussian process (GPR), and bootstrap aggregating regression algorithms.[328] Theoretical/simulation work will be beneficial for better understanding the ink behavior of 2D nanomaterials that governs their utility in device applications.

Overall, unprecedented opportunities and challenges exist in printing colloidal nanoparticles for functional systems and transforming a vast number of nanomaterials into next-generation technologies in a scalable and economic fashion.

Conflicts of interest

There are no conflicts to declare.

Acknowledgements

We acknowledge financial support from the National Science Foundation under award CMMI-1747685, DARPA under DARPA HR00111820030, and the U.S. Department of Energy under awards DE-NE0008712 and DE-NE0008701.

References

1 W. Zeng, L. Shu, Q. Li, S. Chen, F. Wang and X.-M. Tao, *Adv. Mater.*, 2014, **26**, 5310–5336.
2 X. Wang, X. Lu, B. Liu, D. Chen, Y. Tong and G. Shen, *Adv. Mater.*, 2014, **26**, 4763–4782.
3 K. Chen, W. Gao, S. Emaminejad, D. Kiriya, H. Ota, H. Y. Y. Nyein, K. Takei and A. Javey, *Adv. Mater.*, 2016, **28**, 4397–4414.
4 A. Ambrosi and M. Pumera, *Chem. Soc. Rev.*, 2016, **45**, 2740–2755.
5 K. Fu, Y. Yao, J. Dai and L. Hu, *Adv. Mater.*, 2017, **29**, 1603486.
6 Z. Zhan, J. An, Y. Wei, V. T. Tran and H. Du, *Nanoscale*, 2017, **9**, 965–993.
7 A. Kamyshny and S. Magdassi, *Chem. Soc. Rev.*, 2019, **48**, 1712–1740.
8 Z. Cui, *Printed electronics: materials, technologies and applications*, John Wiley & Sons, 2016.
9 L. Lipani, B. G. R. Dupont, F. Doungmene, F. Marken, R. M. Tyrrell, R. H. Guy and A. Ilie, *Nat. Nanotechnol.*, 2018, **13**, 504–511.
10 Y. Ma, N. Liu, L. Li, X. Hu, Z. Zou, J. Wang, S. Luo and Y. Gao, *Nat. Commun.*, 2017, **8**, 1207.
11 S. Borini, R. White, D. Wei, M. Astley, S. Haque, E. Spigone, N. Harris, J. Kivioja and T. Ryhänen, *ACS Nano*, 2013, **7**, 11166–11173.
12 C. Tan, X. Cao, X.-J. Wu, Q. He, J. Yang, X. Zhang, J. Chen, W. Zhao, S. Han, G.-H. Nam, M. Sindoro and H. Zhang, *Chem. Rev.*, 2017, **117**, 6225–6331.
13 Y. Liu, N. O. Weiss, X. Duan, H.-C. Cheng, Y. Huang and X. Duan, *Nat. Rev. Mater.*, 2016, **1**, 16042.
14 V. Nicolosi, M. Chhowalla, M. G. Kanatzidis, M. S. Strano and J. N. Coleman, *Science*, 2013, **340**, 1226419.
15 L. Fu, H. Yang, A. Tang and Y. Hu, *Nano Res.*, 2017, **10**, 2782–2799.
16 A. I. Khan and D. O'Hare, *J. Mater. Chem.*, 2002, **12**, 3191–3198.
17 H. T. Li, R. H. Liu, W. Q. Kong, J. Liu, Y. Liu, L. Zhou, X. Zhang, S. T. Lee and Z. H. Kang, *Nanoscale*, 2014, **6**, 867–873.
18 D. Chimene, D. L. Alge and A. K. Gaharwar, *Adv. Mater.*, 2015, **27**, 7261–7284.
19 M. Singh, H. M. Haverinen, P. Dhagat and G. E. Jabbour, *Adv. Mater.*, 2010, **22**, 673–685.
20 P. Chang, H. Mei, S. Zhou, K. G. Dassios and L. Cheng, *J. Mater. Chem. A*, 2019, **7**, 4230–4258.
21 G. Hu, J. Kang, L. W. T. Ng, X. Zhu, R. C. T. Howe, C. G. Jones, M. C. Hersam and T. Hasan, *Chem. Soc. Rev.*, 2018, **47**, 3265–3300.
22 D. Tian, Y. Song and L. Jiang, *Chem. Soc. Rev.*, 2013, **42**, 5184–5209.
23 Y. Q. Dong, J. W. Shao, C. Q. Chen, H. Li, R. X. Wang, Y. W. Chi, X. M. Lin and G. N. Chen, *Carbon*, 2012, **50**, 4738–4743.
24 K. Hu, X. Xie, T. Szkopek and M. Cerruti, *Chem. Mater.*, 2016, **28**, 1756–1768.
25 K. S. Novoselov, A. K. Geim, S. V. Morozov, D. Jiang, Y. Zhang, S. V. Dubonos, I. V. Grigorieva and A. A. Firsov, *Science*, 2004, **306**, 666–669.
26 A. Geim and K. Novoselov, *Nat. Mater.*, 2007, **6**, 183–191.

27 D. C. Marcano, D. V. Kosynkin, J. M. Berlin, A. Sinitskii, Z. Z. Sun, A. Slesarev, L. B. Alemany, W. Lu and J. M. Tour, *ACS Nano*, 2010, **4**, 4806–4814.
28 M. Zeng, S. A. Shah, D. Huang, D. Parviz, Y.-H. Yu, X. Wang, M. J. Green and Z. Cheng, *ACS Appl. Mater. Interfaces*, 2017, **9**, 30797–30804.
29 Y. Peng, Z. Meng, C. Zhong, J. Lu, W. Yu, Z. Yang and Y. Qian, *J. Solid State Chem.*, 2001, **159**, 170–173.
30 Z. Huang, A. Zhou, J. Wu, Y. Chen, X. Lan, H. Bai and L. Li, *Adv. Mater.*, 2016, **28**, 1703–1708.
31 Z. Tang, Z. Zhang, Y. Wang, S. C. Glotzer and N. A. Kotov, *Science*, 2006, **314**, 274–278.
32 D. J. Late, B. Liu, H. S. S. R. Matte, C. N. R. Rao and V. P. Dravid, *Adv. Funct. Mater.*, 2012, **22**, 1894–1905.
33 Z. Lin, Y. Liu, U. Halim, M. Ding, Y. Liu, Y. Wang, C. Jia, P. Chen, X. Duan, C. Wang, F. Song, M. Li, C. Wan, Y. Huang and X. Duan, *Nature*, 2018, **562**, 254–258.
34 J. Zheng, H. Zhang, S. Dong, Y. Liu, C. Tai Nai, H. Suk Shin, H. Young Jeong, B. Liu and K. Ping Loh, *Nat. Commun.*, 2014, **5**, 2995.
35 B. Huo, B. Liu, T. Chen, L. Cui, G. Xu, M. Liu and J. Liu, *Langmuir*, 2017, **33**, 10673–10678.
36 Y. Kubota, K. Watanabe, O. Tsuda and T. Taniguchi, *Science*, 2007, **317**, 932–934.
37 C. Lee, Q. Li, W. Kalb, X.-Z. Liu, H. Berger, R. W. Carpick and J. Hone, *Science*, 2010, **328**, 76–80.
38 Y. Lin, T. V. Williams, T.-B. Xu, W. Cao, H. E. Elsayed-Ali and J. W. Connell, *J. Phys. Chem. C*, 2011, **115**, 2679–2685.
39 J. D. Wood, S. A. Wells, D. Jariwala, K.-S. Chen, E. Cho, V. K. Sangwan, X. Liu, L. J. Lauhon, T. J. Marks and M. C. Hersam, *Nano Lett.*, 2014, **14**, 6964–6970.
40 J. Kang, S. A. Wells, V. K. Sangwan, D. Lam, X. Liu, J. Luxa, Z. Sofer and M. C. Hersam, *Adv. Mater.*, 2018, **30**, 1802990.
41 X. Zhang, P. Yu, H. Zhang, D. Zhang, X. Sun and Y. Ma, *Electrochim. Acta*, 2013, **89**, 523–529.
42 M. Liu, P.-Y. Chen and R. H. Hurt, *Adv. Mater.*, 2018, **30**, 1705080.
43 A. A. AbdelHamid, J. H. Soh, Y. Yu and J. Y. Ying, *Nano Energy*, 2018, **44**, 399–410.
44 R. Cai, D. Yang, K.-T. Lin, Y. Lyu, B. Zhu, Z. He, L. Zhang, Y. Kitamura, L. Qiu, X. Chen, Y. Zhao, Z. Chen and W. Tan, *J. Am. Chem. Soc.*, 2019, **141**, 1725–1734.
45 X. Rui, Z. Lu, H. Yu, D. Yang, H. H. Hng, T. M. Lim and Q. Yan, *Nanoscale*, 2013, **5**, 556–560.
46 X. Xiao, H. Yu, H. Jin, M. Wu, Y. Fang, J. Sun, Z. Hu, T. Li, J. Wu, L. Huang, Y. Gogotsi and J. Zhou, *ACS Nano*, 2017, **11**, 2180–2186.
47 M. Naguib, O. Mashtalir, J. Carle, V. Presser, J. Lu, L. Hultman, Y. Gogotsi and M. W. Barsoum, *ACS Nano*, 2012, **6**, 1322–1331.
48 Z. P. Xu and G. Q. Lu, *Chem. Mater.*, 2005, **17**, 1055–1062.
49 Y. Kuroda, K. Ito, K. Itabashi and K. Kuroda, *Langmuir*, 2011, **27**, 2028–2035.
50 S. Gao, Y. Lin, X. Jiao, Y. Sun, Q. Luo, W. Zhang, D. Li, J. Yang and Y. Xie, *Nature*, 2016, **529**, 68.
51 B. Mahler, V. Hoepfner, K. Liao and G. A. Ozin, *J. Am. Chem. Soc.*, 2014, **136**, 14121–14127.
52 W. Mai, Y. Zuo, X. Zhang, K. Leng, R. Liu, L. Chen, X. Lin, Y. Lin, R. Fu and D. Wu, *Chem. Commun.*, 2019, **55**, 10241–10244.
53 T. Yu, B. Lim and Y. N. Xia, *Angew. Chem., Int. Ed.*, 2010, **49**, 4484.
54 X. Huang, S. Li, Y. Huang, S. Wu, X. Zhou, S. Li, C. L. Gan, F. Boey, C. A. Mirkin and H. Zhang, *Nat. Commun.*, 2011, **2**, 292.
55 W. Cheng, J. He, T. Yao, Z. Sun, Y. Jiang, Q. Liu, S. Jiang, F. Hu, Z. Xie, B. He, W. Yan and S. Wei, *J. Am. Chem. Soc.*, 2014, **136**, 10393–10398.
56 X.-J. Wu, X. Huang, X. Qi, H. Li, B. Li and H. Zhang, *Angew. Chem., Int. Ed.*, 2014, **53**, 8929–8933.
57 P. Simon, L. Bahrig, I. A. Baburin, P. Formanek, F. Roder, J. Sickmann, S. G. Hickey, A. Eychmuller, H. Lichte, R. Kniep and E. Rosseeva, *Adv. Mater.*, 2014, **26**, 3042.
58 Z. Wu, J. Liu, Y. Li, Z. Cheng, T. Li, H. Zhang, Z. Lu and B. Yang, *ACS Nano*, 2015, **9**, 6315–6323.
59 S. Acharya, B. Das, U. Thupakula, K. Ariga, D. D. Sarma, J. Israelachvili and Y. Golan, *Nano Lett.*, 2013, **13**, 409–415.
60 J. Niu, D. Wang, H. Qin, X. Xiong, P. Tan, Y. Li, R. Liu, X. Lu, J. Wu and T. Zhang, *Nat. Commun.*, 2014, **5**, 3313.
61 K. S. Novoselov, A. K. Geim, S. V. Morozov, D. Jiang, Y. Zhang, S. V. Dubonos, I. V. Grigorieva and A. A. Firsov, *Science*, 2004, **306**, 666.
62 K. S. Novoselov, A. K. Geim, S. V. Morozov, D. Jiang, M. I. Katsnelson, I. V. Grigorieva, S. V. Dubonos and A. A. Firsov, *Nature*, 2005, **438**, 197.
63 K. S. Novoselov, D. Jiang, F. Schedin, T. J. Booth, V. V. Khotkevich, S. V. Morozov and A. K. Geim, *Proc. Natl. Acad. Sci. U. S. A.*, 2005, **102**, 10451.
64 A. K. Geim and K. S. Novoselov, *Nat. Mater.*, 2007, **6**, 183.
65 H. Li, J. Wu, Z. Yin and H. Zhang, *Acc. Chem. Res.*, 2014, **47**, 1067–1075.
66 V. Goyal, D. Teweldebrhan and A. A. Balandin, *Appl. Phys. Lett.*, 2010, **97**, 133117.
67 P. Ares, F. Aguilar-Galindo, D. Rodríguez-San-Miguel, D. A. Aldave, S. Díaz-Tendero, M. Alcamí, F. Martín, J. Gómez-Herrero and F. Zamora, *Adv. Mater.*, 2016, **28**, 6332–6336.
68 Y. Huang, E. Sutter, N. N. Shi, J. Zheng, T. Yang, D. Englund, H. J. Gao and P. Sutter, *ACS Nano*, 2015, **9**, 10612.
69 Y. Hernandez, V. Nicolosi, M. Lotya, F. M. Blighe, Z. Sun, S. De, I. T. McGovern, B. Holland, M. Byrne and Y. K. Gun'Ko, *Nat. Nanotechnol.*, 2008, **3**, 563.
70 L. X. Xu, J. W. McGraw, F. Gao, M. Grundy, Z. B. Ye, Z. Y. Gu and J. L. Shepherd, *J. Phys. Chem. C*, 2013, **117**, 10730.
71 A. O'neill, U. Khan, P. N. Nirmalraj, J. Boland and J. N. Coleman, *J. Phys. Chem. C*, 2011, **115**, 5422.
72 J. N. Coleman, M. Lotya, A. O'Neill, S. D. Bergin, P. J. King, U. Khan, K. Young, A. Gaucher, S. De and R. J. Smith, *Science*, 2011, **331**, 568.
73 J. Kim, S. Kwon, D.-H. Cho, B. Kang, H. Kwon, Y. Kim, S. O. Park, G. Y. Jung, E. Shin, W.-G. Kim, H. Lee, G. H. Ryu,

M. Choi, T. H. Kim, J. Oh, S. Park, S. K. Kwak, S. W. Yoon, D. Byun, Z. Lee and C. Lee, *Nat. Commun.*, 2015, **6**, 8294.
74 X. Dong, Y. Shi, Y. Zhao, D. Chen, J. Ye, Y. Yao, F. Gao, Z. Ni, T. Yu, Z. Shen, Y. Huang, P. Chen and L.-J. Li, *Phys. Rev. Lett.*, 2009, **102**, 135501.
75 M. Zhang, R. R. Parajuli, D. Mastrogiovanni, B. Dai, P. Lo, W. Cheung, R. Brukh, P. L. Chiu, T. Zhou and Z. Liu, *Small*, 2010, **6**, 1100–1107.
76 D. Parviz, S. Das, H. S. T. Ahmed, F. Irin, S. Bhattacharia and M. J. Green, *ACS Nano*, 2012, **6**, 8857–8867.
77 A. Ciesielski and P. Samorì, *Chem. Soc. Rev.*, 2014, **43**, 381–398.
78 S. Eigler and A. Hirsch, *Angew. Chem., Int. Ed.*, 2014, **53**, 7720–7738.
79 Y. T. Liang and M. C. Hersam, *J. Am. Chem. Soc.*, 2010, **132**, 17661.
80 R. J. Smith, P. J. King, M. Lotya, C. Wirtz, U. Khan, S. De, A. O'Neill, G. S. Duesberg, J. C. Grunlan and G. Moriarty, *Adv. Mater.*, 2011, **23**, 3944.
81 G. Guan, S. Zhang, S. Liu, Y. Cai, M. Low, C. P. Teng, I. Y. Phang, Y. Cheng, K. L. Duei and B. M. Srinivasan, *J. Am. Chem. Soc.*, 2015, **137**, 6152.
82 P. May, U. Khan, J. M. Hughes and J. N. Coleman, *J. Phys. Chem. C*, 2012, **116**, 11393.
83 K. R. Paton, E. Varrla, C. Backes, R. J. Smith, U. Khan, A. O'Neill, C. Boland, M. Lotya, O. M. Istrate and P. King, *Nat. Mater.*, 2014, **13**, 624.
84 E. Varrla, C. Backes, K. R. Paton, A. Harvey, Z. Gholamvand, J. McCauley and J. N. Coleman, *Chem. Mater.*, 2015, **27**, 1129–1139.
85 D. Voiry, A. Mohite and M. Chhowalla, *Chem. Soc. Rev.*, 2015, **44**, 2702–2712.
86 L. Niu, M. Li, X. Tao, Z. Xie, X. Zhou, A. P. A. Raju, R. J. Young and Z. Zheng, *Nanoscale*, 2013, **5**, 7202–7208.
87 X. Fan, W. Peng, Y. Li, X. Li, S. Wang, G. Zhang and F. Zhang, *Adv. Mater.*, 2008, **20**, 4490.
88 K. Erickson, R. Erni, Z. Lee, N. Alem, W. Gannett and A. Zettl, *Adv. Mater.*, 2010, **22**, 4467.
89 X. Huang, X. Qi, F. Boey and H. Zhang, *Chem. Soc. Rev.*, 2012, **41**, 666–686.
90 M. Naguib, V. N. Mochalin, M. W. Barsoum and Y. Gogotsi, *Adv. Mater.*, 2014, **26**, 992.
91 X. Wang, S. Kajiyama, H. Iinuma, E. Hosono, S. Oro, I. Moriguchi, M. Okubo and A. Yamada, *Nat. Commun.*, 2015, **6**, 6544.
92 J. Halim, S. Kota, M. R. Lukatskaya, M. Naguib, M. Q. Zhao, E. J. Moon, J. Pitock, J. Nanda, S. J. May, Y. Gogotsi and M. W. Barsou, *Adv. Funct. Mater.*, 2016, **26**, 3118.
93 P. Urbankowski, B. Anasori, T. Makaryan, D. Er, S. Kota, P. L. Walsh, M. Zhao, V. B. Shenoy, M. W. Barsouma and Y. Gogotsi, *Nanoscale*, 2016, **8**, 11385.
94 B. Anasori, Y. Xie, M. Beidaghi, J. Lu, B. Hosler, L. Hultman, P. Kent, Y. Gogotsi and M. W. Barsoum, *ACS Nano*, 2015, **9**, 9507.
95 K. Sano, Y. S. Kim, Y. Ishida, Y. Ebina, T. Sasaki, T. Hikima and T. Aida, *Nat. Commun.*, 2016, **7**, 12559.
96 I. Chowdhury, M. C. Duch, N. D. Mansukhani, M. C. Hersam and D. Bouchard, *Environ. Sci. Technol.*, 2013, **47**, 6288–6296.
97 G. R. Wiese and T. W. Healy, *Trans. Faraday Soc.*, 1970, **66**, 490–499.
98 T. Missana and A. Adell, *J. Colloid Interface Sci.*, 2000, **230**, 150–156.
99 P. He, A. F. Mejia, Z. D. Cheng, D. Z. Sun, H. J. Sue, D. S. Dinair and M. Marquez, *Phys. Rev. E*, 2010, **81**, 026310.
100 X. Sun, D. Luo, J. Liu and D. G. Evans, *ACS Nano*, 2010, **4**, 3381–3389.
101 J. I. Paredes, S. Villar-Rodil, A. Martínez-Alonso and J. M. D. Tascón, *Langmuir*, 2008, **24**, 10560–10564.
102 M. Bystrzejewski, A. Huczko and H. Lange, *Mater. Chem. Phys.*, 2008, **107**, 322–327.
103 J. N. Coleman, M. Lotya, A. O'Neill, S. D. Bergin, P. J. King, U. Khan, K. Young, A. Gaucher, S. De, R. J. Smith, I. V. Shvets, S. K. Arora, G. Stanton, H.-Y. Kim, K. Lee, G. T. Kim, G. S. Duesberg, T. Hallam, J. J. Boland, J. J. Wang, J. F. Donegan, J. C. Grunlan, G. Moriarty, A. Shmeliov, R. J. Nicholls, J. M. Perkins, E. M. Grieveson, K. Theuwissen, D. W. McComb, P. D. Nellist and V. Nicolosi, *Science*, 2011, **331**, 568–571.
104 G. Cunningham, M. Lotya, C. S. Cucinotta, S. Sanvito, S. D. Bergin, R. Menzel, M. S. P. Shaffer and J. N. Coleman, *ACS Nano*, 2012, **6**, 3468–3480.
105 Y. Hernandez, M. Lotya, D. Rickard, S. D. Bergin and J. N. Coleman, *Langmuir*, 2010, **26**, 3208–3213.
106 B. Schmatz, A. W. Lang and J. R. Reynolds, *Adv. Funct. Mater.*, 2019, DOI: 10.1002/adfm.201905266.
107 K.-G. Zhou, N.-N. Mao, H.-X. Wang, Y. Peng and H.-L. Zhang, *Angew. Chem., Int. Ed.*, 2011, **50**, 10839–10842.
108 M. Yi, Z. Shen, S. Ma and X. Zhang, *J. Nanopart. Res.*, 2012, **14**, 1003.
109 X. Li, Y. Qin, C. Liu, S. Jiang, L. Xiong and Q. Sun, *Food Chem.*, 2016, **199**, 356–363.
110 J. K. Lim, S. A. Majetich and R. D. Tilton, *Langmuir*, 2009, **25**, 13384–13393.
111 A. Gupta, V. Arunachalam and S. Vasudevan, *J. Phys. Chem. Lett.*, 2015, **6**, 739–744.
112 S. G. Hashmi, T. Moehl, J. Halme, Y. Ma, T. Saukkonen, A. Yella, F. Giordano, J. D. Decoppet, S. M. Zakeeruddin, P. Lund and M. Grätzel, *J. Mater. Chem. A*, 2014, **2**, 19609–19615.
113 R. J. Smith, P. J. King, M. Lotya, C. Wirtz, U. Khan, S. De, A. O'Neill, G. S. Duesberg, J. C. Grunlan, G. Moriarty, J. Chen, J. Wang, A. I. Minett, V. Nicolosi and J. N. Coleman, *Adv. Mater.*, 2011, **23**, 3944–3948.
114 R. C. T. Howe, R. I. Woodward, G. Hu, Z. Yang, E. J. R. Kelleher and T. Hasan, *Phys. Status Solidi B*, 2016, **253**, 911–917.
115 J. N. Coleman, *Adv. Funct. Mater.*, 2009, **19**, 3680–3695.
116 T. Hasan, F. Torrisi, Z. Sun, D. Popa, V. Nicolosi, G. Privitera, F. Bonaccorso and A. C. Ferrari, *Phys. Status Solidi B*, 2010, **247**, 2953–2957.
117 P. K. Misra, B. K. Mishra and G. B. Behera, *Colloids Surf.*, 1991, **57**, 1–10.

118 S. G. Hashmi, M. Ozkan, J. Halme, K. D. Misic, S. M. Zakeeruddin, J. Paltakari, M. Grätzel and P. D. Lund, *Nano Energy*, 2015, **17**, 206–215.
119 T. Hasan, Z. Sun, F. Wang, F. Bonaccorso, P. H. Tan, A. G. Rozhin and A. C. Ferrari, *Adv. Mater.*, 2009, **21**, 3874–3899.
120 L. Guardia, M. J. Fernández-Merino, J. I. Paredes, P. Solís-Fernández, S. Villar-Rodil, A. Martínez-Alonso and J. M. D. Tascón, *Carbon*, 2011, **49**, 1653–1662.
121 A. Ciesielski, S. Haar, M. El Gemayel, H. Yang, J. Clough, G. Melinte, M. Gobbi, E. Orgiu, M. V. Nardi, G. Ligorio, V. Palermo, N. Koch, O. Ersen, C. Casiraghi and P. Samorì, *Angew. Chem., Int. Ed.*, 2014, **53**, 10355–10361.
122 Y. T. Liang and M. C. Hersam, *J. Am. Chem. Soc.*, 2010, **132**, 17661–17663.
123 F. Kim, B. Kwon, Y. Eom, J. E. Lee, S. Park, S. Jo, S. H. Park, B.-S. Kim, H. J. Im, M. H. Lee, T. S. Min, K. T. Kim, H. G. Chae, W. P. King and J. S. Son, *Nat. Energy*, 2018, **3**, 301–309.
124 J. Li, M. M. Naiini, S. Vaziri, M. C. Lemme and M. Östling, *Adv. Funct. Mater.*, 2014, **24**, 6524–6531.
125 D. McManus, S. Vranic, F. Withers, V. Sanchez-Romaguera, M. Macucci, H. Yang, R. Sorrentino, K. Parvez, S.-K. Son, G. Iannaccone, K. Kostarelos, G. Fiori and C. Casiraghi, *Nat. Nanotechnol.*, 2017, **12**, 343.
126 X. Ma, Z. Xie, Z. Yang, G. Zeng, M. Xue and X. Zhang, *Mater. Res. Express*, 2018, **6**, 015025.
127 P. He, J. R. Brent, H. Ding, J. Yang, D. J. Lewis, P. O'Brien and B. Derby, *Nanoscale*, 2018, **10**, 5599–5606.
128 W. Yang, J. Yang, J. J. Byun, F. P. Moissinac, J. Xu, S. J. Haigh, M. Domingos, M. A. Bissett, R. A. W. Dryfe and S. Barg, *Adv. Mater.*, 2019, **0**, 1902725.
129 T. Varghese, C. Hollar, J. Richardson, N. Kempf, C. Han, P. Gamarachchi, D. Estrada, R. J. Mehta and Y. Zhang, *Sci. Rep.*, 2016, **6**, 33135.
130 M. Saeidi-Javash, W. Kuang, C. Dun and Y. Zhang, *Adv. Funct. Mater.*, 2019, **29**, 1901930.
131 T. Carey, S. Cacovich, G. Divitini, J. Ren, A. Mansouri, J. M. Kim, C. Wang, C. Ducati, R. Sordan and F. Torrisi, *Nat. Commun.*, 2017, **8**, 1202.
132 S. Santra, G. Hu, R. C. T. Howe, A. De Luca, S. Z. Ali, F. Udrea, J. W. Gardner, S. K. Ray, P. K. Guha and T. Hasan, *Sci. Rep.*, 2015, **5**, 17374.
133 J. Baker, D. Deganello, D. T. Gethin and T. M. Watson, *Mater. Res. Innovations*, 2014, **18**, 86–90.
134 E. B. Secor, S. Lim, H. Zhang, C. D. Frisbie, L. F. Francis and M. C. Hersam, *Adv. Mater.*, 2014, **26**, 4533–4538.
135 Y. Xu, M. G. Schwab, A. J. Strudwick, I. Hennig, X. Feng, Z. Wu and K. Müllen, *Adv. Energy Mater.*, 2013, **3**, 1035–1040.
136 K. Fu, Y. Wang, C. Yan, Y. Yao, Y. Chen, J. Dai, S. Lacey, Y. Wang, J. Wan, T. Li, Z. Wang, Y. Xu and L. Hu, *Adv. Mater.*, 2016, **28**, 2587–2594.
137 G. Xiao, Y. Li, W. Shi, L. Shen, Q. Chen and L. Huang, *Appl. Surf. Sci.*, 2017, **404**, 334–341.
138 G. Pangalos, J. M. Dealy and M. B. Lyne, *J. Rheol.*, 1985, **29**, 471–491.
139 X. Yang, C. Guo, L. Ji, Y. Li and Y. Tu, *Langmuir*, 2013, **29**, 8103–8107.
140 D. Kleshchanok, M. Heinen, G. Nägele and P. Holmqvist, *Soft Matter*, 2012, **8**, 1584–1592.
141 A. Goldschmidt and H.-J. Streitberger, *BASF Handbook on Basics of Coating Technology*, William Andrew, 2003.
142 C. B. Highley, C. B. Rodell and J. A. Burdick, *Adv. Mater.*, 2015, **27**, 5075–5079.
143 W. A. Zisman, in *Contact Angle, Wettability, and Adhesion*, American Chemical Society, 1964, ch. 1, vol. 43, pp. 1–51.
144 G. Pariani, R. Castagna, L. Oggioni, L. Colella, A. Nardi, S. Anzani, C. Bertarelli and A. Bianco, *Adv. Mater. Technol.*, 2018, **3**, 1700325.
145 B. Xin and J. Hao, *Chem. Soc. Rev.*, 2010, **39**, 769–782.
146 W.-K. Lee, W.-B. Jung, D. Rhee, J. Hu, Y.-A. L. Lee, C. Jacobson, H.-T. Jung and T. W. Odom, *Adv. Mater.*, 2018, **30**, 1706657.
147 M. Zeng, P. Wang, J. Luo, B. Peng, B. Ding, L. Zhang, L. Wang, D. Huang, I. Echols, E. Abo Deeb, E. Bordovsky, C.-H. Choi, C. Ybanez, P. Meras, E. Situ, M. S. Mannan and Z. Cheng, *ACS Appl. Mater. Interfaces*, 2018, **10**, 22793–22800.
148 T. Trantidou, Y. Elani, E. Parsons and O. Ces, *Microsyst. Nanoeng.*, 2017, **3**, 16091.
149 G. Hu, T. Albrow-Owen, X. Jin, A. Ali, Y. Hu, R. C. T. Howe, K. Shehzad, Z. Yang, X. Zhu, R. I. Woodward, T.-C. Wu, H. Jussila, J.-B. Wu, P. Peng, P.-H. Tan, Z. Sun, E. J. R. Kelleher, M. Zhang, Y. Xu and T. Hasan, *Nat. Commun.*, 2017, **8**, 278.
150 P. G. Campbell, E. D. Miller, G. W. Fisher, L. M. Walker and L. E. Weiss, *Biomaterials*, 2005, **26**, 6762–6770.
151 T. Jungst, W. Smolan, K. Schacht, T. Scheibel and J. Groll, *Chem. Rev.*, 2016, **116**, 1496–1539.
152 H. Sirringhaus, T. Kawase, R. H. Friend, T. Shimoda, M. Inbasekaran, W. Wu and E. P. Woo, *Science*, 2000, **290**, 2123–2126.
153 R. Cobas, S. Muñoz-Pérez, S. Cadogan, M. C. Ridgway and X. Obradors, *Adv. Funct. Mater.*, 2015, **25**, 768–775.
154 R. E. Saunders and B. Derby, *Int. Mater. Rev.*, 2014, **59**, 430–448.
155 D. Soltman and V. Subramanian, *Langmuir*, 2008, **24**, 2224–2231.
156 R. D. Deegan, O. Bakajin, T. F. Dupont, G. Huber, S. R. Nagel and T. A. Witten, *Nature*, 1997, **389**, 827–829.
157 Y. Li, Q. Yang, M. Li and Y. Song, *Sci. Rep.*, 2016, **6**, 24628.
158 S. V. Murphy and A. Atala, *Nat. Biotechnol.*, 2014, **32**, 773.
159 T. J. Coogan and D. O. Kazmer, *J. Rheol.*, 2019, **63**, 141–155.
160 K. Arapov, E. Rubingh, R. Abbel, J. Laven, G. de With and H. Friedrich, *Adv. Funct. Mater.*, 2016, **26**, 586–593.
161 S. J. Rowley-Neale, G. C. Smith and C. E. Banks, *ACS Appl. Mater. Interfaces*, 2017, **9**, 22539–22548.
162 L. Chen, L. Huang, Y. Lin, L. Sai, Q. Chang, W. Shi and Q. Chen, *Sens. Actuators, B*, 2018, **255**, 1482–1490.
163 C. Dun, W. Kuang, N. Kempf, M. Saeidi-Javash, D. J. Singh and Y. Zhang, *Adv. Sci.*, 2019, in press.
164 M. S. Saleh, C. Hu and R. Panat, *Sci. Adv.*, 2017, **3**, e1601986.

165 F. Withers, H. Yang, L. Britnell, A. P. Rooney, E. Lewis, A. Felten, C. R. Woods, V. Sanchez Romaguera, T. Georgiou, A. Eckmann, Y. J. Kim, S. G. Yeates, S. J. Haigh, A. K. Geim, K. S. Novoselov and C. Casiraghi, *Nano Lett.*, 2014, **14**, 3987–3992.
166 C. Casiraghi, M. Macucci, K. Parvez, R. Worsley, Y. Shin, F. Bronte, C. Borri, M. Paggi and G. Fiori, *Carbon*, 2018, **129**, 462–467.
167 K. Chi, Z. Zhang, J. Xi, Y. Huang, F. Xiao, S. Wang and Y. Liu, *ACS Appl. Mater. Interfaces*, 2014, **6**, 16312–16319.
168 C. Yuan, D. J. Roach, C. K. Dunn, Q. Mu, X. Kuang, C. M. Yakacki, T. J. Wang, K. Yu and H. J. Qi, *Soft Matter*, 2017, **13**, 5558–5568.
169 D. Zhang, B. Chi, B. Li, Z. Gao, Y. Du, J. Guo and J. Wei, *Synth. Met.*, 2016, **217**, 79–86.
170 Y. Liu, W. Zhang, F. Zhang, J. Leng, S. Pei, L. Wang, X. Jia, C. Cotton, B. Sun and T.-W. Chou, *Compos. Sci. Technol.*, 2019, **181**, 107692.
171 Y. Kim, H. Yuk, R. Zhao, S. A. Chester and X. Zhao, *Nature*, 2018, **558**, 274–279.
172 Y. Huang, H. Wu, L. Xiao, Y. Duan, H. Zhu, J. Bian, D. Ye and Z. Yin, *Mater. Horiz.*, 2019, **6**, 642–683.
173 Z. Yin, Y. Huang, N. Bu, X. Wang and Y. Xiong, *Chin. Sci. Bull.*, 2010, **55**, 3383–3407.
174 B.-J. de Gans and U. S. Schubert, *Macromol. Rapid Commun.*, 2003, **24**, 659–666.
175 J. Noh, D. Yeom, C. Lim, H. Cha, J. Han, J. Kim, Y. Park, V. Subramanian and G. Cho, *IEEE Trans. Electron. Packag. Manuf.*, 2010, **33**, 275–283.
176 F. Torrisi, T. Hasan, W. Wu, Z. Sun, A. Lombardo, T. S. Kulmala, G.-W. Hsieh, S. Jung, F. Bonaccorso, P. J. Paul, D. Chu and A. C. Ferrari, *ACS Nano*, 2012, **6**, 2992–3006.
177 E. B. Secor, P. L. Prabhumirashi, K. Puntambekar, M. L. Geier and M. C. Hersam, *J. Phys. Chem. Lett.*, 2013, **4**, 1347–1351.
178 J. Li, F. Ye, S. Vaziri, M. Muhammed, M. C. Lemme and M. Östling, *Adv. Mater.*, 2013, **25**, 3985–3992.
179 R. Danaei, T. Varghese, M. Ahmadzadeh, J. McCloy, C. Hollar, M. Sadeq Saleh, J. Park, Y. Zhang and R. Panat, *Adv. Eng. Mater.*, 2019, **21**, 1800800.
180 J. A. Paulsen, M. Renn, K. Christenson and R. Plourde, *2012 Future of Instrumentation International Workshop (FIIW) Proceedings*, Piscataway, NJ, 2012.
181 D. Zhao, T. Liu, J. G. Park, M. Zhang, J.-M. Chen and B. Wang, *Microelectron. Eng.*, 2012, **96**, 71–75.
182 C. Cao, J. B. Andrews and A. D. Franklin, *Adv. Electron. Mater.*, 2017, **3**, 1700057.
183 K. Wang, Y.-H. Chang, C. Zhang and B. Wang, *Carbon*, 2016, **98**, 397–403.
184 W. Xie, X. Zhang, C. Leighton and C. D. Frisbie, *Adv. Electron. Mater.*, 2017, **3**, 1600369.
185 Y. Xiao, Developing aerosol jet printable regenerated silk fibroin solutions, M.S. thesis, Georgia Institute of Technology, 2019.
186 R. Leach, *The Printing Ink Manual*, Springer Science & Business Media, 2012.
187 C. Xu, B. Xu, Y. Gu, Z. Xiong, J. Sun and X. S. Zhao, *Energy Environ. Sci.*, 2013, **6**, 1388–1414.
188 D. W. Zhang, X. D. Li, H. B. Li, S. Chen, Z. Sun, X. J. Yin and S. M. Huang, *Carbon*, 2011, **49**, 5382–5388.
189 A. M. Joseph, B. Nagendra, E. Bhoje Gowd and K. P. Surendran, *ACS Omega*, 2016, **1**, 1220–1228.
190 M. Jung, J. Kim, H. Koo, W. Lee, V. Subramanian and G. Cho, *J. Nanosci. Nanotechnol.*, 2014, **14**, 1303–1317.
191 J. Hast, M. Tuomikoski, R. Suhonen, K.-L. Väisänen, M. Välimäki, T. Maaninen, P. Apilo, A. Alastalo and A. Maanineny, *SID Symp. Dig. Tech. Pap.*, 2013, **44**, 192–195.
192 B. Y. Ahn, E. B. Duoss, M. J. Motala, X. Guo, S.-I. Park, Y. Xiong, J. Yoon, R. G. Nuzzo, J. A. Rogers and J. A. Lewis, *Science*, 2009, **323**, 1590–1593.
193 J. J. Adams, E. B. Duoss, T. F. Malkowski, M. J. Motala, B. Y. Ahn, R. G. Nuzzo, J. T. Bernhard and J. A. Lewis, *Adv. Mater.*, 2011, **23**, 1335–1340.
194 M. A. Skylar-Scott, S. Gunasekaran and J. A. Lewis, *Proc. Natl. Acad. Sci.*, 2016, **113**, 6137–6142.
195 J. A. Lewis, J. E. Smay, J. Stuecker and J. Cesarano, *J. Am. Ceram. Soc.*, 2006, **89**, 3599–3609.
196 E. García-Tuñon, S. Barg, J. Franco, R. Bell, S. Eslava, E. D'Elia, R. C. Maher, F. Guitian and E. Saiz, *Adv. Mater.*, 2015, **27**, 1688–1693.
197 Y. Zhang, F. Zhang, Z. Yan, Q. Ma, X. Li, Y. Huang and J. A. Rogers, *Nat. Rev. Mater.*, 2017, **2**, 17019.
198 P. C. Sherrell and C. Mattevi, *Mater. Today*, 2016, **19**, 428–436.
199 Y. Lin, Y. Gao, F. Fang and Z. Fan, *Nano Res.*, 2018, **11**, 3065–3087.
200 X. Wei, D. Li, W. Jiang, Z. Gu, X. Wang, Z. Zhang and Z. Sun, *Sci. Rep.*, 2015, **5**, 11181.
201 S. S. K. Mallineni, Y. Dong, H. Behlow, A. M. Rao and R. Podila, *Adv. Energy Mater.*, 2018, **8**, 1702736.
202 H. Ragones, S. Menkin, Y. Kamir, A. Gladkikh, T. Mukra, G. Kosa and D. Golodnitsky, *Sustainable Energy Fuels*, 2018, **2**, 1542–1549.
203 N. Singh, C. Galande, A. Miranda, A. Mathkar, W. Gao, A. L. M. Reddy, A. Vlad and P. M. Ajayan, *Sci. Rep.*, 2012, **2**, 481.
204 Q. Zhang, F. Zhang, S. P. Medarametla, H. Li, C. Zhou and D. Lin, *Small*, 2016, **12**, 1702–1708.
205 S. Tibbits, *Architectural Design*, 2014, **84**, 116–121.
206 R. Bogue, *Assembly Autom.*, 2014, **34**, 16–22.
207 E. Pei, *Assembly Autom.*, 2014, **34**, 310–314.
208 G. Liu, Y. Zhao, G. Wu and J. Lu, *Sci. Adv.*, 2018, **4**, eaat0641.
209 A. Sydney Gladman, E. A. Matsumoto, R. G. Nuzzo, L. Mahadevan and J. A. Lewis, *Nat. Mater.*, 2016, **15**, 413.
210 M. Acerce, E. K. Akdoğan and M. Chhowalla, *Nature*, 2017, **549**, 370.
211 Z. Lei, W. Zhu, S. Sun and P. Wu, *Nanoscale*, 2016, **8**, 18800–18807.
212 S. Dadbakhsh, M. Speirs, J.-P. Kruth, J. Schrooten, J. Luyten and J. Van Humbeeck, *Adv. Eng. Mater.*, 2014, **16**, 1140–1146.

213 D. Raviv, W. Zhao, C. McKnelly, A. Papadopoulou, A. Kadambi, B. Shi, S. Hirsch, D. Dikovsky, M. Zyracki, C. Olguin, R. Raskar and S. Tibbits, *Sci. Rep.*, 2014, **4**, 7422.
214 A. Kotikian, R. L. Truby, J. W. Boley, T. J. White and J. A. Lewis, *Adv. Mater.*, 2018, **30**, 1706164.
215 Q. Ge, H. J. Qi and M. L. Dunn, *Appl. Phys. Lett.*, 2013, **103**, 131901.
216 X.-Y. Tsai and L.-W. Chen, *Compos. Struct.*, 2002, **56**, 235–241.
217 W. Xu and D. H. Gracias, *ACS Nano*, 2019, **13**, 4883–4892.
218 D. Davis, R. Mailen, J. Genzer and M. D. Dickey, *RSC Adv.*, 2015, **5**, 89254–89261.
219 H. Yang, B. S. Yeow, T.-H. Chang, K. Li, F. Fu, H. Ren and P.-Y. Chen, *ACS Nano*, 2019, **13**, 5410–5420.
220 K. J. Stevenson, V. Ozoliņš and B. Dunn, *Acc. Chem. Res.*, 2013, **46**, 1051–1052.
221 Z. Yang, J. Zhang, M. C. W. Kintner-Meyer, X. Lu, D. Choi, J. P. Lemmon and J. Liu, *Chem. Rev.*, 2011, **111**, 3577–3613.
222 L. E. Bell, *Science*, 2008, **321**, 1457–1461.
223 G. J. Snyder and E. S. Toberer, *Nat. Mater.*, 2008, **7**, 105.
224 C. Dun, C. A. Hewitt, Q. Li, Y. Guo, Q. Jiang, J. Xu, G. Marcus, D. C. Schall and D. L. Carroll, *Adv. Mater.*, 2017, **29**, 1702968.
225 C. Dun, C. A. Hewitt, Q. Li, J. Xu, D. C. Schall, H. Lee, Q. Jiang and D. L. Carroll, *Adv. Mater.*, 2017, **29**, 1700070.
226 A. J. Minnich, M. S. Dresselhaus, Z. F. Ren and G. Chen, *Energy Environ. Sci.*, 2009, **2**, 466–479.
227 J. H. We, S. J. Kim and B. J. Cho, *Energy*, 2014, **73**, 506–512.
228 S. J. Kim, H. Choi, Y. Kim, J. H. We, J. S. Shin, H. E. Lee, M.-W. Oh, K. J. Lee and B. J. Cho, *Nano Energy*, 2017, **31**, 258–263.
229 Z. Lu, M. Layani, X. Zhao, L. P. Tan, T. Sun, S. Fan, Q. Yan, S. Magdassi and H. H. Hng, *Small*, 2014, **10**, 3551–3554.
230 L. Yang, Z.-G. Chen, M. S. Dargusch and J. Zou, *Adv. Energy Mater.*, 2018, **8**, 1701797.
231 M. Orrill and S. LeBlanc, *J. Appl. Polym. Sci.*, 2017, **134**, 44256.
232 B. Zhang, J. Sun, H. E. Katz, F. Fang and R. L. Opila, *ACS Appl. Mater. Interfaces*, 2010, **2**, 3170–3178.
233 T. Juntunen, H. Jussila, M. Ruoho, S. Liu, G. Hu, T. Albrow-Owen, L. W. T. Ng, R. C. T. Howe, T. Hasan, Z. Sun and I. Tittonen, *Adv. Funct. Mater.*, 2018, **28**, 1800480.
234 C. Han, G. Tan, T. Varghese, M. G. Kanatzidis and Y. Zhang, *ACS Energy Lett.*, 2018, **3**, 818–822.
235 M. Saeidijavash, W. Kuang, C. Dun and Y. Zhang, *Adv. Funct. Mater.*, 2019, **35**, 1901930.
236 Y. Shao, M. F. El-Kady, L. J. Wang, Q. Zhang, Y. Li, H. Wang, M. F. Mousavi and R. B. Kaner, *Chem. Soc. Rev.*, 2015, **44**, 3639–3665.
237 P. Simon and Y. Gogotsi, *Nat. Mater.*, 2008, **7**, 845.
238 R. Raccichini, A. Varzi, S. Passerini and B. Scrosati, *Nat. Mater.*, 2014, **14**, 271.
239 M. Xu, T. Liang, M. Shi and H. Chen, *Chem. Rev.*, 2013, **113**, 3766–3798.
240 C. W. Foster, M. P. Down, Y. Zhang, X. Ji, S. J. Rowley-Neale, G. C. Smith, P. J. Kelly and C. E. Banks, *Sci. Rep.*, 2017, **7**, 42233.
241 R. Gusmão, M. P. Browne, Z. Sofer and M. Pumera, *Electrochem. Commun.*, 2019, **102**, 83–88.
242 G. Sun, J. An, C. K. Chua, H. Pang, J. Zhang and P. Chen, *Electrochem. Commun.*, 2015, **51**, 33–36.
243 Y. Jiang, Z. Xu, T. Huang, Y. Liu, F. Guo, J. Xi, W. Gao and C. Gao, *Adv. Funct. Mater.*, 2018, **28**, 1707024.
244 C. Zhang, M. P. Kremer, A. Seral-Ascaso, S. H. Park, N. McEvoy, B. Anasori, Y. Gogotsi and V. Nicolosi, *Adv. Funct. Mater.*, 2018, **28**, 1705506.
245 S. D. Lacey, D. J. Kirsch, Y. Li, J. T. Morgenstern, B. C. Zarket, Y. Yao, J. Dai, L. Q. Garcia, B. Liu, T. Gao, S. Xu, S. R. Raghavan, J. W. Connell, Y. Lin and L. Hu, *Adv. Mater.*, 2018, **30**, 1705651.
246 K. Shen, H. Mei, B. Li, J. Ding and S. Yang, *Adv. Energy Mater.*, 2018, **8**, 1701527.
247 J. Ding, K. Shen, Z. Du, B. Li and S. Yang, *ACS Appl. Mater. Interfaces*, 2017, **9**, 41871–41877.
248 C. W. Foster, G.-Q. Zou, Y. Jiang, M. P. Down, C. M. Liauw, A. Garcia-Miranda Ferrari, X. Ji, G. C. Smith, P. J. Kelly and C. E. Banks, *Batteries Supercaps*, 2019, **2**, 448–453.
249 M. Shanmugam, C. A. Durcan, R. Jacobs-Gedrim and B. Yu, *Nano Energy*, 2013, **2**, 419–424.
250 J.-M. Yun, Y.-J. Noh, C.-H. Lee, S.-I. Na, S. Lee, S. M. Jo, H.-I. Joh and D.-Y. Kim, *Small*, 2014, **10**, 2319–2324.
251 J.-Y. Lin, C.-Y. Chan and S.-W. Chou, *Chem. Commun.*, 2013, **49**, 1440–1442.
252 D. Barpuzary, A. Banik, G. Gogoi and M. Qureshi, *J. Mater. Chem. A*, 2015, **3**, 14378–14388.
253 A. Agresti, S. Pescetelli, A. L. Palma, A. E. Del Rio Castillo, D. Konios, G. Kakavelakis, S. Razza, L. Cinà, E. Kymakis, F. Bonaccorso and A. Di Carlo, *ACS Energy Lett.*, 2017, **2**, 279–287.
254 X. Meng, X. Cui, M. Rager, S. Zhang, Z. Wang, J. Yu, Y. W. Harn, Z. Kang, B. K. Wagner, Y. Liu, C. Yu, J. Qiu and Z. Lin, *Nano Energy*, 2018, **52**, 123–133.
255 J. Yoon, H. Sung, G. Lee, W. Cho, N. Ahn, H. S. Jung and M. Choi, *Energy Environ. Sci.*, 2017, **10**, 337–345.
256 C.-C. Chung, S. Narra, E. Jokar, H.-P. Wu and E. Wei-Guang Diau, *J. Mater. Chem. A*, 2017, **5**, 13957–13965.
257 S. G. Hashmi, D. Martineau, X. Li, M. Ozkan, A. Tiihonen, M. I. Dar, T. Sarikka, S. M. Zakeeruddin, J. Paltakari, P. D. Lund and M. Grätzel, *Adv. Mater. Technol.*, 2017, **2**, 1600183.
258 H.-C. Fu, V. Ramalingam, H. Kim, C.-H. Lin, X. Fang, H. N. Alshareef and J.-H. He, *Adv. Energy Mater.*, 2019, **9**, 1900180.
259 X. Cao, C. Tan, X. Zhang, W. Zhao and H. Zhang, *Adv. Mater.*, 2016, **28**, 6167–6196.
260 F. Brunetti, A. Operamolla, S. Castro-Hermosa, G. Lucarelli, V. Manca, G. M. Farinola and T. M. Brown, *Adv. Funct. Mater.*, 2019, **29**, 1806798.
261 S. G. Hashmi, J. Halme, Y. Ma, T. Saukkonen and P. Lund, *Adv. Mater. Interfaces*, 2014, **1**, 1300055.
262 S. G. Hashmi, M. Özkan, J. Halme, S. M. Zakeeruddin, J. Paltakari, M. Grätzel and P. D. Lund, *Energy Environ. Sci.*, 2016, **9**, 2453–2462.

263 D. Dodoo-Arhin, R. C. T. Howe, G. Hu, Y. Zhang, P. Hiralal, A. Bello, G. Amaratunga and T. Hasan, *Carbon*, 2016, **105**, 33–41.
264 Y. Chen, D. Wang, Y. Lin, X. Zou and T. Xie, *Electrochim. Acta*, 2019, **316**, 248–256.
265 D. S. Hecht, L. Hu and G. Irvin, *Adv. Mater.*, 2011, **23**, 1482–1513.
266 X. Ling, H. Wang, S. Huang, F. Xia and M. S. Dresselhaus, *Proc. Natl. Acad. Sci.*, 2015, **112**, 4523–4530.
267 T.-Y. Kim, J. Ha, K. Cho, J. Pak, J. Seo, J. Park, J.-K. Kim, S. Chung, Y. Hong and T. Lee, *ACS Nano*, 2017, **11**, 10273–10280.
268 K. K. Manga, S. Wang, M. Jaiswal, Q. Bao and K. P. Loh, *Adv. Mater.*, 2010, **22**, 5265–5270.
269 S. Wu, Z. Zeng, Q. He, Z. Wang, S. J. Wang, Y. Du, Z. Yin, X. Sun, W. Chen and H. Zhang, *Small*, 2012, **8**, 2264–2270.
270 K.-J. Huang, L. Wang, Y.-J. Liu, T. Gan, Y.-M. Liu, L.-L. Wang and Y. Fan, *Electrochim. Acta*, 2013, **107**, 379–387.
271 J. Li, Z. Yang, Y. Tang, Y. Zhang and X. Hu, *Biosens. Bioelectron.*, 2013, **41**, 698–703.
272 T.-W. Lin, C.-J. Liu and C.-S. Dai, *Appl. Catal., B*, 2014, **154–155**, 213–220.
273 V. Dua, S. P. Surwade, S. Ammu, S. R. Agnihotra, S. Jain, K. E. Roberts, S. Park, R. S. Ruoff and S. K. Manohar, *Angew. Chem., Int. Ed.*, 2010, **49**, 2154–2157.
274 J. H. Kim, W. S. Chang, D. Kim, J. R. Yang, J. T. Han, G.-W. Lee, J. T. Kim and S. K. Seol, *Adv. Mater.*, 2015, **27**, 157–161.
275 P. Liu, A. T. Liu, D. Kozawa, J. Dong, J. F. Yang, V. B. Koman, M. Saccone, S. Wang, Y. Son, M. H. Wong and M. S. Strano, *Nat. Mater.*, 2018, **17**, 1005–1012.
276 C. Anichini, W. Czepa, D. Pakulski, A. Aliprandi, A. Ciesielski and P. Samorì, *Chem. Soc. Rev.*, 2018, **47**, 4860–4908.
277 Y. Yuan, R. Li and Z. Liu, *Anal. Chem.*, 2014, **86**, 3610–3615.
278 C.-H. Lu, H.-H. Yang, C.-L. Zhu, X. Chen and G.-N. Chen, *Angew. Chem., Int. Ed.*, 2009, **48**, 4785–4787.
279 S. Mao, J. Chang, H. Pu, G. Lu, Q. He, H. Zhang and J. Chen, *Chem. Soc. Rev.*, 2017, **46**, 6872–6904.
280 C. Singhal, M. Khanuja, N. Chaudhary, C. S. Pundir and J. Narang, *Sci. Rep.*, 2018, **8**, 7734.
281 X. Gan, H. Zhao and X. Quan, *Biosens. Bioelectron.*, 2017, **89**, 56–71.
282 B. Ryu, H. Nam, B.-R. Oh, Y. Song, P. Chen, Y. Park, W. Wan, K. Kurabayashi and X. Liang, *ACS Sens.*, 2017, **2**, 274–281.
283 M. Kukkar, A. Sharma, P. Kumar, K.-H. Kim and A. Deep, *Anal. Chim. Acta*, 2016, **939**, 101–107.
284 D. Katerinopoulou, P. Zalar, J. Sweelssen, G. Kiriakidis, C. Rentrop, P. Groen, G. H. Gelinck, J. van den Brand and E. C. P. Smits, *Adv. Electron. Mater.*, 2019, **5**, 1800605.
285 C. Bali, A. Brandlmaier, A. Ganster, O. Raab, J. Zapf and A. Hübler, *Mater. Today: Proc.*, 2016, **3**, 739–745.
286 J. Zikulnig, C. Hirschl, L. Rauter, M. Krivec, H. Lammer, F. Riemelmoser and A. Roshanghias, *Flexible Printed Electron.*, 2019, **4**, 015008.
287 D. Kong, L. T. Le, Y. Li, J. L. Zunino and W. Lee, *Langmuir*, 2012, **28**, 13467–13472.
288 S. Afroj, N. Karim, Z. Wang, S. Tan, P. He, M. Holwill, D. Ghazaryan, A. Fernando and K. S. Novoselov, *ACS Nano*, 2019, **13**, 3847–3857.
289 J. Zhao, Y. Zhang, Y. Huang, X. Zhao, Y. Shi, J. Qu, C. Yang, J. Xie, J. Wang, L. Li, Q. Yan, S. Hou, C. Lu, X. Xu and Y. Yao, *J. Mater. Chem. A*, 2019, **7**, 972–978.
290 T. Vuorinen, J. Niittynen, T. Kankkunen, T. M. Kraft and M. Mäntysalo, *Sci. Rep.*, 2016, **6**, 35289.
291 T.-H. Chang, K. Li, H. Yang and P.-Y. Chen, *Adv. Mater.*, 2018, **30**, 1802418.
292 X. Shi, S. Liu, Y. Sun, J. Liang and Y. Chen, *Adv. Funct. Mater.*, 2018, **28**, 1800850.
293 H. Song, I. Karakurt, M. Wei, N. Liu, Y. Chu, J. Zhong and L. Lin, *Nano Energy*, 2018, **49**, 7–13.
294 Z. Chen, Y. Hu, H. Zhuo, L. Liu, S. Jing, L. Zhong, X. Peng and R.-c. Sun, *Chem. Mater.*, 2019, **31**, 3301–3312.
295 G. Hassan, J. Bae, A. Hassan, S. Ali, C. H. Lee and Y. Choi, *Composites, Part A*, 2018, **107**, 519–528.
296 J. Z. Gul, M. Sajid and K. H. Choi, *J. Mater. Chem. C*, 2019, **7**, 4692–4701.
297 X. Fan, N. Wang, F. Yan, J. Wang, W. Song and Z. Ge, *Adv. Mater. Technol.*, 2018, **3**, 1800030.
298 R. Zhang, B. Peng and Y. Yuan, *Compos. Sci. Technol.*, 2018, **168**, 118–125.
299 P. Kruse, *J. Phys. D: Appl. Phys.*, 2018, **51**, 203002.
300 Q. Yang, A. J. Yu, J. Simonton, G. Yang, Y. Dohrmann, Z. Kang, Y. Li, J. Mo and F.-Y. Zhang, *J. Mater. Chem. A*, 2017, **5**, 17841–17847.
301 H. An, T. Habib, S. Shah, H. Gao, A. Patel, I. Echols, X. Zhao, M. Radovic, M. J. Green and J. L. Lutkenhaus, *ACS Appl. Nano Mater.*, 2019, **2**, 948–955.
302 S.-J. Choi, H. Yu, J.-S. Jang, M.-H. Kim, S.-J. Kim, H. S. Jeong and I.-D. Kim, *Small*, 2018, **14**, 1703934.
303 Z. Zhen, Z. Li, X. Zhao, Y. Zhong, L. Zhang, Q. Chen, T. Yang and H. Zhu, *Small*, 2018, **14**, 1703848.
304 Z. Yang, A. Liu, C. Wang, F. Liu, J. He, S. Li, J. Wang, R. You, X. Yan, P. Sun, Y. Duan and G. Lu, *ACS Sens.*, 2019, **4**, 1261–1269.
305 P. Yasaei, A. Behranginia, T. Foroozan, M. Asadi, K. Kim, F. Khalili-Araghi and A. Salehi-Khojin, *ACS Nano*, 2015, **9**, 9898–9905.
306 D. J. Late, *Microporous Mesoporous Mater.*, 2016, **225**, 494–503.
307 M. B. Erande, M. S. Pawar and D. J. Late, *ACS Appl. Mater. Interfaces*, 2016, **8**, 11548–11556.
308 D. S. Dolzhnikov, H. Zhang, J. Jang, J. S. Son, M. G. Panthani, T. Shibata, S. Chattopadhyay and D. V. Talapin, *Science*, 2015, **347**, 425–428.
309 D. Luo, F. Wang, J. Zhu, F. Cao, Y. Liu, X. Li, R. C. Willson, Z. Yang, C.-W. Chu and Z. Ren, *Proc. Natl. Acad. Sci.*, 2016, 201608135.
310 I. Raj, M. Qu, L. Xiao, J. Hou, Y. Li, T. Liang, T. Yang and M. Zhao, *Fuel*, 2019, **251**, 514–522.
311 J. Luo, M. Zeng, B. Peng, Y. Tang, L. Zhang, P. Wang, L. He, D. Huang, L. Wang, X. Wang, M. Chen, S. Lei, P. Lin,

Y. Chen and Z. Cheng, *Angew. Chem., Int. Ed.*, 2018, **57**, 11752–11757.

312 L. Zhang, Q. Lei, J. Luo, M. Zeng, L. Wang, D. Huang, X. Wang, S. Mannan, B. Peng and Z. Cheng, *Sci. Rep.*, 2019, **9**, 163.

313 X. Wang, M. Zeng, Y.-H. Yu, H. Wang, M. S. Mannan and Z. Cheng, *ACS Appl. Mater. Interfaces*, 2017, **9**, 7852–7858.

314 S. G. Bucella, A. Luzio, E. Gann, L. Thomsen, C. R. McNeill, G. Pace, A. Perinot, Z. Chen, A. Facchetti and M. Caironi, *Nat. Commun.*, 2015, **6**, 8394.

315 M. Shusteff, A. E. M. Browar, B. E. Kelly, J. Henriksson, T. H. Weisgraber, R. M. Panas, N. X. Fang and C. M. Spadaccini, *Sci. Adv.*, 2017, **3**, eaao5496.

316 B. E. Kelly, I. Bhattacharya, H. Heidari, M. Shusteff, C. M. Spadaccini and H. K. Taylor, *Science*, 2019, **363**, 1075–1079.

317 A. Reiser, M. Lindén, P. Rohner, A. Marchand, H. Galinski, A. S. Sologubenko, J. M. Wheeler, R. Zenobi, D. Poulikakos and R. Spolenak, *Nat. Commun.*, 2019, **10**, 1853.

318 X. Chen, X. Liu, M. Ouyang, J. Chen, O. Taiwo, Y. Xia, P. R. N. Childs, N. P. Brandon and B. Wu, *Sci. Rep.*, 2019, **9**, 3973.

319 J. T. Muth, D. M. Vogt, R. L. Truby, Y. Mengüç, D. B. Kolesky, R. J. Wood and J. A. Lewis, *Adv. Mater.*, 2014, **26**, 6307–6312.

320 H. Cui, R. Hensleigh, D. Yao, D. Maurya, P. Kumar, M. G. Kang, S. Priya and X. Zheng, *Nat. Mater.*, 2019, **18**, 234–241.

321 M. Zeng, D. King, D. Huang, C. Do, L. Wang, M. Chen, S. Lei, P. Lin, Y. Chen and Z. Cheng, *Proc. Natl. Acad. Sci.*, 2019, 201906511, DOI: 10.1073/pnas.1906511116.

322 M. Chen, A. Shinde, L. Wang, C. Ye, M. Zeng, Q. Yan, P. Lin, Y. Chen and Z. Cheng, *2D Materials*, 2019, **6**, 025031.

323 G. Xin, W. Zhu, Y. Deng, J. Cheng, L. T. Zhang, A. J. Chung, S. De and J. Lian, *Nat. Nanotechnol.*, 2019, **14**, 168–175.

324 Y. Xia, T. S. Mathis, M.-Q. Zhao, B. Anasori, A. Dang, Z. Zhou, H. Cho, Y. Gogotsi and S. Yang, *Nature*, 2018, **557**, 409.

325 D. Voiry, J. Yang, J. Kupferberg, R. Fullon, C. Lee, H. Y. Jeong, H. S. Shin and M. Chhowalla, *Science*, 2016, **353**, 1413–1416.

326 Y. Wang, G. Qiu, R. Wang, S. Huang, Q. Wang, Y. Liu, Y. Du, W. A. Goddard, M. J. Kim, X. Xu, P. D. Ye and W. Wu, *Nat. Electron.*, 2018, **1**, 228–236.

327 A. Puthirath Balan, S. Radhakrishnan, C. F. Woellner, S. K. Sinha, L. Deng, C. d. l. Reyes, B. M. Rao, M. Paulose, R. Neupane, A. Apte, V. Kochat, R. Vajtai, A. R. Harutyunyan, C.-W. Chu, G. Costin, D. S. Galvao, A. A. Martí, P. A. van Aken, O. K. Varghese, C. S. Tiwary, A. Malie Madom Ramaswamy Iyer and P. M. Ajayan, *Nat. Nanotechnol.*, 2018, **13**, 602–609.

328 A. C. Rajan, A. Mishra, S. Satsangi, R. Vaish, H. Mizuseki, K.-R. Lee and A. K. Singh, *Chem. Mater.*, 2018, **30**, 4031–4038.

